MCNP5 AND GEANT4 COMPARISONS FOR PRELIMINARY FAST NEUTRON PENCIL BEAM DESIGN AT THE UNIVERSITY OF UTAH TRIGA SYSTEM

by

Christian Amevi Adjei

A thesis submitted to the faculty of
The University of Utah
in partial fulfillment of the requirements for the degree of

Master of Science

in

Nuclear Engineering

Department of Civil and Environmental Engineering

University of Utah

December 2012

The University of Utah Graduate School

STATEMENT OF THESIS APPROVAL

The thesis of **Christian Amevi Adjei**

has been approved by the following supervisory committee members:

Tatjana Jevremovic	, Chair	**10/25/2012** Date Approved
Dong-Ok Choe	, Member	**10/25/2012** Date Approved
Haori Yang	, Member	**10/25/2012** Date Approved

and by **Chris Pantelides** , Chair of

the Department of **Civil and Environmental Engineering**

and by Charles A. Wight, Dean of The Graduate School.

ABSTRACT

The main objective of this thesis is twofold. The starting objective was to develop a model for meaningful benchmarking of different versions of GEANT4 against an experimental set-up and MCNP5 pertaining to photon transport and interactions. The following objective was to develop a preliminary design of a Fast Neutron Pencil Beam (FNPB) Facility to be applicable for the University of Utah research reactor (UUTR) using MCNP5 and GEANT4. The three various GEANT4 code versions, GEANT4.9.4, GEANT4.9.3, and GEANT4.9.2, were compared to MCNP5 and the experimental measurements of gamma attenuation in air. The average gamma dose rate was measured in the laboratory experiment at various distances from a shielded cesium source using a Ludlum model 19 portable NaI detector. As it was expected, the gamma dose rate decreased with distance. All three GEANT4 code versions agreed well with both the experimental data and the MCNP5 simulation. Additionally, a simple GEANT4 and MCNP5 model was developed to compare the code agreements for neutron interactions in various materials.

Preliminary FNPB design was developed using MCNP5; a semi-accurate model was developed using GEANT4 (because GEANT4 does not support the reactor physics modeling, the reactor was represented as a surface neutron source, thus a semi-accurate model). Based on the MCNP5 model, the fast neutron flux in a sample holder of the FNPB is obtained to be 6.52×10^7 n/cm^{2}s, which is one order of magnitude lower than gigantic fast neutron pencil beam facilities existing

elsewhere. The MCNP5 model-based neutron spectrum indicates that the maximum expected fast neutron flux is at a neutron energy of ~1 MeV. In addition, the MCNP5 model provided information on gamma flux to be expected in this preliminary FNPB design; specifically, in the sample holder, the gamma flux is to be expected to be around 10^8 γ/cm^{2}s, delivering a gamma dose of 4.54×10^3 rem/hr. This value is one to two orders of magnitudes below the gamma exposure as exists in the currently used fast neutron irradiation facility at the UUTR. The GEANT4.9.4 semi-accurate model of the FNPB design provided higher values for neutron and gamma fluxes, indicating the importance of transfering the data from MCNP5 rather than using the GEANT4 default neutron spectra.

CONTENTS

ABSTRACT iii

LIST OF FIGURES vii

LIST OF TABLES ix

ACKNOWLEDGEMENTS x

Chapters

1. INTRODUCTION 1

1.1. Motivation 1
1.2. Thesis Objectives 1
1.3. Organization of the Thesis 2

2. BASICS ON GEANT4 AND MCNP5 CODES 4

2.1. GEANT4 Code 4
2.1.1. Applications of GEANT4 5
2.1.2. GEANT4 Physics Models 5
2.1.3. GEANT4 Functionality 9
2.1.4. GEANT4 Benchmark and Accuracy 11
2.2. MCNP5 Code 12
2.2.1. Applications of MCNP5 13
2.2.2. MCNP5 Physics Processes 14
2.2.3. MCNP5 Functionality 15
2.2.4. MCNP5 Benchmark and Accuracy 16
2.3. Summary of GEANT4 and MCNP5 Similarities and Differences 18

3. EXPERIMENTAL ASSESSMENT OF DIFFERENT GEANT4 CODE VERSIONS AND COMPARISON TO MCNP5 20

3.1. Description of Experiment to Benchmark GEANT4 and MCNP5 20
3.2. Modeling of Gamma Interactions in GEANT4 and MCNP5 23
3.2.1. Modeling of Gamma Interactions in GEANT4 23
3.2.2. Modeling of Gamma Interactions in MCNP5 27
3.3. Experiment Assessment of Gamma Interactions Modeling using GEANT4 and MCNP5 29

4. BASICS ON FAST NEUTRON PENCIL BEAM FACILITY 35

4.1. About Fast Neutrons 35
4.2. Fast Neutron Facilities 37
4.2.1. Application of Fast Neutron Facilities 38
4.2.2. Application of Fast Neutron Pencil Beam Facilities 41

5. PRELIMINARY DESIGN OF THE FAST NEUTRON PENCIL BEAM FACILITY AT THE UNIVERSITY OF UTAH TRIGA (UUTR) 44

5.1. General Characteristics of the UUTR 44
5.2. Conceptual Design of the Fast Neutron Pencil Beam Facility at the UUTR 46
5.3. MCNP5 Model of the Fast Neutron Pencil Beam Facility at the UUTR 55
5.4. GEANT4 Model of the Fast Neutron Pencil Beam Facility at the UUTR 57
5.5 Comparison of GEANT4 and MCNP5 in Modeling Neutron Interactions 57
5.6. Comparison between MCNP5 and GEANT4.9.4 Models of the Fast Neutron Pencil Beam Facility at the UUTR 62
5.7 Comparison of UUTR FNPB design with other fast neutron pencil beam facilities 69

6. CONCLUSION AND FUTURE WORK 71

6.1. Conclusion 71
6.2. Recommendations for Future Work 73

Appendices

A. MCNP5 INPUT FILE FOR PHOTON EXPERIMENT 75

B. GEANT4.9.4 INPUT FILE FOR PHOTON EXPERIMENT 79

C. MCNP5 INPUT FILE FOR NEUTRON INTERACTION 84

D. GEANT4.9.4 INPUT FILE FOR NEUTRON INTERACTION 87

E. MCNP5 INPUT FILE OF UUTR FNPB 92

F. GEANT4.9.4 INPUT FILE OF UUTR FNPB 107

REFERENCES 117

LIST OF FIGURES

2-1 Applications of GEANT4 6

2-2 GEANT4 class categories 10

2-3 Applications of MCNP5 13

2-4 MCNP5 categories 16

3-1 ^{137}Cs decay scheme 20

3-2 Diagram of cesium source in Pig shielding 22

3-3 Block diagram of the experimental set-up at UNEP facitly (MEB1205) 23

3-4 Comparison of GEANT4.9.2, GEANT4.9.3 and GEANT4.9.4 gamma dose rate as a function of distance from the source 33

3-5 Comparison of gamma dose rate as a function of distance from the source between the measured and calculated values using GEANT4 and MCNP5 . 33

4-1 Classification of neutron energies and interactions 36

5-1 Cross section diagram of the UUTR 100-kWt TRIGA research reactor 45

5-2 Vertical cross-section diagram of FNIF 47

5-3 Outline of UUTR reactor and FNIF 47

5-4 UUTR FNPB model 48

5-5 Cross-section plots of aluminum, Al 49

5-6 Cross-section plots of boron, B-10 51

5-7 Cross-section plots of graphite, C 51

5-8 Cross-section plots of lead, Pb 52

5-9 Cross-section plots of Hydrogen, H 53

5-10 Model of aluminum casing and FNPB sample holder 54

5-11 Cross-section model of UUTR FNPB 55

5-12 MCNP5 3-D model of UUTR FNPB 56

5-13 MCNP5 cross section view of UUTR FNPB 56
5-14 GEANT4 model of UUTR FNPB 58
5-15 GEANT4 and MCNP5 simulation of neutron interaction with boron-10 59
5-16 GEANT4 and MCNP5 simulation of neutron interaction with lead 60
5-17 GEANT4 and MCNP5 simulation of neutron interaction with paraffin 61
5-18 MCNP5 - Neutron spectrum of UUTR FNPB 64
5-19 MCNP5 - Gamma spectrum of UUTR FNPB 67
5-20 Comparison of UUTR FNPB spectrum with literature 70

LIST OF TABLES

2-1 Electromagnetic interactions as modeled in GEANT4 8

3-1 Background dose rate at various distance around experimental area 30

3-2 GEANT4 and MCNP dose rate in comparison to experimental measurements 34

3-3 Percentage difference of experimental measurements with GEANT4 and MCNP5 simulations..... 34

4-1 Applications of fast neutron facilities 38

4-2 Fast Neutron Therapy (FNT) facilities around the world 42

5-1 MCNP5 and GEANT4 comparison of neutron interactions 62

5-2 MCNP reactor physics neutron simulation of UUTR FNPB..... 63

5-3 MCNP neutron flux simulation of UUTR FNPB 65

5-4 MCNP reactor physics gamma simulation of UUTR FNPB..... 66

5-5 MCNP gamma flux simulation of UUTR FNPB 66

5-6 GEANT4 summary of UUTR FNPB simulation 68

5-7 GEANT4 simulation of neutron and gamma fluence in the UUTR FNPB..... 68

5-8 Comparison of MCNP5 and GEANT4.9.4 simulation of UUTR FNPB 69

ACKNOWLEDGEMENTS

Foremost, glory and honour to God, for the opportunity given me to take up this study. I am indebted to my advisor, Professor Tatjana Jevremovic, for her unconditional guidance, advice, support, and opportunities she has provided for my academic development in my graduate studies. Sincere gratitude to Professor Dong-Ok Choe and Professor Haori Yang for their support and guidance. I would like to express my gratitude to Dr. Hermilo Hernandez for his support and encouragement. Also, I would like to thank my colleagues and friends, Avdo Cutic, Andrey Rybalkin, Can Liao, Philip Babitz, Todd Sherman, Jason Rapich, and Chris Dances, for their help and support. Finally, my heartfelt gratitude to my parents (Andrew A. Adjei and Cecilia Adjei), my siblings (Rose Siedu and Andrew Adjei Jr.), brother in-law (Frederick Siedu), nephew (Joshua Anglamaga), and nieces (Nomu Anglamaga, Zunou Anglamaga, and Pupil Anglama), for their prayers and support.

CHAPTER 1

INTRODUCTION

1.1. Motivation

The University of Utah TRIGA Reactor (UUTR) is licensed to operate at a maximum power of 100 kW, and it is used for research, teaching, and training. The UUTR has four neutron irradiation ports used for a number of applications, such as, but not limited to: Neutron Activation Analysis (NAA), irradiation of samples, cadmium ratio measurements, studies on irradiation damage to materials, effects of radiation on some electronic components, and basic studies on biological effects of radiation. Currently, the UUTR has no Fast Neutron Pencil Beam (FNPB) irradiation port. Design and installation of such a facility would open up a variety of new applications, such as fast neutron irradiation studies to understand the effect of fast neutrons on biological cells, by-standard effects, impact on materials and nanoparticles, as well as for benchmarking numerical simulations based on various codes, such as, for example, GEANT4 and MCNP5/X.

1.2. Thesis Objectives

The main objective of this thesis is to develop a preliminary design of the Fast Neutron Pencil Beam facility and assess the feasibility of its installation in the UUTR pool. In order to develop such a design, two known codes used in the nuclear industry are adopted; GEANT4 [1] and MCNP5/X [2]. The MCNP5 code was

developed, and continues to be modified, in the United States; the GEANT4 code was developed, and continues to be modified, in Europe. Both codes are based on the Monte Carlo method for tracking particles in the geometry of interest. GEANT4, being an open software code, suffered numerous changes, so that now, a number of subversions are available with no clear understanding of the accuracy of each subversion. MCNP5/X is closed to public domain and therefore, its accuracy is strictly controlled and tracked with every new code version. Therefore, in order to understand what the best subversion of GEANT4 code is, a few comparisons were performed developing experimental and numerical examples.

Detailed objectives of this thesis are summarized as follows:

1. Perform experimental assessment to validate different versions of the GEANT4 code and compare it to MCNP5 focusing at photon transport and interactions.
2. Compare MCNP5/X and GEANT4 in modeling neutron transport in various media.
3. Design a preliminary model of a Fast Neutron Pencil Beam facility at the UUTR using MCNP5/X and GEANT4.

1.3. Organization of the Thesis

The basic description of GEANT4 and MCNP5, similarities, and differences are provided in Chapter 2. In Chapter 3, the experimental assessment of gamma interactions using different GEANT4 code versions in comparison to MCNP5 are described. The basics of a Fast Neutron Pencil Beam facility are described in

Chapter 4. In Chapter 5, the preliminary design of a fast neutron irradiation facility at the University of Utah TRIGA (UUTR) is described. The comparison of MCNP5 and GEANT4 models of the preliminary design of the fast neutron pencil beam are also evaluated. Chapter 6 outlines the future work and conclusion of this research study.

CHAPTER 2

BASICS ON GEANT4 AND MCNP5 CODES

2.1. GEANT4 Code

GEANT4 is a Monte Carlo-based code that is a successor of GEANT3 developed in two independent studies at CERN and KEK in 1993 [1]. Both groups researched how modern computing techniques could be applied to improve existing FORTRAN-based GEANT3 simulation programs, and finally developed GEANT4 in 1994. The main objective of developing the GEANT4 code was to have a simulation program which had the flexibility and functionality to meet the essentials and needs of subatomic physics experiments. The development of GEANT4 has grown to become a large international collaboration of over hundred (100) scientist, physicist programmers, and software engineers from a number of institutions and universities participating in a wide range of research experiments in Europe, Japan, Canada, and the United States [3].

GEANT4 is a modern object oriented (OO) environment code based on C++ that exploits advanced software-engineering techniques and object-oriented technology to achieve transparency. GEANT4 is one of the largest and most ambitious open source codes in terms of the size and scope. Every section of the GEANT4 code is individually managed by a group of experts known as the international GEANT4 collaboration group. In addition, there is a working group for testing, quality assurance, software management, and documentation of the

software. The GEANT4 code is freely available, accompanied by an installation guide and an extensive set of documentation [1, 3].

2.1.1. Applications of GEANT4

GEANT4 is a software toolkit based on Monte Carlo simulation of particle transport and interaction with matter. One of the GEANT4 code's powerful applications is its use in instrumentation studies of the High Energy Physics (HEP), and Large Hadron Collider (LHC) experiment [4], simulation of the BaBar experiment [5], large HEP experiments ATLAS [4, 5], among others. GEANT4 users come from a variety of fields, including space and radiation science, medical science, and technology transfer, which basically allows the user to incorporate other subroutine programs from other simulation codes into GEANT4 (Figure 2-1). Specifically, the interest from the space and medical communities stems from the following aspects of the toolkit [6, 7]: freely available software with long-term support, object-oriented design and component approach, a wide choice of geometry shapes, geometry and tracks visualization, particle tracking in fields, and a rich set of physics models. GEANT4 provides users the ability to construct stand-alone applications built upon another object-oriented framework.

2.1.2. GEANT4 Physics Models

GEANT4 consist of a number of various physics models supporting the interactions of particles with matter across a wide range of energies. It provides the user with interfaces, built-in steering routines, and commands at every level of simulation.

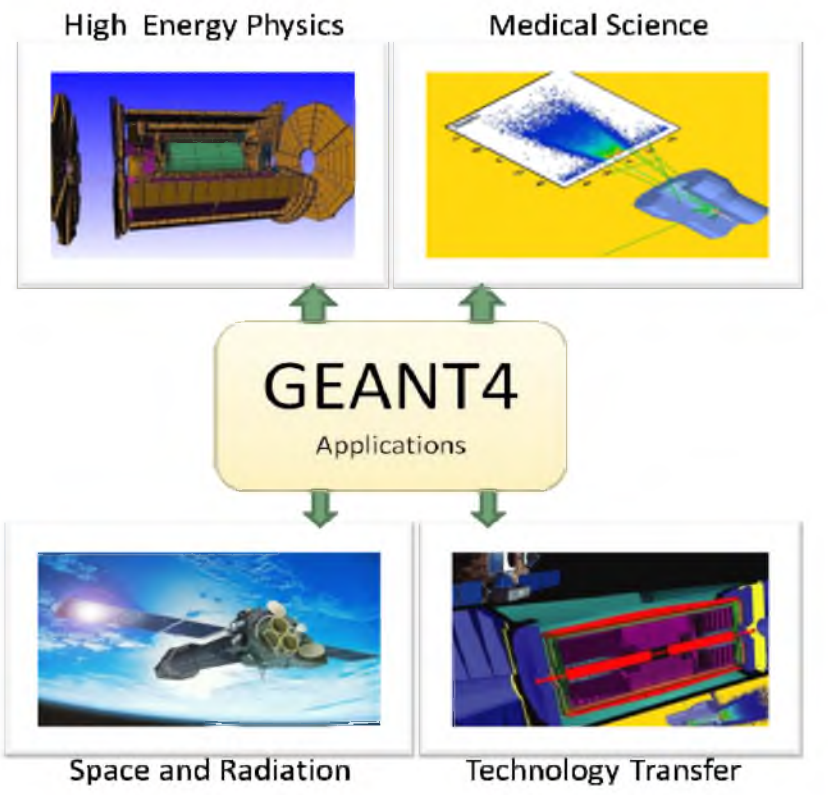

Figure 2-1. Applications of GEANT4. Adapted from [1]

A limitation with older versions of the GEANT4 was the difficulty of adding new physics models, due to the complexity and interdependence of physics procedures which are "hard coded" into the code. In contrast, the object-oriented approach helped manage complexity and limit dependencies by defining a uniform interface and common organizational principles used for all physics models. Within the GEANT4, the functionality of models can easily be recognized and understood, making the creation and addition of new physics models easy and well defined [3-5].

All aspects of the simulation process that can be included in the code are: geometry of a system to be modeled, materials, particles of interest, generation of primary events, tracking of particles, physics processes governing particle

interactions, storage of events and tracks, visualization of the detector and particle trajectories, and analysis of simulation data [7, 8, 9]. GEANT4 physics modules include [10, 11]:

- *Particle transport*: particle transport determines the geometrical limits of a step (i.e. the point of interaction of the particle) by calculating the length of step with which a track (i.e. the path of the particle) crosses into another volume.
- *Particle decay*: is simulated by the G4Decay class implemented into the GEANT4 physics process based on the branching ratios. Each of the decay modes are implemented as a class and generate secondary particles produced from the decay process.
- *Electromagnetic interactions*: are listed in Table 2-1. GEANT4 has three different physics package models implemented for electromagnetic particle interactions, standard electromagnetic physics model, Livermore electromagnetic physics model, and Penelope electromagnetic physics model. *Hadronic interactions*: GEANT4 includes photonuclear interactions of muons. A muon interacts electromagnetically with a nucleus, exchanging a virtual photon. At energies above a few GeV, the photon interacts hadronically with the nucleus and produces hadronic secondary particles [12, 13]. An example of the hadronic process is the use of the Large Hadron Collider to accelerate subatomic particles at very high energies, and colliding them together to understand conditions that prevailed in the universe trillions of years ago after the big bang, and also to understand the Higgs boson.

Table 2-1. Electromagnetic interactions as modeled in GEANT4

ELECTROMAGNETIC INTERACTIONS	
Type of Particle	**Interaction Process**
Charged Particles	Ionization
	Coulomb scattering
	Cerenkov effect
	Scintillation
	Transition radiation
Muons	Pair production
	Bremsstahlung
	Nuclear interactions
Electrons and Positrons	Bremsstahlung
	e+ annihilation
Photons	Photoelectric effect
	Compton effect
	Coherent scattering
	Incoherent scattering
Optical Photons	Reflection and refraction
	Adsorption
	Rayleigh scattering

- *Neutron interactions*: when a neutron interacts with a nucleus, two major types of interactions occur: either the neutron is scattered or it is absorbed. If a neutron is scattered (either elastically or inelastically) by a nucleus, its speed and direction are changed, but the nucleus is left with the same number of protons and neutrons. The nucleus will also have some recoil velocity, and may be left in an excited state that will lead to a release of gamma radiation. When a neutron is absorbed by a nucleus, different types of radiations can be emitted (either charge particle or gamma), or fission can be induced.

2.1.3. GEANT4 Functionality

The GEANT4 class categories are shown in Figure 2-2, and explained as follows [8]:

- *Global* category covers the system of units, constants, numerics, and random number handling.
- *Materials* and *particles* categories are implemented to describe the physical properties of particles and materials for the simulation of particle interactions.
- *Geometry* module is used to describe a geometrical model and propagate particles.
- There are also categories required for describing the tracking of particles and the physical processes they undergo. The *track* category contains classes for tracking the particle interactions and steps, while the *processes* categories contain implementations of models of physical interactions.
- *Tracking* category manages the evolution of a track's state and provides information in sensitive volumes for hits and digitization.
- *Event* category manages events in terms of the particle tracks, and the *run* category manages collections of events that share a common beam and detector implementation.
- *Readout* category allows the user to print the desired information.

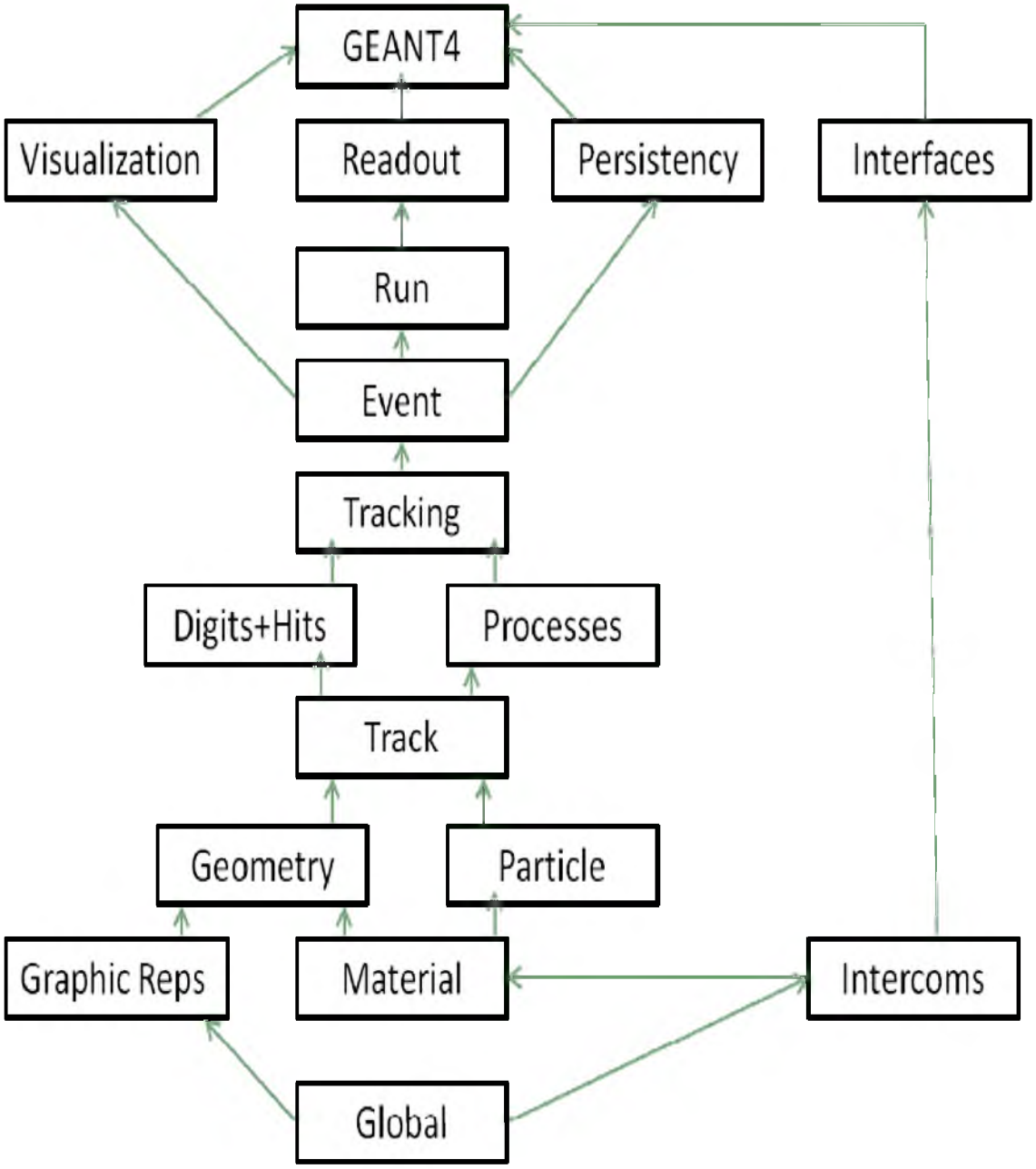

Figure 2-2. GEANT4 class categories. Adapted from [7, 8]

- Finally, capabilities that use all of these categories and connect them together within the GEANT4 code through abstract interfaces by providing *visualization*, *persistency,* and user *interface* capabilities [1, 7, 8].

2.1.4. GEANT4 Benchmark and Accuracy

Electromagnetic processes can easily be described using theoretical methods for very low to high energies. The precision of simulations most often depends on a choice of implementation methods; therefore, validation of simulation codes depends on direct comparison between simulation results, theoretical predictions, and experimental work. At lower energies below 1 MeV generally, the analytical theory tends not to be inaccurate [13], because it is necessary to describe the wave function of atomic electrons in media. Cross-sections, stopping powers, and other physical data are provided in evaluated data libraries. Simulation of electromagnetic processes as well as other physics processes depends on tracking methods of the particle that the user selects. The user can also specify the cut of energy of the particle and the particle track path. Hence, the precision of most simulation codes depends on chosen theoretical and physics models, parameterization methods, and tracking parameters that are implemented by the user.

Regular regression tests and benchmarks are performed for all the physics models implemented in GEANT4 [7, 8, 13]. Before the release of any GEANT4 package, the verification and validation of the electromagnetic (EM) physics models are benchmarked and tested against known accurate data by the GEANT4 system testing team [14]. For example, A. Lechner developed a benchmark experiment for

GEANT4 on electron backscattering energy deposition in semi-infinite media using Sandia data. The electron energy of 0.1 – 1 MeV was evaluated and beam angles were from 0 and 75 degrees, and GEANT4 results showed good accuracy with existing data [15, 16]. Benchmarking of electromagnetic interactions was performed at ATLAS using a barrel simplified calorimeter, and results showed no change of energy of resolution [15, 16]. Validation and improvements of the GEANT4 standard electromagnetic package at low energies performed by Vladimir Grichine, by propagating particles through different target materials (Al, Au, Cu, and Si), showed that the standard models have good agreement with the experiment (dE/dX) for electron energy interval 0.01 – 10 MeV, and GEANT4 models for Bremsstahlung benchmarked against experimental data also showed good agreement [17, 18]. Due to the fact that GEANT4 is an open source code that has undergone many generations of modifications pertaining to electromagnetic processes leading to the release of different versions, not many benchmark experiments have been conducted to compare some released versions of GEANT4. In Chapter 3, the benchmark of different versions of GEANT4 codes used to model photon interactions are evaluated against experimental data and MCNP5 modeling.

2.2. MCNP5 Code

The Monte Carlo N-Particle (MCNP) code is currently being managed by the Diagnostic Application Group (Group X-5) in the Applied Physics Division (X Division) at the Los Alamos National Laboratory [19]. MCNP is a general purpose code that can be used to simulate neutron, photon, and electron transport. It is

capable of modeling complex 3D geometries and utilizes extensive point-wise cross-section data libraries in a continuous energy spectrum. It is applicable to modeling nuclear interactions in medical physics, boron neutron capture therapy (BNCT), high energy physics, radiation detection and shielding, particle accelerator models, space study analysis, nuclear reactor simulations, and criticality calculations [19].

2.2.1. Applications of MCNP5

MCNP5 code is a Monte Carlo-based simulation of particle transport and interactions with matter. MCNP5 is mostly used by nuclear engineers and scientist around the world for a vast number of research simulations. MCNP5 has a wide range of applications in the fields of medical physics, reactor physics calculations, reactor safety calculations, and radiation dose estimates, as shown in Figure 2-3, [20].

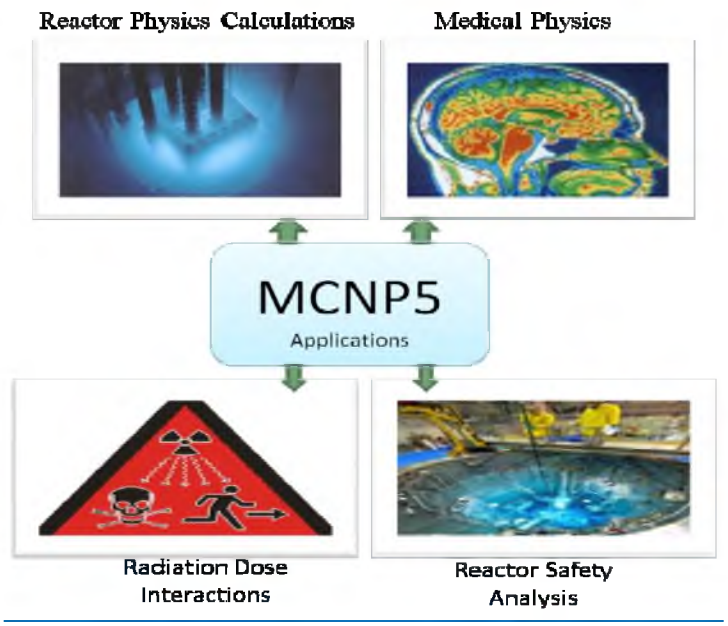

Figure 2-3. Applications of MCNP. Adapted from [2]

2.2.2. MCNP5 Physics Processes

The very essence of MCNP is based on the probability of a physics interaction of a neutron, photon, or electron. The MCNP is associated with having complete accurate nuclear and atomic data libraries [19]. Data libraries provided in MCNP contain information relating to the probability of unique particle interactions per elements used during simulation. MCNP includes nine classes of data tables [20]: (1) Continuous-energy neutron interaction data; (2) Discrete reaction neutron interaction data; (3) Continuous-energy photoatomic interaction data;

(4) continuous-energy photonuclear interaction data; (5) neutron dosimetry cross-sections; (6) neutron S(α,ß) thermal data; (7) multigroup neutron, coupled neutron/photon, and charged particles masquerading as neutrons; (8) multigroup photon; and (9) electron interaction data. Physics interactions implemented in the MCNP code for simulations include particle weight calculation, particle tracking, neutron interactions, photon interactions, electron interactions, electromagnetic interactions, and many more. During neutron interactions, a particle may collide with a nucleus and will either be absorbed or scattered. Photon interactions include coherent scattering and account for fluorescent photons after photoelectric absorption, the Compton scattering from free electrons, photonuclear interactions, and pair production. The transport of electrons and other charged particles is fundamentally different from that of neutrons and photons. The interaction of neutral particles is characterized by relatively infrequent isolated collisions, with simple free flight between collisions. In contrast, the transport of electrons is

dominated by the Coulomb force, resulting in large numbers of small interactions, Bremsstahlung, Cerenkov radiations, and other nuclear reactions [19, 20, 21].

2.2.3. MCNP5 Functionality

The MCNP5 input file contains five main categories as illustrated in Figure 2-4, namely [2]:

- *Geometry category* – In order to describe the geometry of a model, one has to specify the *cell* and the *surfaces* that make up the model. The material composition of the cell is also specified in the geometry category.
- *Source category* – User specifies types of reactions and source(s) to be simulated; for example, whether a source is a neutron source, or gamma source. The user has the option to specify the energy or activity of the source and the direction at which the source emits particles.
- *Material card category* – User chooses the elemental compositions that make up the specified material in the geometry category and the data libraries associated with the elements.
- *Run mode category* – This category determines a type of simulation being performed; for example, either criticality calculation or particle interaction. In addition, the run category gives a user an option to specify nuclear reactions desired for the simulation as well as production of secondary particles.

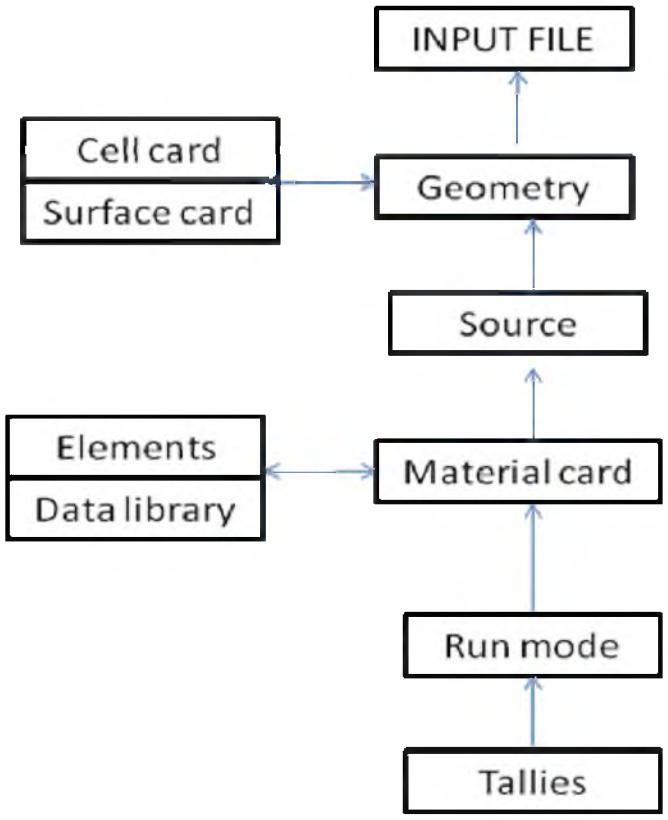

Figure 2-4. MCNP5 categories. Adapted from [2]

- *Tallies category* – Provides summary information to a user related to particle interactions, collision, creation and loss of particles, energy of particles, radiation dose, particle flux, and much other useful information needed for problem analysis.

2.2.4. MCNP5 Benchmark and Accuracy

Benchmarking of MCNP5 simulation codes against existing data for verification and validation is very important due to the wide range of different physics models, different code options, and different data libraries implemented within the code. The verification of the simulation code is normally performed by

developers, and it involves performing a series of calculations to determine whether a code solves the equations, computational models, and physical models it was designed to solve [21, 22]. Validation of the MCNP5 simulation code is normally performed by the end-users, and it involves the determination of whether the code reproduces the true values of the simulated experiment or research or application. Verification and validation also includes the comparison of the simulated results to other codes, to analytical benchmarks, or to experiments [22].

MCNP5 developers have verified that MCNP5 produces accurate and the same results as previous versions such as MCNP4 for a set of over a hundred test experiments. For example, MCNP5 develops performed benchmarking of criticality calculations by comparing MCNP5 simulations to previous versions of MCNP4 and existing criticality data, and MCNP5 simulations showed good accuracy of criticality calculations [22]. In addition, Y. Danon developed a benchmark experiment of neutron resonance scattering models using MCNP. Experimental measurements of elastic neutron scattering from U-238 resonances were used to benchmark neutron scattering models in Monte Carlo transport codes. He found that MCNP5 elastic free gas models have been improved to provide accurate simulation of the experimental results [23]. Hanna Koivunoro performed simulations pertaining to the accuracy of the electron transport in MCNP5 and its suitability for ionization chamber response simulations [24]. She reported that the electron beam studies had some discrepancies (>3%) at electron beam energies of 0.1 and 0.05 MeV. She also concluded that MCNP5 provides dose distributions that agree better with other

reference codes, and MCNP5 results are highly dependent on the chosen electron track length.

2.3. Summary of GEANT4 and MCNP5 Similarities and Differences

GEANT4 and MCNP5 are two simulation codes with similar features embedded within the heart of the codes, yet different in their own unique aspects. One of the most common features implemented in both codes are the Monte Carlo methods. Monte Carlo methods are statistical principles that employ a class of computational algorithms that rely on repeated random sampling to solve problems that are of a probabilistic nature: for example, the interaction of nuclear particles with materials. The Monte Carlo methods are also used to solve complex problems that cannot be modeled with computational deterministic methods [2, 19]. Both GEANT4 and MCNP5 codes are developed to be easily run along a wide range of computer operation system platforms, such as Linux (GCC (g++)), and Mac OS X (GCC (g++), Xcode 3 or 4) [1, 20]. Both codes are used for a wide range of research applications, such as, but not limited to, high energy physics, medical sciences, space radiation, nuclear engineering, and radiation science.

GEANT4 and MCNP5 have distinctive differences, including, but not limited to, the following: (1) MCNP5 is developed by the Los Alamos National Laboratory requiring individual licenses, while GEANT4, developed at CERN, is an open source. (2) GEANT4 has several affiliated visualization codes such as OpenGL, OpenInventor visualization, and X11 RayTracer [7, 8], while MCNP has its own inbuilt visualization tool, VISED [20]. (3) MCNP5 requires INPUT file, whereas

GEANT4 is versatile and gives a user ability to program/code a desired geometry and material definition, physics models, nuclear interactions, and output results. (4) MCNP5 implements comprehensive physics models which include all nuclear interactions processes possible, but GEANT4 has three different physics model packages implemented within the code, namely, the Livermore physics model, Standard physics model, and Penelope physics model [7, 15]. (5) One major difference between MCNP5 and GEANT4 is the implementation of nuclear data libraries used by both simulations codes; MCNP5 uses the Evaluated Nuclear Data Files ENDF/B-VI [2] which are updated frequently, whereas GEANT4 implements some data libraries extracted from the ENDF/B-VI and also, most of the data libraries implemented are the EPDL97, EEDL, and EADL [16, 21].

CHAPTER 3

EXPERIMENTAL ASSESSMENT OF DIFFERENT GEANT4 CODE VERSIONS AND COMPARISON TO MCNP5

3.1. Description of Experiment to Benchmark GEANT4 and MCNP5

In order to benchmark versions of GEANT4 to determine which version provides accurate simulation relative to photon transport and interaction, a photon interaction experiment was conducted to benchmark experimental data with simulation of different versions of GEANT4 and MCNP5 code using a cesium-137 source (^{137}Cs). Cesium-137 has a half-life of 30.08 years, and specific activity of 3.214 TBq/g. The decay scheme of ^{137}Cs is shown in Figure 3-1. Cesium-137 decays via beta decay mode into a daughter nucleus of Barium-137 (^{137}Ba) with maximum beta energies of 0.512 MeV (94.6% probability) and 1.174 MeV (5.4% probability), and emits gamma rays with energy of 0.6617 MeV during the transition from a meta-

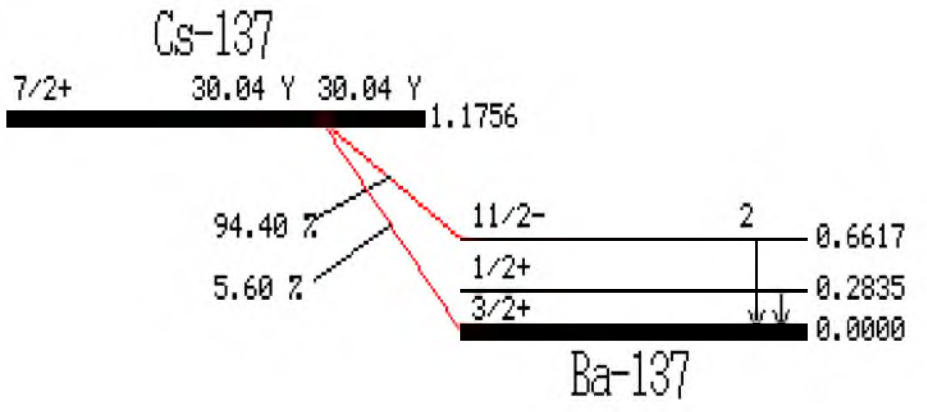

Figure 3-1. ^{137}Cs decay scheme. Adapted from [25]

stable to the ground state of ^{137}Ba (Figure 3-1). Cesium-137 is used for a wide variety of applications, both in the medical and industrial field, and not limited to treatment of cancer, measurement of fluid flow in oil pipelines, well logging, and many more. The Cesium- 137 gamma source was placed in the hollow cylindrical lead shielding to minimize any unnecessary radiation dose to the researchers since the source is very radioactive, and then placed on the open floor of the Nuclear Engineering Facility, as shown in Figure 3-2. The gamma dose rates were measured at various distances around the cesium- 137 source by placing a Ludlum model 19 potable NaI detector at one foot intervals up to a distance of 8 ft around the set-up, as shown in Figure 3-3. The Ludlum model 19 detector is a photomultiplier coupled to a 1" x 1" NaI(TI) crystal, mounted inside the instrument housing. The detector is constructed as a cast and aluminium cover with computer-beige powdercoating finish and printed membrane front panel. The experimental measurement was repeated at least five times to account for experimental error. The research was to simulate the experimental set-up shown in Figures 3-2 and 3-3, using different versions of Geant4. Benchmarking the experimental results with the Geant4 simulated results to ascertain which version of Geant4 provides more accurate simulations pertaining to photon transport, since the different versions of Geant4 have differences in their physics models. Validation of the results was done with MCNP5.

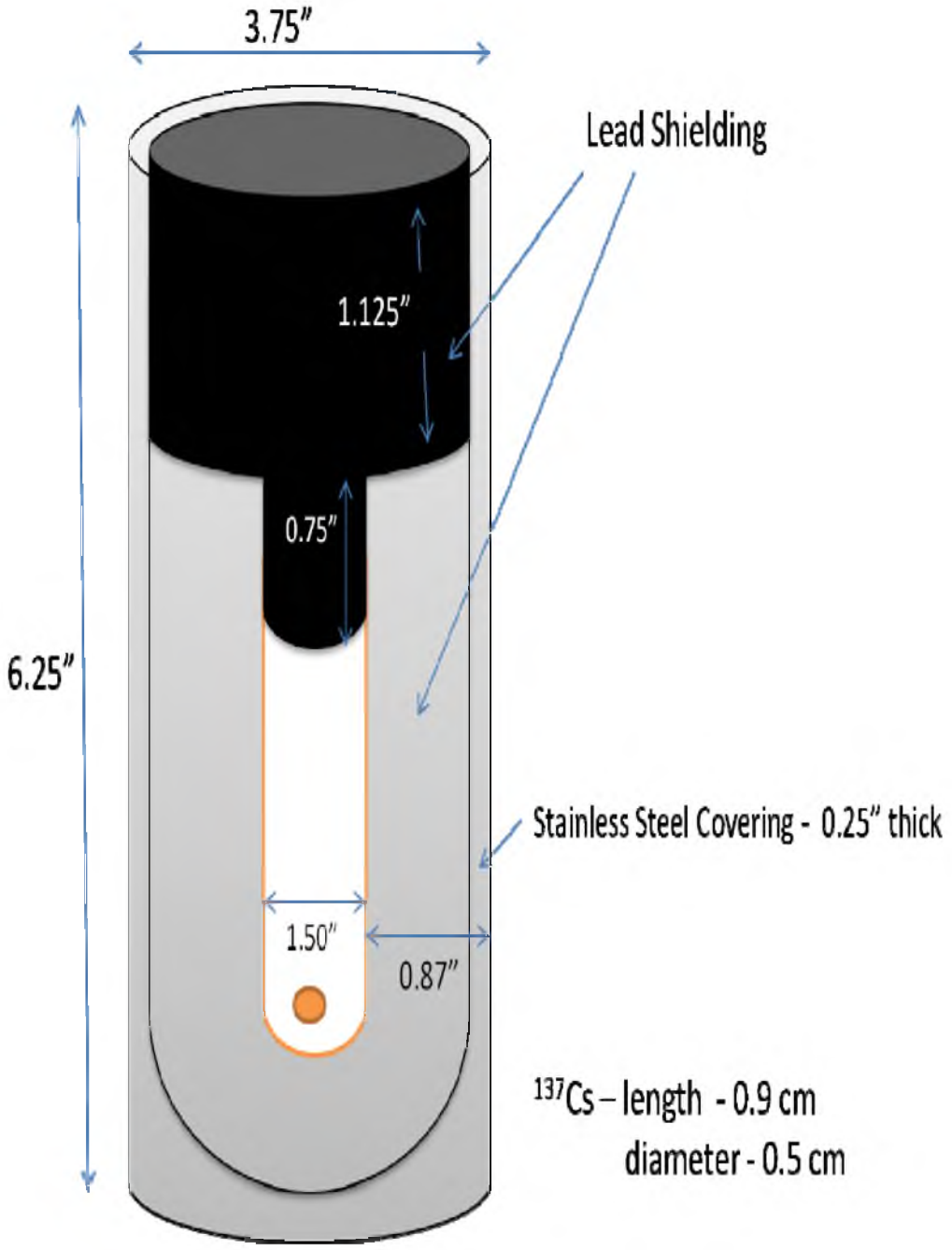

Figure 3-2. Diagram of cesium source in Pig shielding (Not to scale)

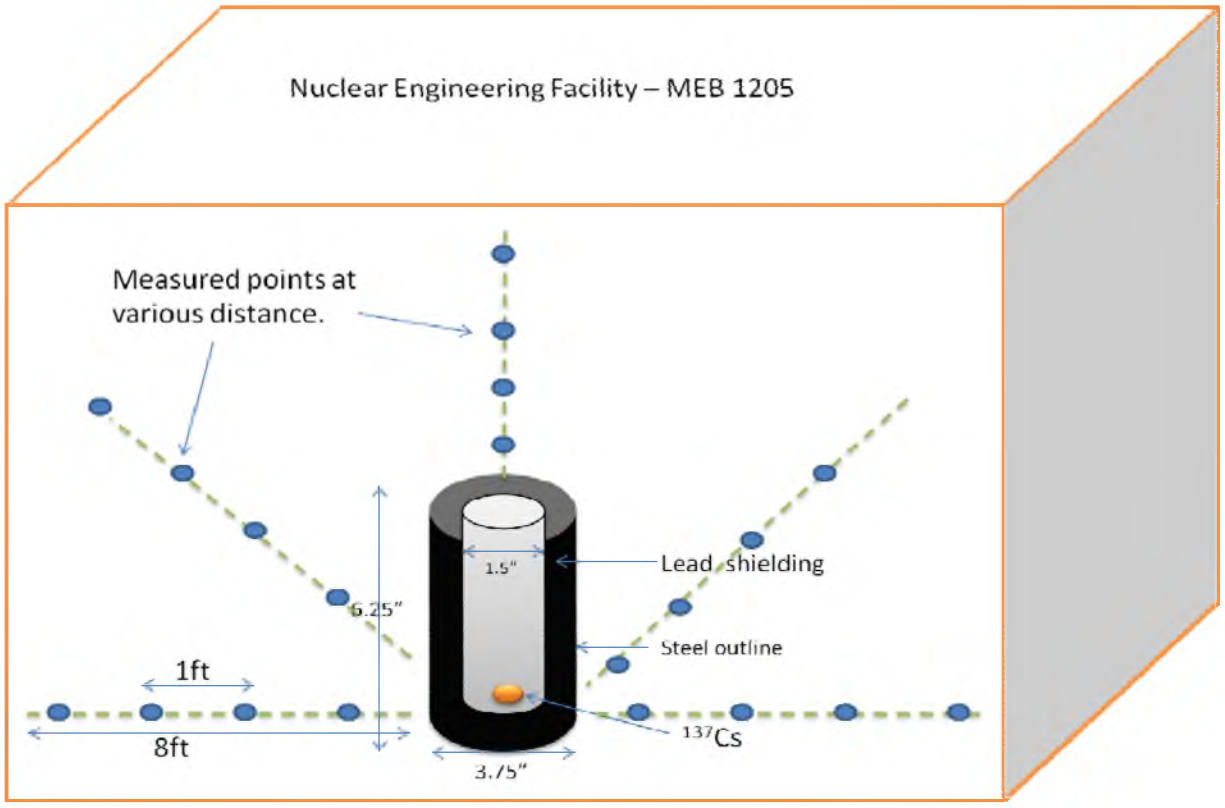

Figure 3-3. Block diagram of the experimental set-up at UNEP facility (MEB 1205) (Not to scale)

3.2. Modeling of Gamma Interactions in GEANT4 and MCNP5

Different versions of GEANT4 (versions 4.9.2, 4.9.3, and 4.9.4) and MCNP5 codes (Appendix A and B) were used to simulate the experimental set-up in Figure 3-2 and Figure 3-3. The simulated data were compared and benchmarked against obtained experimental data.

3.2.1. Modeling of Gamma Interactions in GEANT4

Versions of GEANT4.9.2, 4.9.3, and 4.9.4 have similar electromagnetic models implemented within the code, but have unique different features. GEANT4

version 4.9.2 has three different independent electromagnetic physics package models implemented within the heart of the code, namely, the Standard EM package, Livermore EM package, and Penelope EM package. Each of the models has different processes for describing photon interactions; for example, *G4PhotoElectricEffect* (from the Standard EM package), *G4LowEnergyPhotoElectric* (Livermore package) and *G4PenelopePhotoElectric* (Low Energy Penelope package) [14].

GEANT4 version 4.9.3 is an improvement of GEANT4 version 4.9.2 that has a few changes in its physics model. The low energy EM process in GEANT4.9.3 had been migrated to follow the same software interface that was developed for the Standard EM package. As a result, in the new approach, there is only one process (e.g. *G4PhotoElectricEffect*) and multiple independent models that can be registered to the process, in different energy ranges, e.g. *G4PEEffectModel* (Standard), *G4LivermorePho-toElectricModel* (LIVERMORE), and *G4PenelopePhoto-ElectricModel* (PENELOPE). New versions of two data sets were added : a low-energy data set, G4EMLOW.6.9, and a new data set for optical surface reflectance [26].

GEANT4 version 4.9.4 was developed to improve/address some shortcomings of GEANT4.9.3. Geant4.9.4 includes modeling of pair production in the electric field of secondary particles. The Bertini Cascade (BERT) model implemented in GEANT4.9.3 was rewritten for Geant4.9.4 to improve memory management, and to provide better energy/momentum conservation. Alongside, there was the addition of a new physics list for BERT and CHIPS for shielding, and improved inelastic cross-

sections at high energies. Also, eight new cross-section data sets for nuclear interactions at low-energies were added to this package. Extensive validation of physics models, which is fundamental to guarantee the accuracy and reliability of Geant4-based simulations, has been documented by G.A.P. Cirrone *et al.* 2010 [14].

Photon interactions processes considered are as follows: The total cross-sections as a function of energy are derived from the evaluated data for all the processes considered. For each process, the total cross-section at a given energy E is obtained by interpolating the available data, according to the equation [10]:

$$\log(\sigma(E)) = \log(\sigma_1)\frac{\log(E_2)-\log(E)}{\log(E_2)-\log(E_1)} + \log(\sigma_2)\frac{\log(E)-\log(E_1)}{\log(E_2)-\log(E_1)} \qquad (3.1)$$

where E_1 and E_2 are the closest lower and higher energy for which cross-section σ_1 and σ_2 are available in the data libraries. In the photoelectric effect, the incident photon is absorbed and an electron of direction identical to the one of the incident photon is emitted. The subshell from which the electron is emitted is selected according to the cross-sections of the subshell. The interaction leaves the atom in an excited state, with excitation energy equal to the binding energy of the subshell from which the electron has been emitted. The de-excitation of the atom proceeds via the emission of fluorescence photons. The transition probabilities from a subshell to lower energies are extracted from the EADL data library [26]. The fluorescence photons are generated with energy determined by the energy difference of the subshells involved in the transition and with isotropical distribution [10]. The Livermore and Penelope cross-sections are tabulated according to EPDL97 and EPDL89, respectively, and they are both in agreement with the NIST data cross-

section; however, the Standard model with respect to NIST data has a 10% deviation [14]. During Compton scattering, the scattered photon energy is distributed according to the product of the Klein-Nishina formula [10]:

$$\sigma(k) = 2\pi r^2 Z\left[\left(\frac{\kappa^2 - 2\kappa - 2}{2\kappa^3}\right)\ln(2\kappa+1) + \frac{\kappa^3 + 9\kappa^2 + 8\kappa + 2}{4\kappa^4 + 4\kappa^3 + \kappa^2}\right] \tag{3.2}$$

where: r is classical electron radius, $\kappa = k/mc^2$

$$\phi(\in) \cong \left[\frac{1}{\in} + \in\right]\left[1 - \frac{\in \sin^2(\theta)}{1+\in^2}\right] \tag{3.3}$$

photon scattering functions *F(q)*:

$$P(\in, q) = \phi(\in)\cdot F(q) \tag{3.4}$$

where $\in$ is the ratio between the scattered photon energy and the incident photon energy. The scattering functions *F(q)* at the transferred momentum $q = E\cdot\sin^2(\theta/2)$ corresponding to the energy E are calculated from the values available in the EPDL97 data library. The angular distribution of the scattered photons is obtained from the same procedure. The cross-section of the Standard package model (G4KleinNishinaCompton) is derived from an empirical parameterized approach, whose accuracy is estimated to be 10% between 10 and 20 keV, and 5-6% above 20 keV. The cross-section of the Geant4 Livermore model is tabulated according to the EPDL97 library. The Penelope model is determined from an analytical parameterization that takes into account atomic binding effects and Doppler broadening for energies below 5 MeV, and uses the Klein-Nishina formula for energy above 5 MeV [10, 14]. In the Rayleigh effect, the angular distribution of the scattered photon is described by

$$\phi(E,\theta) = \left[1 + \cos^2(\theta)\right] \cdot F^2(q) \qquad (3.5)$$

where $q = E \cdot \sin^2(\theta/2)$ is the transferred momentum corresponding to energy E and $F(q)$ is the form factor. Form factors are obtained from the EPDL97 data libraries; their dependence on the momentum transfer is taken into account by interpolating the available data. The Standard EM package of Geant4 does not contain its own model to describe Rayleigh scattering; only Livermore and Penelope models describe Rayleigh scattering in Geant4. The cross-section of the G4LivermoreRayleighModel is based on the EPDL97 database, while the cross-section of the Penelope model is determined by numerical integration from an analytical parameterization [10, 14].

3.2.2. Modeling of Gamma Interactions in MCNP5

MCNP5 simulation code (Appendix A) was used to model the photon interaction experiment depicted in Figure 3-3. There are two photon interaction models implemented in MCNP: the Simple and Detailed model. The Simple photon interaction physics model ignores coherent scattering and fluorescent photons from photoelectric adsorption, and it is mostly used for high-energy photon problems [2]. The Detailed photon interaction physics model includes coherent scattering and accounts for fluorescent photons after photoelectric absorption, and form factors as well as Compton process are used to account for electron binding effects [2].

The photon interactions considered in MCNP are [2]: the total cross-section calculation does not use the Klein-Nishina differential cross-section calculations. Thus, the total cross-section σ_t is regarded as the sum of three components: the photoelectric cross-section-σ_{pe}, Compton scattering-σ_s, and pair production-σ_{pp}.

$$\sigma_t = \sigma_{pe} + \sigma_{pp} + \sigma_s \qquad (3.6)$$

- *Photoelectric effect:* The incident photon is absorbed and an electron of direction identical to the one of the incident photon is emitted, and treated as a pure absorption by implicit capture with corresponding reduction in the photon weight WGT, and hence does not result in the loss of the particle history.
- *Compton scattering:* in the interaction process of Compton scattering, the physics is to determine the energy E' of the scattered photon, and $\mu = cos\theta$ for the angle θ of the deflection from the line of flight. This yields the energy WGT (E – E') deposited at the point of collision and the new direction of the scattered photon. The differential cross-section for the process is given by the Klein-Nishina formula

$$K(\alpha,\mu)d\mu = \pi r_o^2 \left(\frac{\alpha'}{\alpha}\right)^2 \left[\frac{\alpha'}{\alpha} + \frac{\alpha}{\alpha'} + \mu^2 - 1\right] d\mu \qquad (3.7)$$

where r_o is the classical electron radius 2.817938 x 10^{-13} *cm*, α and α' are the incident and final photon energies in units of 0.511 MeV ($\alpha = E/(mc^2)$, where m is the mass of the electron and c is the speed of light, and $\alpha' = \alpha/(1+\alpha(1-\mu))$.

- *Pair production*: in pair production, an electron-positron pair is created for further transport and the photon disappears, or it is assumed that the kinetic energy of the electron positron pair produced is deposited as thermal energy at the time and point of collision, with isotropic production of one photon of energy 0.511 MeV in one direction and another photon of the same energy in the opposite direction.

3.3. Experiment Assessment of Gamma Interactions Modeling using GEANT4 and MCNP5

The background dose rate at UNEP facility room MEB 1205 were measured at various distances around the experimental area before the experimental set-up was performed (Table 3-1) using the NaI detector. The NaI detector has a linearity reading within ± 10% of true value. The NaI detector has a two-scale meter face presenting 0-50 μR/hr with full-scale range positions of 5000, 500, 50, and 0-25 μR/hr with full-scale range of 250 and 25. The measured gamma dose obtained from the Ludlum model 19 potable NaI detector was recorded in mR/hr and converted to mrem/hr with a conversion of 1 Roentgen (R) equal to 0.87 rems in dry air and 0.96 rems in tissue. Roentgen (R) is a measure of exposure to gamma ray or x-ray radiation. One Roentgen is the amount of gamma radiation that will deposit enough energy to strip about two billion electrons from their orbits in one cubic centimeter of dry air. Rem is based on the biological damage casued by ionization in human body tissue. The rem is also a term for dose equivalence and equals the biological damage that would be caused by one rad of dose. Experimental data obtained were benchmarked against versions of GEANT4 simulation and MCNP5. The dose measurements were performed three times at each measured distance and the average gamma dose, standard deviation, and standard error at each distance was calculated.

Table 3-1. Background dose rate at various distances around experimental area

Distance (ft)	Time (min)	Average Background (mrem/hr)
1	0:30	0.0035
2	1:00	0.0035
3	1:30	0.0035
4	2:00	0.0035
5	2:30	0.0035
6	3:00	0.0035
7	3:30	0.0035
8	4:00	0.0035

The gamma dose rate can be calculated by either using the dose tallies in the MCNP code or analytically by using the dose equations:

$$D\left(\frac{Gy}{source}\right) = \frac{C}{N}\sum_{j=1}^{N}\sum_{i=1}^{T}\varphi\sigma_T(E)H(E) \tag{3.8}$$

$$\text{where } C = \left(1.602x10^{-10}\frac{Gy}{MeV/g}\right)\left(1.10^{-24}\frac{cm^2}{barn}\right)\left(\frac{N_a\eta}{M}\right) \tag{3.9}$$

Na = Avagadro's constant = 6.022x1023 mol-1;

η = number of atoms per molecule;

M = molar mass of material in grams;

φ = fluence score in particles/cm2;

σ_T = total atomic cross-section at energy of scoring track in barns;

H = heating number in MeV per collision at energy of scoring track;

N = number of source particles; and

T = number of scoring source particle tracks.

The equivalent dose could also be calculated depending on the energy deposited within the target tissue based on the equation:

$$\dot{H} = \frac{EnergyDeposited}{mass} \cdot 18.5mCi \cdot \frac{1.602x10^{-13}\ J/MeV}{1} \cdot g \tag{3.10}$$

$$\text{where } g = \frac{4\pi}{\mu}\left(1 - e^{-\mu R}\right) \tag{3.11}$$

The average gamma dose rate can be expressed as:

$$\bar{n} = \frac{\sum_{i=1}^{N} n_i}{N}, \tag{3.12}$$

where $\bar{n}$ is the average dose rate at each distance, n_i is the dose rate, and N is the number of dose rate measured. The standard error equation is expressed as:

$$\sigma_{err} = \sqrt{\frac{\sum_{i=1}^{N} (n_i - n)^2}{N(N-1)}} \tag{3.13}$$

The two main photon interactions considered during simulation were photoelectric effect and Compton scattering because the energy of emitted photon particles from the cesium-137 source was 0.6617 MeV. Different versions of the Geant4 codes were used to simulate the experimental set-up and simulations presented in Table 3-2. The results obtained from the simulations of different versions of Geant4 were benchmarked against MCNP5 simulation code and data obtained in experiments. Gamma dose rate measured one foot away from the cesium source was very high and decreased with an increase in measured distance away from the cesium source. As expected, the gamma dose rate decreased as the distance increased from the lead shielding. The trend of graphs obtained in Figures 3-4 and

3-5 follow the gamma exponential attenuation law. The slight differences in simulation of GEANT4 versions and MCNP simulation was due to the different data libraries implemented in codes. Even though the GEANT4 versions had different physics models implemented for photon interactions, the simulations of GEANT4 versions presented good agreement with experimental data and MCNP5 simulation, as indicated in Figure 3-4 and 3-5. Statistical analysis of error propagation with both GEANT4 and MCNP5 simulation indicates good accuracy with dose rate measured close to the source as compared to a further distance away from the detector; this is due to particle angular dispersion as the particle traverses distance away from the source (Table 3-2). The percentage difference between experimental results in comparison to GEANT4 and MCNP5 is presented in Table 3-3, indicating marginal differences between experimental results and simulations.

To calculate the percentage difference is given as: Percentage difference (Pd %) = (1- (Simulated results/ experimental results)). For example, the percentage difference between experimental results and MCNP5 at a distance of one feet (1 ft) could be calculated as, $Pd\% = (1 - (27 / 27.667)) = 0.0241$.

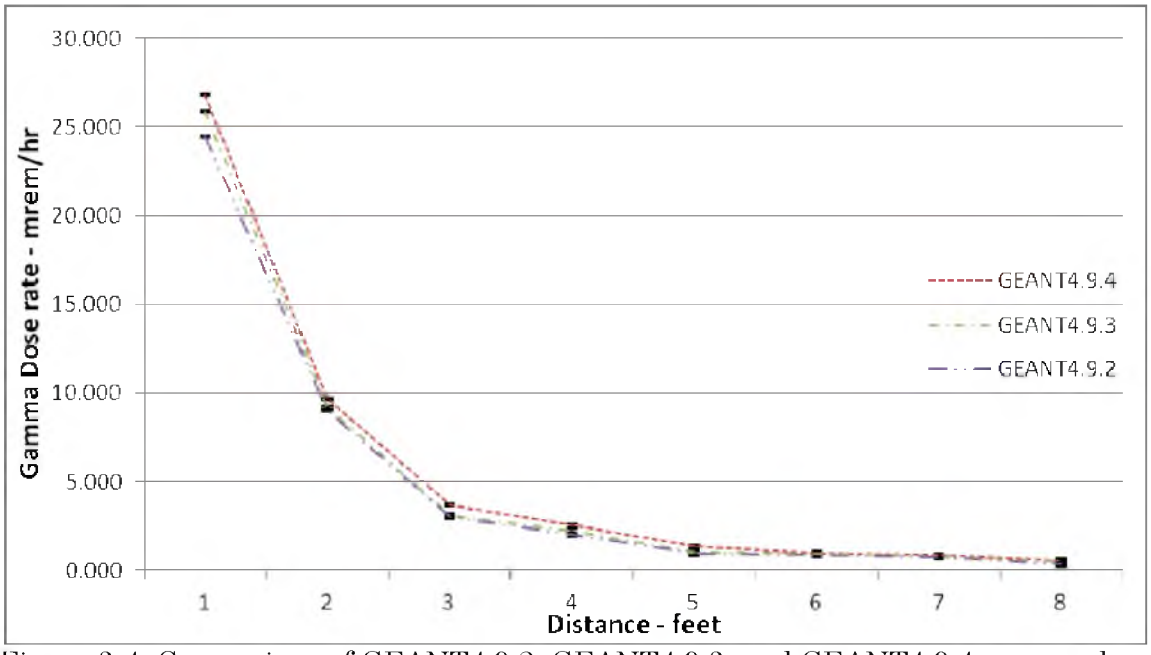

Figure 3-4. Comparison of GEANT4.9.2, GEANT4.9.3, and GEANT4.9.4 gamma dose rate as a function of distance from the source

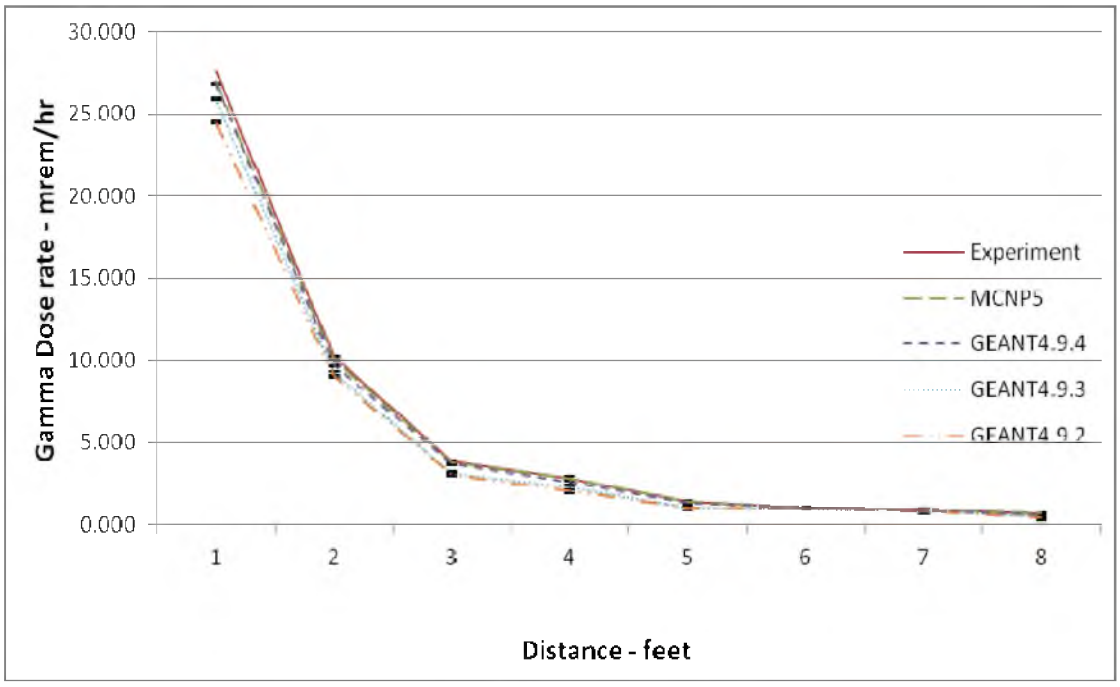

Figure 3-5. Comparison of gamma dose rate as a function of distance from the source between the measured and calculated values using GEANT4 and MCNP5

Table 3-2. GEANT4 and MCNP5 dose rate in comparison to experimental measurements

Distance – feet	Experiment – mrem/hr	MCNP5 – mrem/hr	GEANT4.9.4 – mrem/hr	GEANT4.9.3 mrem/hr	GEANT4.9.2 – mrem/hr
1	27.667 ± 0.026	27.000 ± 0.051	26.843 ± 0.053	25.913 ± 0.063	24.500 ± 0.057
2	10.170 ± 0.089	10.000 ± 0.083	9.680 ± 0.084	9.200 ± 0.089	9.010 ± 0.085
3	3.830 ± 0.041	3.760 ± 0.087	3.712 ± 0.083	3.110 ± 0.093	3.001 ± 0.091
4	2.830 ± 0.128	2.810± 0.092	2.560 ± 0.101	2.240 ± 0.121	2.030 ± 0.113
5	1.420 ± 0.013	1.400 ± 0.094	1.348 ± 0.120	1.018 ± 0.133	0.990 ± 0.127
6	1.020 ± 0.013	1.000 ± 0.101	0.999 ± 0.123	0.960 ± 0.142	0.910 ± 0.131
7	0.920 ± 0.014	0.900 ± 0.137	0.870 ± 0.130	0.830 ± 0.150	0.789 ± 0.138
8	0.670 ± 0.015	0.700 ±0.142	0.580 ± 0.148	0.498 ± 0.153	0.401 ± 0.142

Table 3-3. Percentage difference between experimental measurements with GEANT4 and MCNP5 simulations

Distance - feet	MCNP5 (%)	Geant4.9.4 (%)	Geant4.9.3 (%)	Geant4.9.2 (%)
1	0.0241	0.02978	0.0634	0.1145
2	0.0167	0.04818	0.0954	0.1141
3	0.0183	0.03081	0.1880	0.2164
4	0.0071	0.09541	0.2085	0.2827
5	0.0141	0.05070	0.2831	0.3028
6	0.0196	0.02098	0.0588	0.1078
7	0.0217	0.05435	0.0978	0.1424
8	0.0448	0.13433	0.2567	0.4015

CHAPTER 4

BASICS ON FAST NEUTRON PENCIL BEAM FACILITY

4.1. About Fast Neutrons

In 1932, James Chadwick discovered the neutron particle. He performed series of experiments at the University of Cambridge showing that the gamma ray hypothesis was illogical and concluded that the new radiation consisted of uncharged particles of approximately the mass of the proton. James Chadwick called these uncharged particles neutrons [27]. James Chadwick's discovery proved that there is a neutral particle in the nucleus and that there are no free electrons in the nucleus, as postulated by Ernest Rutherford. The neutron is a subatomic hadron particle, which has no electric charge, and therefore does not cause direct ionization of matter. Neutrons are found within the atomic nucleus as they bind with protons via the nuclear force. Neutrons do not interact with electrons but interact with the nucleus. The number of neutrons in a nucleus determines the isotope of an element [28]. Free neutrons decay with a half-life of about 10.3 min [28]. There are two types of neutron interactions: Compound Interactions – the neutron as a projectile interacts with a target nucleus, forming a compound nucleus (half-life ~10^{-16} sec) and decays in different channels and has no memory of its formation; and Direct Interactions – an incoming neutron interacts with the nucleus but does not disturb other nucleons within the target nucleus; thus, the time for a neutron as a projectile particle to traverse a target nucleus is ~ 10^{-22} sec [27, 28].

Fast neutrons are free neutrons with kinetic energy levels higher than 50 keV, and have speeds of 14,000 km/s or higher [29]. They are named fast neutrons to distinguish them from lower-energy thermal neutrons, and higher-energy neutrons produced in cosmic showers and accelerators [29]. Fast neutrons can undergo the following neutron interaction depending on the material's affinity to fast neutrons (Figure 4-1): fission, elastic scattering, radiative capture, and inelastic scattering. The type of neutron interactions depends on the neutron energy and the material's affinity toward neutrons. Neutrons are classified based solely on their energy (Figure 4-1).

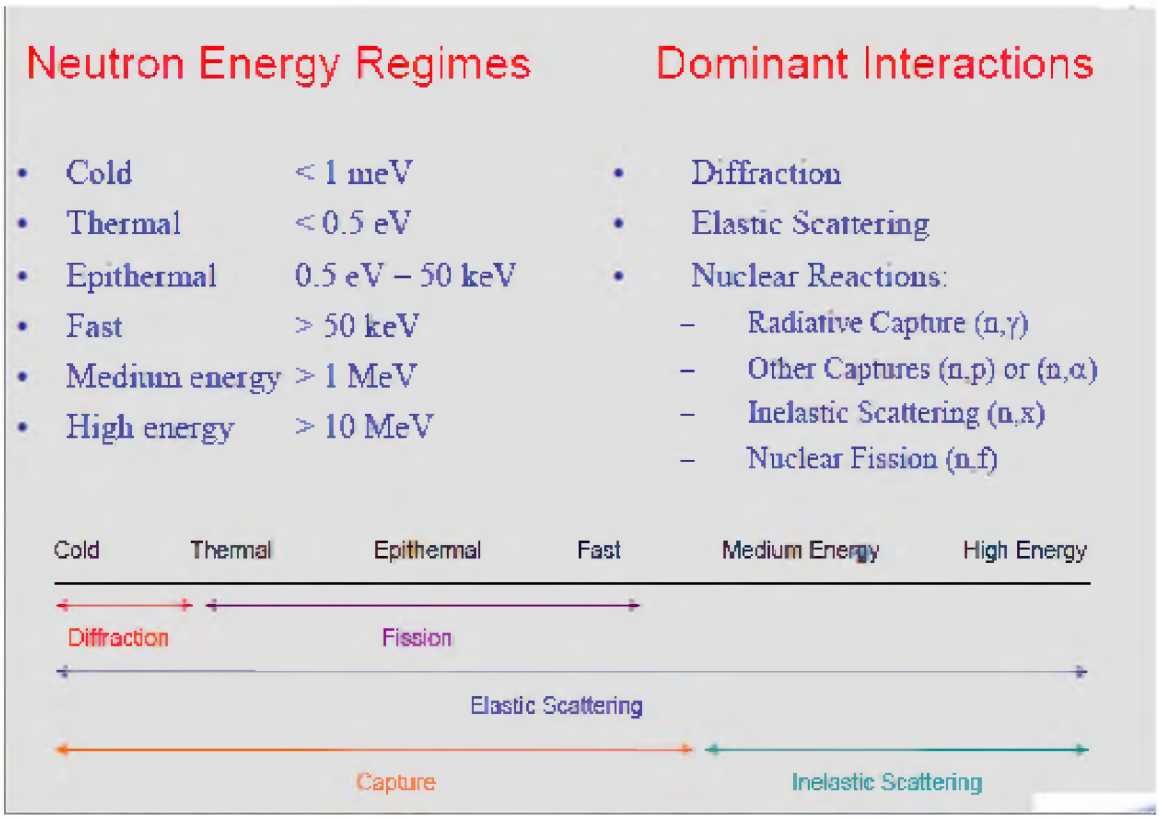

Figure 4-1. Classification of neutron energies and interactions. Adapted from [28]

Fast neutrons can be produced, found, or generated from a wide variety of different neutron sources: from neutron accelerators, operating research reactors, spallation neutron source, radioisotopes which decay with alpha particles packed in a low-Z elemental matrix (e.g. Am-Be) [27], and isotopes that produce neutrons spontaneously (e.g. $_{98}Cf^{252}$) [27]. The main sources of fast neutron production are by nuclear fission, which produces fast neutrons with a mean energy of 2 MeV (200 TJ/kg, i.e. 20,000 km/s) [27, 29]; and by particle accelerator with the emission of a proton particle to hit a tungsten, target producing fast neutrons with energies of about 14.1 MeV (1400 TJ/kg, i.e. 52,000 km/s, 17.3% of the speed of light) [27, 29] and can easily fission uranium-238 and other nonfissile actinides.

4.2. Fast Neutron Facilities

Fast neutron facilities can be classified based upon the neutron flux produced, neutron energy, size and type of source, costs, government regulations, and application. Fast neutron sources can be used for a wide diverse range of applications. Most common applications of these neutron facilities are in the areas of engineering, medicine, nuclear weapons, petroleum exploration, biology, chemistry, nuclear power, applied nuclear physics, and other industries (Table 4-1). Fast neutron facilities are located all around the world; to mention a few: The Institute of Neutron Science Laboratory – Institute for Solid State Physics (University of Tokyo), Oak Ridge Neutron Facilities (SNS/HFIR), Los Alamos Neutron Science Centre (LANSCE), Bhabha Atomic Research Centre (Mumbai India), FRM-II Lab (Munich Germany), Bragg Institute (ANSTO Australia), Braunschweig Accelerator Facility, and many other facilities.

Table 4-1. Applications of fast neutron facilities [30]

General Area	Specific Applications
Geophysical Science	Mine mineral mapping and analysis Petroleum exploration Quarry mineral mapping and analysis Uranium exploration Nuclear well logging
Industrial	Cement processing Coal quality analysis Wall thickness analysis Metal fracture detection
Security	Explosives detections and identification Chemical weapon agent detection and identification Special nuclear materials detection and identification Land mine detection Unexploded ordnance inspection Fast neutron radiography
Medicinal Sciences	Nuclear medicine Fast neutron therapy
Nuclear Engineering	Fast breeder reactors Nuclear reactor analysis Fast neutron reference source for instrumentation Calibration source for neutrino observatory instrumentation Studies of radiation damage to electronic component Spallation neutron source
Environment	Nuclear waste assay Waste assay for resource conservation and recovery Carbon sequestration quantification in soil

4.2.1. Application of Fast Neutron Facilities

Fast neutron facilities are used in a myriad of applications, including neutron therapy for the irradiation of cancer cells and tumors, neutron detection for the detection of nuclear materials and neutron radiography, and industrial applications for nuclear well logging, and detection of cracks in concrete and metals. Applications of fast neutron facilities include, but are not limited to, the following:

- *Fast neutron irradiation facility*: there is vast number of fast neutron irradiation facilities in the world used for a wide range of research. Most institutes with research reactors have a fast neutron irradiation facility used for a wide range of research. For example, The University of Utah Triga reactor has a Fast Neutron Irradiation Facility (FNIF), mainly used for research in the field of Neutron Activation Analysis (NAA). The University of Massachusetts Lowell also has a fast neutron irradiation facility used for fast neutron irradiation of samples for elemental analysis. Also, the fast neutron facility at the ISIS Spallation neutron source is used for irradiation tests of electronic components and the beam line has a neutron energy range above 10 MeV [31].
- *Fast neutron detection facility*: There are a couple of institutions that deal with the detection of fast neutrons, which is a technique that could be used for detection of nuclear materials. Most neutron detection techniques rely on observing a neutron-induced nuclear reaction, but the captured cross-sections for fast neutron-induced reactions tend to be small and hard to detect compared to neutrons at lower energies. Two approaches are normally used by detection facilities, namely, Thermalized and Capture (fast neutrons are thermalized in order to detect) and Elastic scatter from protons at high energy (observed recoils for TOF techniques) [32].
- *Linear accelerator facilities*: electron or proton beams produced in linear accelerators can be used to efficiently produce fast neutrons by photonuclear reactions. This process involves the acceleration of collimated electron or

proton beams at high velocity to hit a beryllium (Be) or tungsten target to produce fast neutrons at high energies of about 14 MeV. Neutron accelerator facilities have a broad range of research applications in the areas of industrial, medical dosimetry, homeland security, radiation hardness testing, and radiation effects on materials. An example of such a facility is the NIST accelerator facility used for a number of research such as [33]: (a) broad-energy range calibration of charged-particle spectrometers used in space-flight applications, (b) calibration of a beta spectrometer employed in a fundamental nuclear physics measurement of the neutron lifetime, (c) solar cell performance validation studies at several different electron energies and fluencies, and (d) development of a variable-speed radiation scanning system.

- *Fast neutron therapy facility*: fast neutron facilities have been applied in the medical sciences for the treatment of cancer, and plasma and beam physics research for years. Clinical institutions began supporting clinical fast neutron clinical studies in the world beginning in the early 1970s using physics-based cyclotrons and linear accelerators at a number of facilities around the world. The clinical treatment of cancers and tumors using fast neutrons is being researched and continue to be modified due to advancement in technology by accredited research institutions around the world. Some hospital-based neutron facilities currently being operated in the United States are the University of Washington in Seattle, University of California in Los Angeles, the University of Texas System Cancer Center in Houston, and many other institutions.

4.2.2. Application of Fast Neutron Pencil Beam Facilities

Fast Neutron Pencil Beam (FNPB) facilities around the world (Table 4-2) are applied in a couple of fields; most common amongst the applications are for fast neutron therapy for the cure of cancer and tumors and also for studying the radiation effects on electronic component's displacement damage and ionization. A fast neutron pencil beam is produced using neutron reflective materials to collimate fast neutrons to produce a thin fast neutron beam. The diameter of the fast neutron beam is mostly between 2 cm to 3 cm. A variety of fast neutron facilities have been used to study the response of electronics to displacement damage and ionization in electronic components. The test model is important for the study of radiation damage and hardness of electronic components associated with aircraft and space exploration. A new test methodology using FNPB produced from a 6.5 MeV tandem accelerator alongside high fidelity computational models has been used to study this effect [36]. Fast neutron pencil beams are mostly produced using neutron generators for Fast Neutron Therapy (FNT), such as cyclotron accelerators and reactors. The FNPB uses the effects of high-LET (linear energy transfer) radiation (secondary recoil protons and alpha particles, respectively) to attack/irradiate radio-resistant tumors and cancers, considering hazardous effects for irradiated healthy tissue. In research conducted by E. Bourhis-Martin at the University of Essen, Germany, the fast neutron pencil beam for therapy is produced by a nuclear reaction of 14.3 MeV deuterons emitted on a thick beryllium target (diameter of 30 mm and thickness of 5 mm) according to the nuclear reaction: $^{9}Be+^{2}H \rightarrow ^{10}B+n+Q$, with $Q = 4.36$ MeV, and $^{9}Be+^{2}H \rightarrow ^{9}Be+n+p+Q$ with $Q = 2.2$ MeV.

Table 4-2. Fast Neutron Therapy (FNT) facilities around the world [37]

Country, Location References	Source Reaction	Approx. mean n-Energy [MeV]	50-%-depth [cm]	Beam Direction	Collimator	First Treatment	Patient number	Status	Main indications	Treatment planning system
US Batavia/IL Fermilab [4, 5]	LINAC p(66)+Be	25	16	horizontal	Inserts	1976	3300+	active	H&N	Inhouse, modified MINUIT
US Seattle/WA Univ. of Washington CNTS [6-10]	Cyclotron d(50.5)+Be	20	14	Isocentric horizontal	MLC* Inserts	1984	2800+	active	Salivary gland, sarcomas	Prism, now modified Pinnacle
US Detroit/MI Harper Hospital/WSU [11-13]	Cyclotron d(48.5)+Be	20	13	Isocentric, IMRT	MLC	1990	2140	active (refurbishment)	Lung cancer, late prostate	VRSplan (modified GRATIS)
ZA Somerset West [14-18]	Cyclotron p(66)+Be	25	16	Isocentric	Variable jaws + multiblade trimmer	1988	1635+	active	salivary gland, H&N, soft tissue, sarcoma, osteosarcoma, breast, malignant melanoma	VIRTUOS (from DKFZ**)
RU Tomsk Polytechnic University [19]	Cyclotron d(13.5)+Be	6.3	6	Horizontal	Inserts	1984	1500+	active	H&N, salivary gland, breast	MCNP
RU Snezhinsk VNIITF [20-22]	D-T-Generator	10.5	8	Horizontal	Inserts	1999	990+	Standby	Nose, throat, thyroid	SERA/ PRIZM
DE Garching/Munich FRM-I/FRM-II [23, 24]	Fission of uranium	1.9	5.0	Horizontal	Inserts/MLC	1985/2007	820	active	Recurrent breast cancer, malignant melanoma	SERA, MCNPX

The energy spectrum of fast neutrons has a mean and maximum energy of 5.5 and 18 MeV with a fast neutron flux within a range of ~10^6 to 10^8 n/cm^{2}s, respectively, for patient treatments [35]. Other neutron sources for FNT have been cyclotrons, D-T neutron generators, and the accelerator at the FERMI-Lab. Earlier, a fast reactor (BR-10 at Obninsk, Russia) and ^{252}Cf have also been used with average neutron energies from 2 MeV (fission neutrons) to about 25 MeV for cyclotrons [36].

According to research conducted by F. M. Wagner [37], FNT has been administered to over 30,000 patients world-wide. From formerly 40 facilities around the world, now only eight are operational. This is due to the technical and economic conditions and also the side effects associated with damage of healthy tissue and insufficient proof of clinical results in the early years. FNT is not recommended for all cancers, but rather for predominantly adeno-cystic carcinoma (ACC) of salivary glands, as this type of tumor is rare. FNT is also administered in palliative situations where the tumor/cancer is recurrent or irresectable and for very extended tumors [37]. One such facility is the Detroit FNT facility located at Harper Hospital, Gershenson Radiation Oncology Center, Karmanos Cancer Institute, and Wayne State University (KCC/WSU) in Detroit. The FNT is produced by a gantry-mounted superconducting cyclotron, with a 120-leaf collimator that delivers more radiation dose to the tumor [37]. Overall, FNT has its niche in routine medical treatment of selected malign tumors and their recurrences [37].

CHAPTER 5

PRELIMINARY DESIGN OF THE FAST NEUTRON PENCIL BEAM FACILITY AT THE UNIVERSITY OF UTAH TRIGA (UUTR)

5.1. General Characteristics of the UUTR

The University of Utah TRIGA (Training, Research, Isotope, General Atomics) is a pool-type research reactor that operates at 100 kilowatt thermal power. The core of the reactor is a hexagonal lattice of an aluminum grid structure submerged at the bottom of a deep tank filled with purified water, [38] as shown in Figure 5-1. The TRIGA reactor is mostly used by educational and research institutions for research, teaching, and training. The UUTR uses light water as coolant and the cooling process is by natural convection circulated through a mixed-resin bed ion-exchange system to maintain high purity of the water. The UUTR also uses light water as a neutron moderator, and radiation shielding, in addition to representing a heat sink [38]. The UUTR reactor core has a heterogeneous assembly of standard fuel elements made of zirconium hydride mixed within the uranium matrix, and deuterium oxide (D_2O, "heavy water") and graphite element as reflective material. Both the heavy water and graphite elements surround the core and moderate leakage neutrons from the reactor core and provide an isotropic thermal neutron environment suited for neutron activation via (n, γ) reaction. UUTR has

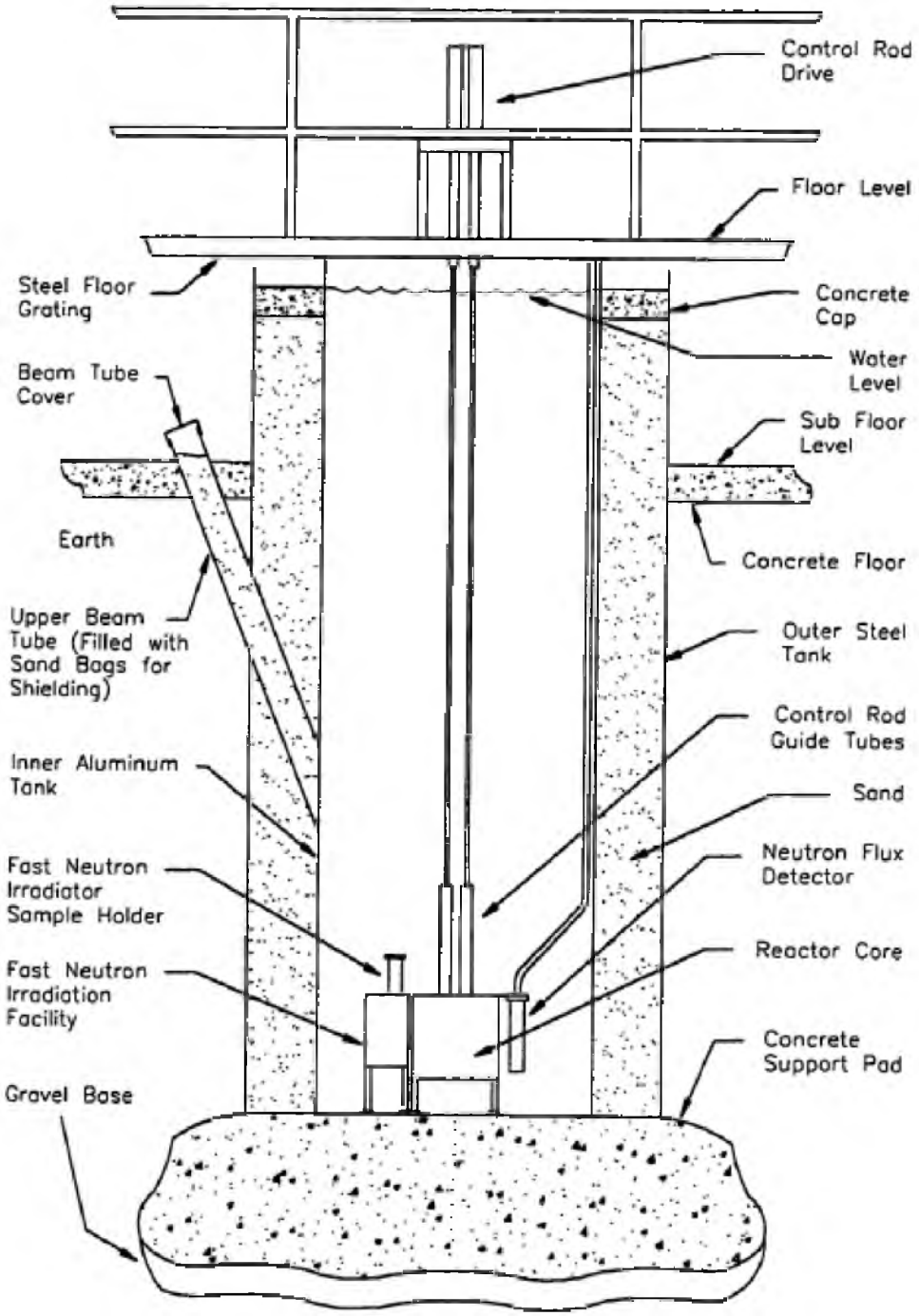

Figure 5-1. Cross-section diagram of the UUTR 100-kWt TRIGA research reactor. Adapted from [41]

three neutron-absorbing control rods (CR) containing boron carbide (B_4C). The UUTR has four neutron irradiation ports: a thermal neutron irradiation (IT) port, fast neutron irradiation facility (FNIF), central neutron irradiation (CI) port, and pneumatic neutron irradiation port.

5.2. Conceptual Design of the Fast Neutron Pencil Beam Facility at the UUTR

The goal of this research is to develop a preliminary study and a model of a fast neutron pencil beam facility at the UUTR for various research applications. The UUTR has only one fast neutron irradiation port (FNIF). This port is capable of providing fast neutrons necessary for the fast neutron pencil beam facility. The FNIF is composed of a heavy lead manufactured box, with a sample holder lid made of aluminum [40]. Figure 5-2 shows a cross-sectional diagram of the FNIF showing its vertical orientation relative to the reactor core [41]. The FNIF was purposely designed to provide fast neutron irradiation with a quasi-fission energy spectrum and low photon exposure, due to the heavy lead material shielding. Fuel elements are adjacent to the FNIF in providing a planar fission neutron source with fast neutron component being dominant. The FNIF is placed very close to the reactor core to minimize the moderation of fast neutrons by the pool water (Figure 5-3). The concept design of the FNPB facility is to optimize the design to provide enough space for fast neutrons from the FNIF to be collimated through a thin tube of space. The FNPB is designed as box with an air space that will be placed on top of the FNIF to enable fast neutrons to flow from the air gap. The FNPB consists of three parts: an aluminum casing, the FNPB box, and the sample holder, as shown in Figure 5-4.

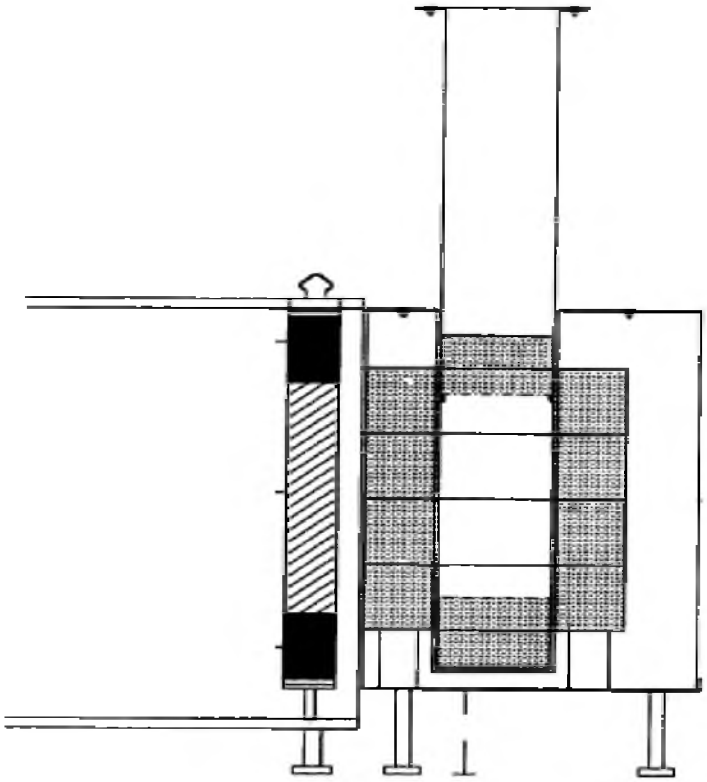

Figure 5-2. Vertical cross-section diagram of FNIF. Adapted from [41]

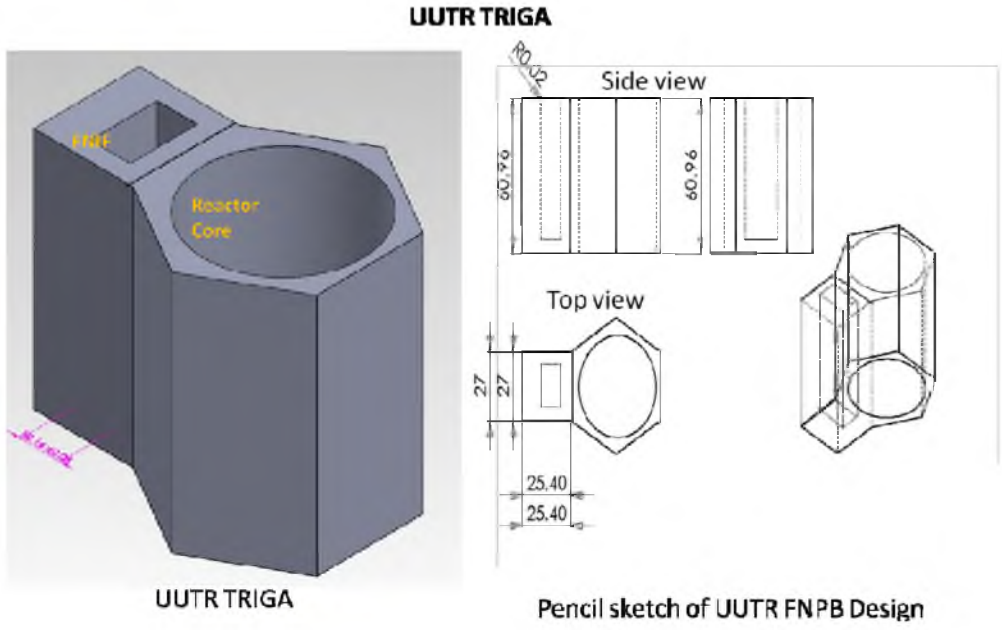

Figure 5-3. Outline of UUTR reactor and FNIF

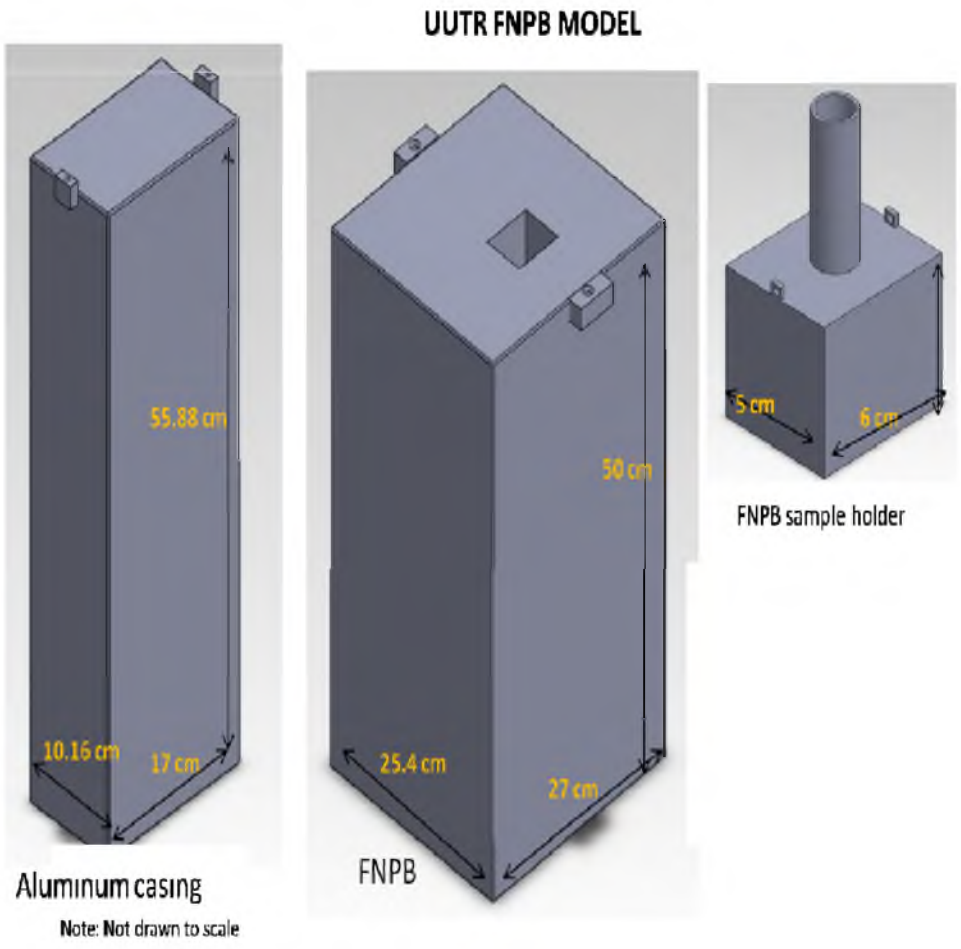

Figure 5-4. UUTR FNPB model

The aluminum casing is hollow with a one inch lead layer at the bottom to enable it to sink beneath into the FNIF to block the air gap and prevent water from entering, since the water will moderate the fast neutrons to thermal neutrons. The FNPB box sits on top of the aluminum casing and the FNIF. The sample holder fits inside the top of the FNPB box. Material composition normally considered for collimation of fast neutrons should be a neutron reflector. When a neutron interacts

with matter, it is either absorbed or scattered. The materials should have the tendency to scatter fast neutrons. To select the materials best suitable for neutron scattering, the material cross-sections related to elastic scattering, absorption, and secondary particle production are closely examined. The materials selected have high affinity for elastic and inelastic scattering for fast neutrons. The resonance peaks occur when there is intermediate formation of compound nucleus. Materials considered for modeling the UUTR FNPB are: aluminum, boron10, paraffin, lead, and graphite.

Aluminum: based on cross-sections, the aluminum does not have high absorption nor a scattering cross-section for fast neutrons (Figure 5-5). Aluminum is a low-Z element with density of 2.7 g/cm^3. Pure aluminum has good material properties with water due to its ability to resist corrosion; therefore, aluminum thickness of 0.5 cm is used to model the aluminum

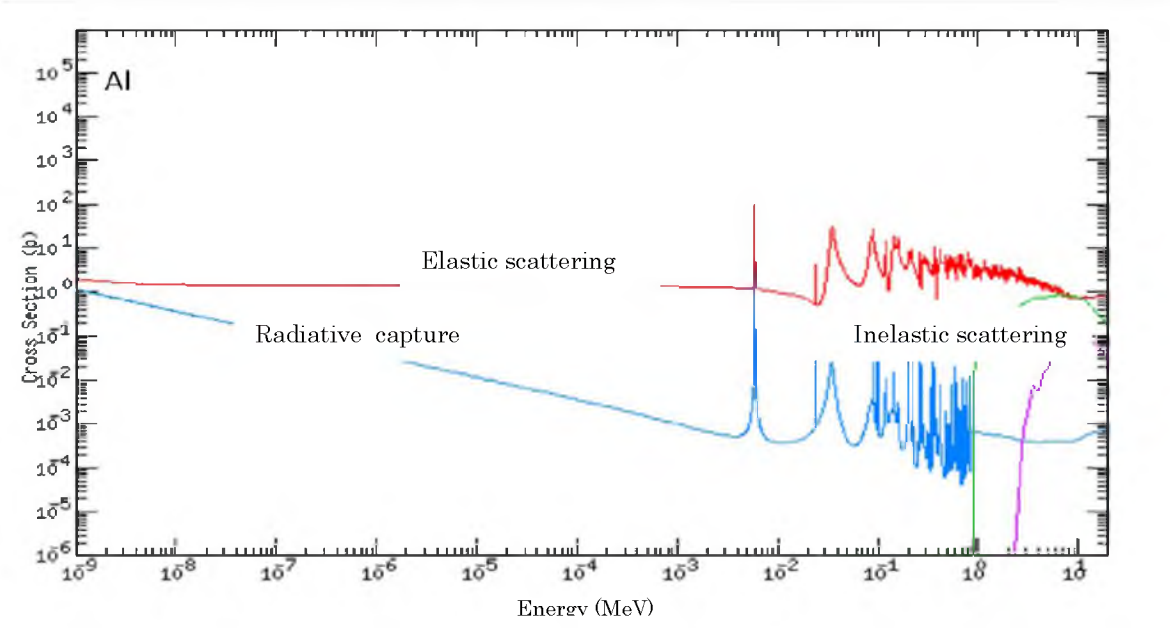

Figure 5-5. Cross-section plots of aluminum-Al. Adapted from [42]

casing to cover the FNIF air gap, and also to cover both the out layer of the FNPB box and the sample holder box.

- *Boron-10*: boron (B-10) has density of 2.08 g/cm^3, and has a high (n, α) reaction and absorption cross-section for thermal neutrons in a ($n, \square$) reaction, but does not absorb fast neutrons, based on cross-section plots in Figure 5-6. Boron (B-10) with thickness of 0.5 cm is used to line the inner surface of the FNPB box to absorb thermalized fast neutrons within the pool water that propagates through the aluminum covering. A thin layer of B-10, of about 0.2 cm, is also placed at the window tip of the collimation tube to absorb moderated neutrons to reduce a thermal neutron flux of pencil beam entering the sample holder.
- *Graphite*: graphite is a good material used in most rectors to reflect leaked neutrons back into the reactor core, and has a density of 1.7 g/cm^3. Figure 5-7 indicates that the graphite is a good moderating material and has good propensity to scatter neutrons. Graphite is one of the materials considered for the collimation of fast neutron pencil beam based on its nuclear properties.
- *Lead*: lead is a very good shielding material for attenuating gamma rays, and has poor affinity for neutrons, based on cross-section plots in Figure 5-8. Lead is a very dense material with density of 11.354 g/cm^3. An inch of lead is modeled within the bottom of the aluminum casing to enable it to sink into the reactor pool and FNIF. The inner layer of the sample holder is made of 0.5 cm of lead to attenuate gammas emitted from the top of the core to prevent radiation damage to the sample, in case of a biological sample.

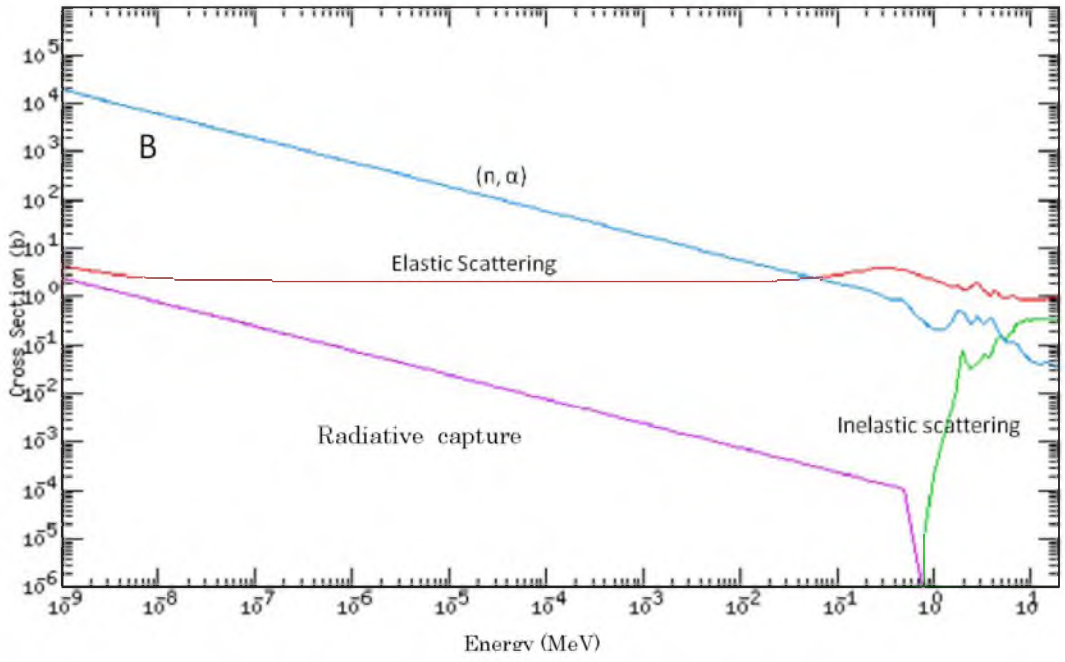

Figure 5-6. Cross-section plots of boron-(B-10). Adapted from [42]

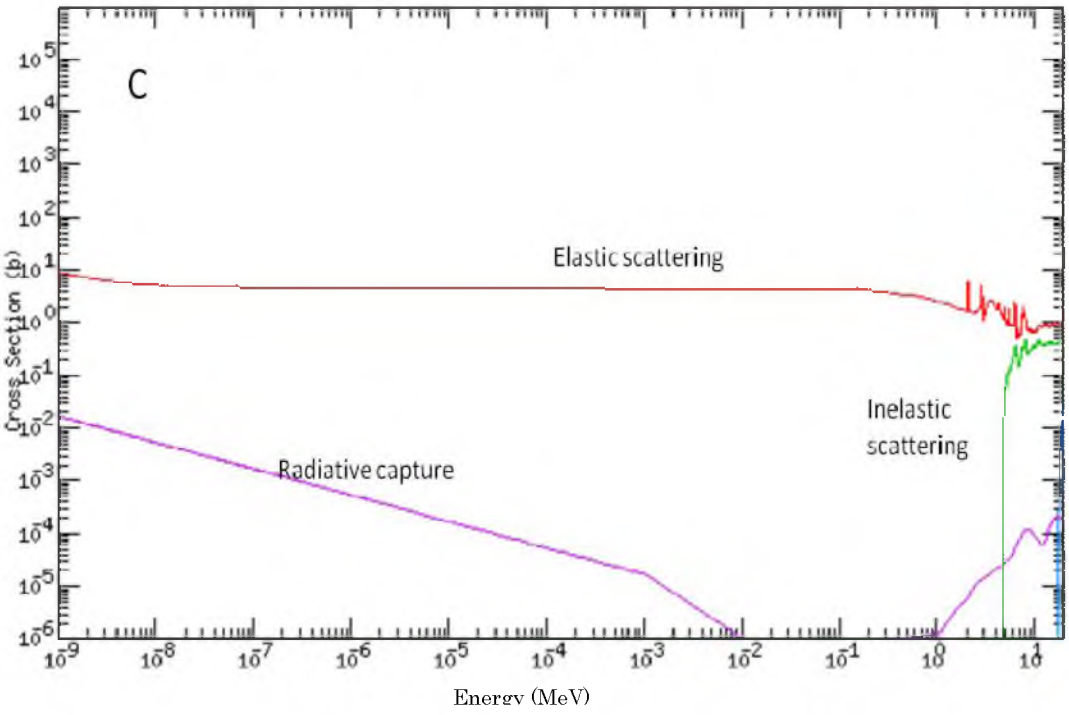

Figure 5-7. Cross-section plots of graphite-C. Adapted from [42]

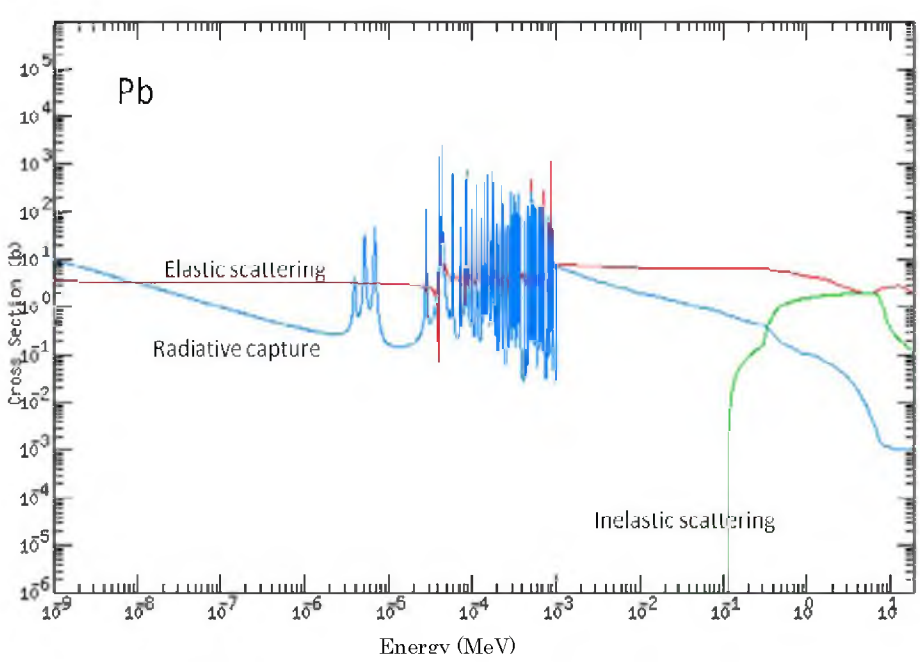

Figure 5-8. Cross-section plots of lead-Pb. Adapted from [42]

- *Paraffin*: paraffin is composed of 85.4% carbon and 14.6% hydrogen; its chemical compound is $C_{20}H_{42}$ to $C_{40}H_{82}$. Hydrogen has no excited states, therefore, it has no formation of a compound nucleus or resonances. Hydrogen has good affinity to absorb thermal neutrons and has good scattering ability for fast neutrons, as shown in Figure 5-9. Hydrogen mixed with carbon to form paraffin provides good scattering of fast neutrons, and could be used either as reflective material or for neutron shielding.

The following is the description of the preliminary design of the fast neutron pencil beam facility at the UUTR:

- *Aluminum casing*: The aluminum casing is made of pure aluminum with an inch thickness of lead molded to the bottom of the casing to enable it to sink

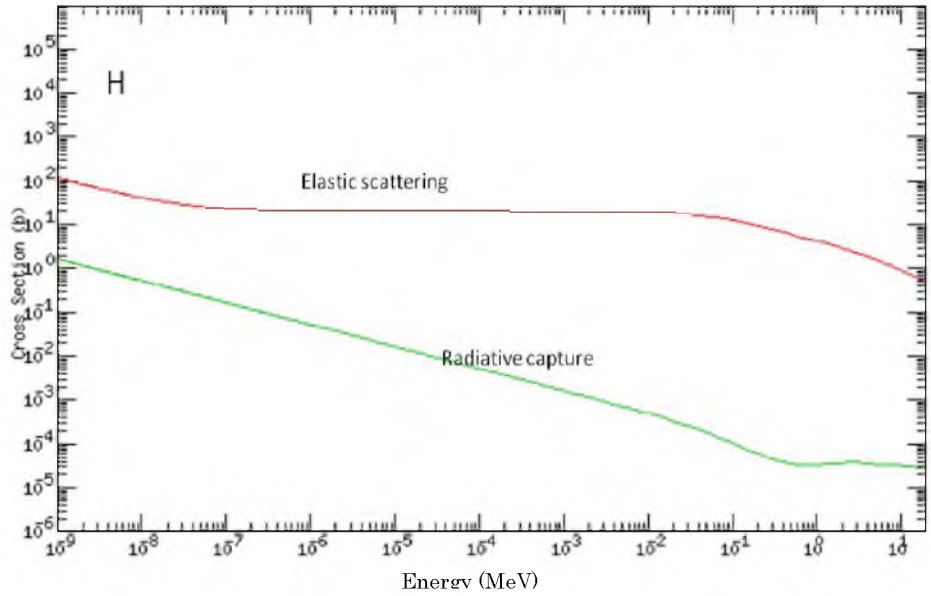

Figure 5-9. Cross-section plots of Hydrogen-H. Adapted from [42]

deep into the reactor pool to cover the FNIF air gap and thus prevent water from entering. The aluminum casing is about 0.5 cm thick, has a height of 55.88 cm, a length of 10.16 cm, and a width of 17 cm, and has two small holding handles at the side for easy removal or placement within the pool, as shown in Figure 5-10.

- *FNPB sample holder*: The FNPB sampler holder is designed to house any sample to be irradiated via the fast neutron pencil beam. The sampler holder is hollow, coated with pure aluminum, with a 0.5 cm inner layer of lead to reduce gamma flux within sample holder. The sample holder is a box of 6 cm height, 6 cm width, 5 cm in length, and has a polyethylene tube at the top for easy placement and removal of samples. The sample holder fits on top of the FNPB box, and has two small handles for easy placement and removal, as shown in Figure 5-10.

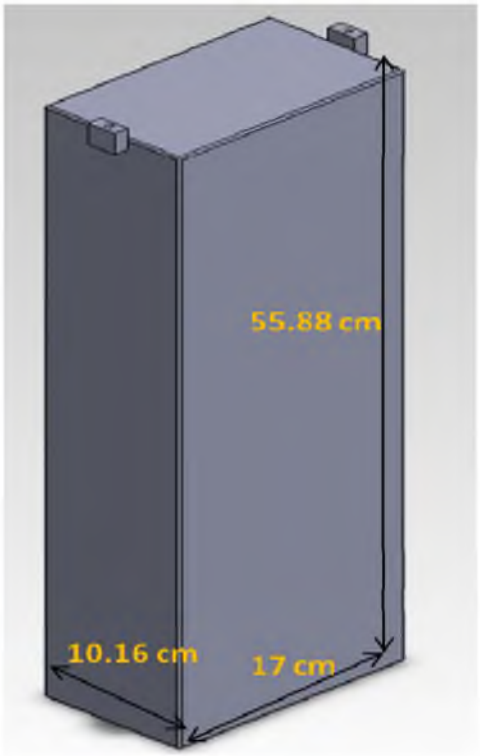

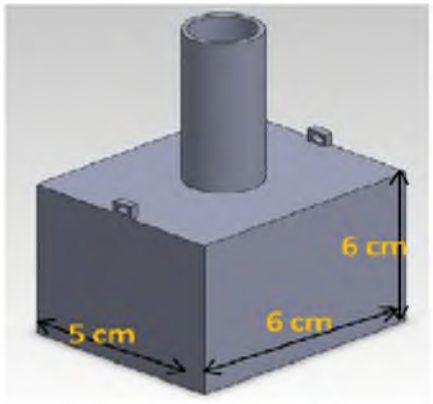

Figure 5-10. Model of aluminum casing and FNPB sample holder

- *FNPB box:* The FNPB is modeled as a box with 50 cm height, 27 cm width, and 25.4 cm length. It has a 0.5 cm thick aluminum casing on the outside casing, a 0.5 cm thick boron-10 layer in the inside, and paraffin within the box as collimation material. The inner space of the collimation path is shaped like a tip of a pencil, with inner length of 16 cm, width of 10.16 cm, and height of 43 cm. The tip of the pencil beam is 5 cm long and shaped as a tube with radius of 1.5 cm to collimate fast neutrons, as shown in the cross-section diagram in Figure 5-11. The square space on top of the FNPB is the sample holder space. The FNPB sits on top of the aluminum casing and the FNIF.

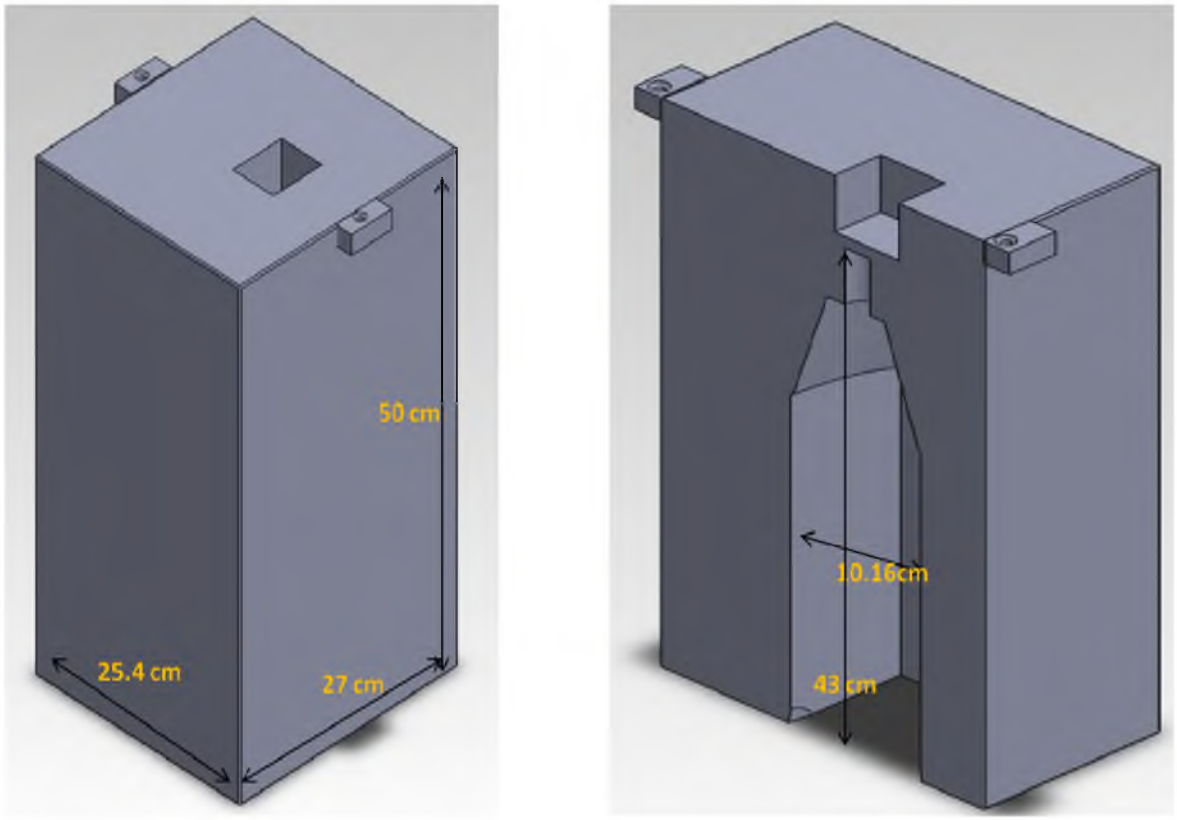

Figure 5-11. Cross-section model of UUTR FNPB

5.3. MCNP5 Model of the Fast Neutron Pencil Beam Facility at the UUTR

The UUTR FNPB was modeled using the MCNP5 following the design as described. Figures 5-12 and 5-13 show the 3-D and the cross-sectional diagram of the UUTR FNPB design, respectively. The MCNP5 FNPB facility model includes the exact model of the UUTR reactor core, with all fuel specifications, moderator material, reflector material, and control rods. The data libraries used for simulation are ENDF-VII data libraries at temperature of 300 K. The source of fast neutron was generated from fission simulation of reactor fuel within the reactor core.

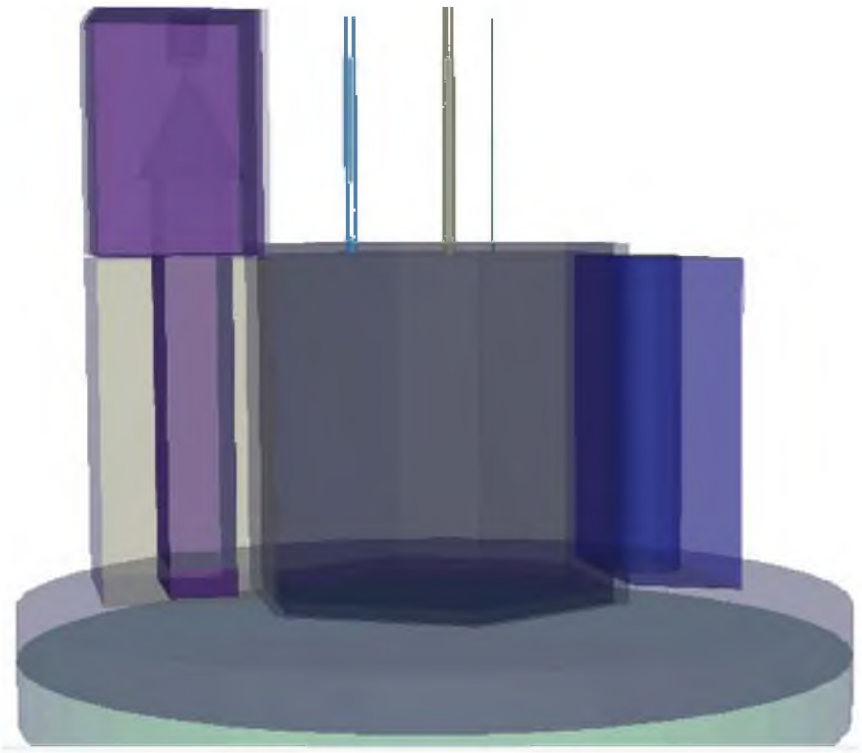

Figure 5-12. MCNP5 3-D model of UUTR FNPB

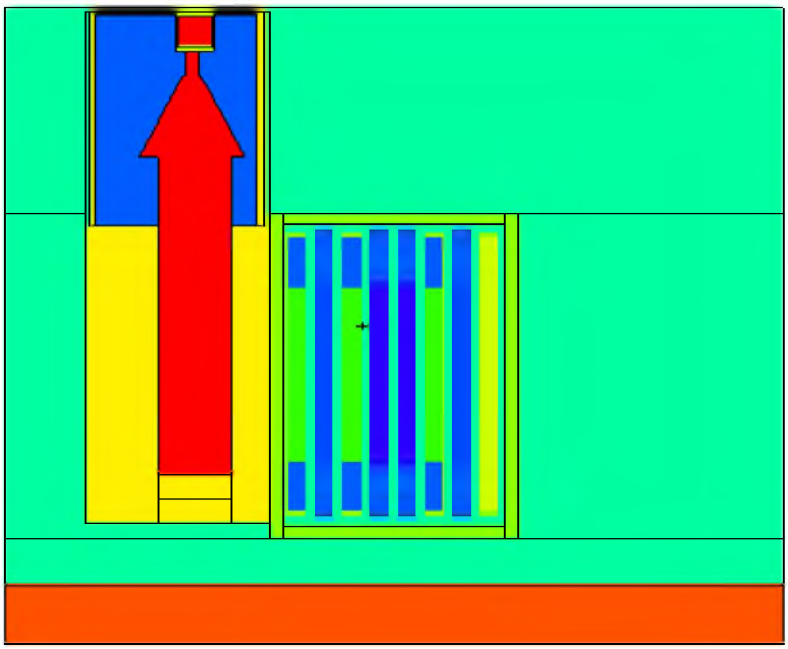

Figure 5-13. MCNP5 cross-section view of UUTR FNPB

5.4. GEANT4 Model of the Fast Neutron Pencil Beam Facility at the UUTR

The UUTR FNPB was modeled using GEANT4.9.4 simulation code (Appendix F). The GEANT4.9.4 classes implemented are the following: *G4DectorConstruction* class was implemented for the construction of the UUTR FNPB geometry, and material specifications; *G4PhysicsList* was used to specify the physics interaction of the neutron interactions with matter; the neutron source was implemented using the *G4GeneralParticleSource* class, and modeled as a square planar source with a Maxwellian energy spectrum placed at the side of FNIF, as shown in Figure 5-14; and *G4SteppingAction* was used to get desired information needed from the simulation, such as change in energy and direction of the particle printed as a text document. Neutron data libraries implemented in GEANT4.9.4 used for the simulation are some imported ENDF-VII MCNP data libraries and EPDL97 data libraries.

5.5. Comparison of GEANT4 and MCNP5 in Modeling Neutron Interactions

Despite the fact that both GEANT4 and MCNP5 codes are based on Monte Carlo methods, they are different in various aspects, as described in Chapter 2. GEANT4 and MCNP5 (Appendix C and D) simulation of neutron interactions with selected materials were assessed based on a simple model represented as a rectangular cubic box with the following dimensions: length 4 cm, height 4 cm, and width 2 cm.

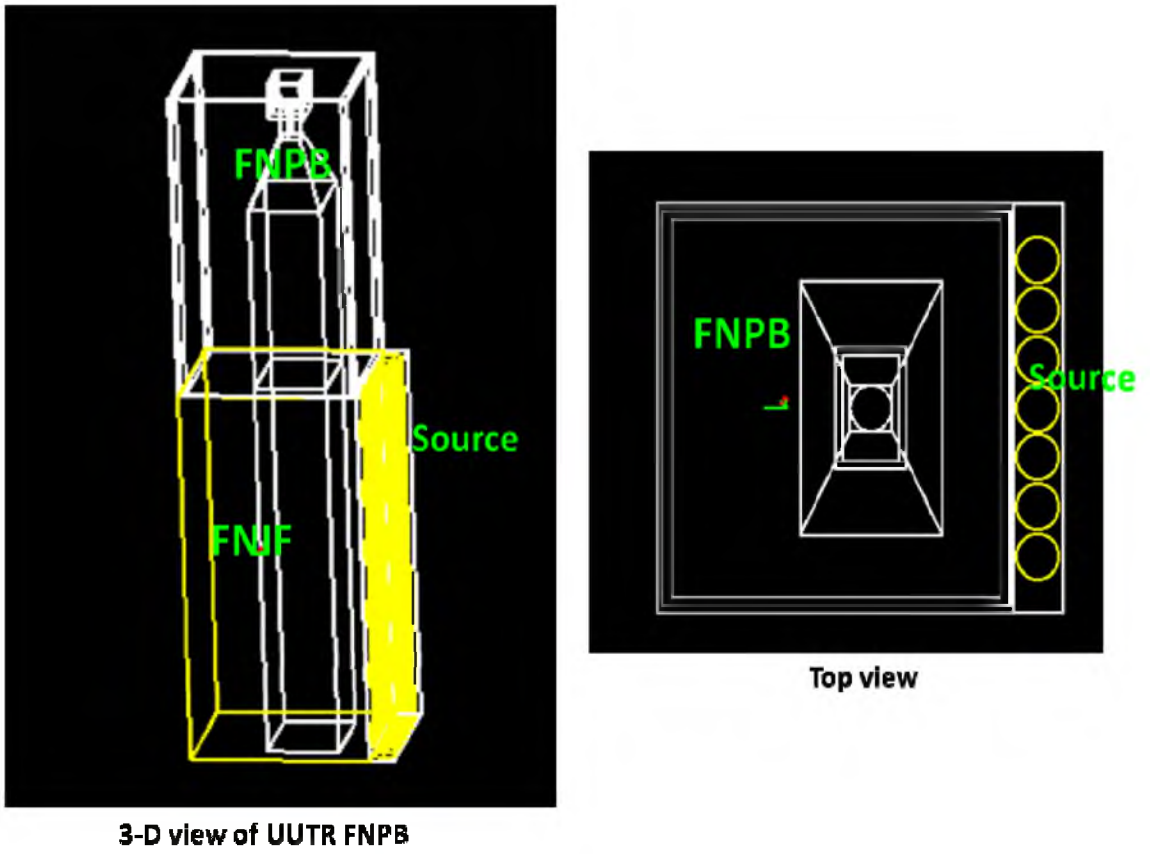

Figure 5-14. GEANT4 model of UUTR FNPB

The neutron source was modeled as a disc surface source placed at the centre of one side of the cube; the neutron source was assumed to be mono-energetic and two different energies were considered: 0.025 eV and 2 MeV. Materials are selected based on the basic materials as used in the preliminary design of FNPB at the UUTR, i.e. lead, boron, and paraffin. Figures 5-15 to 5-17 show the GEANT4 and MCNP5 resulting neutron interactions at different energies with boron-10, lead, and paraffin. Table 5-1 summarizes a comparison of GEANT4 and MCNP5 results as follows: for 10,000,000 neutron particles, the effect of interactions with selected materials at two different neutron energies of 0.025 eV and 2 MeV, neutron and

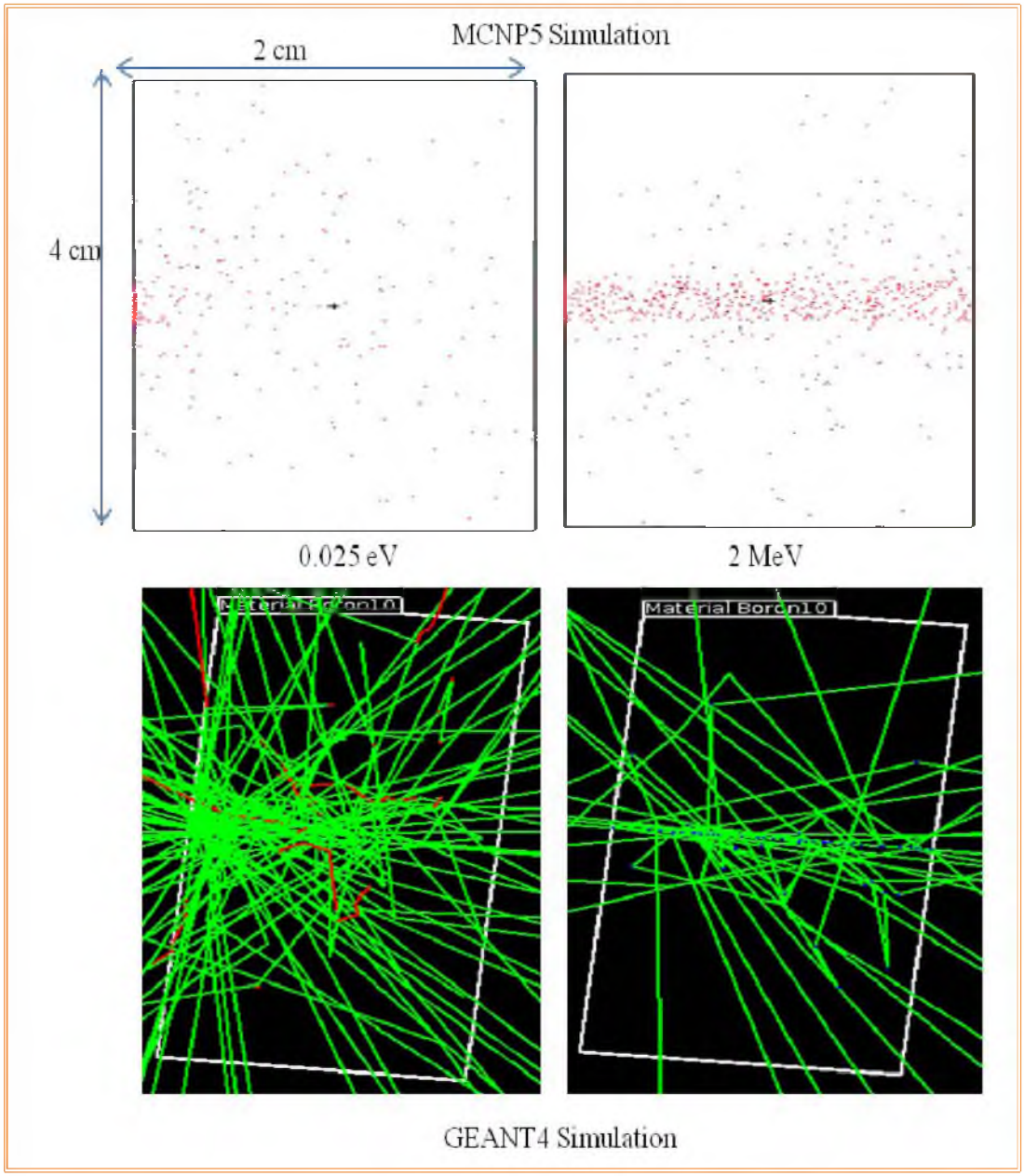

Figure 5-15. GEANT4 and MCNP5 simulation of neutron interactions with boron-10

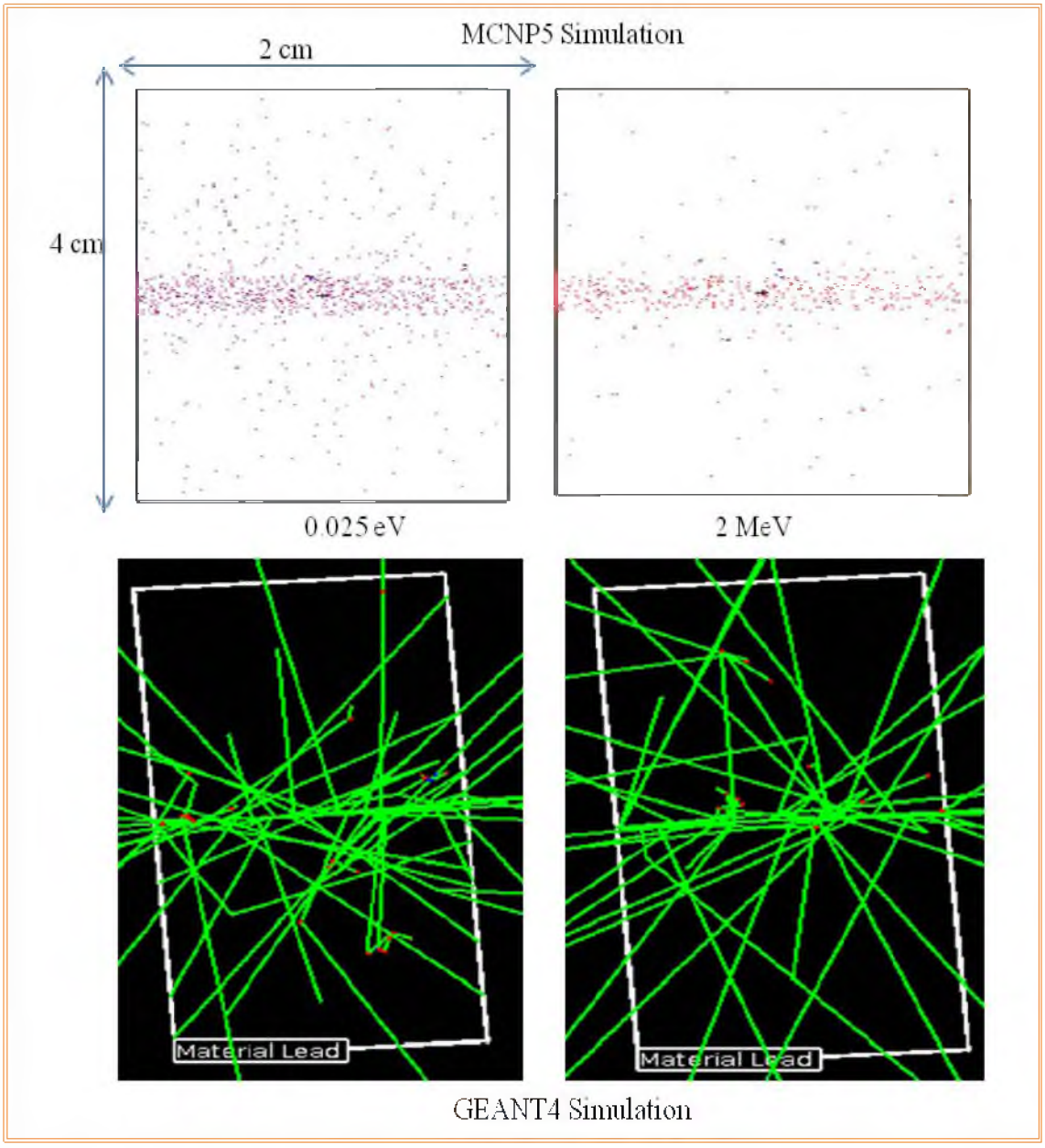

Figure 5-16. GEANT4 and MCNP5 simulation of neutron interactions with lead

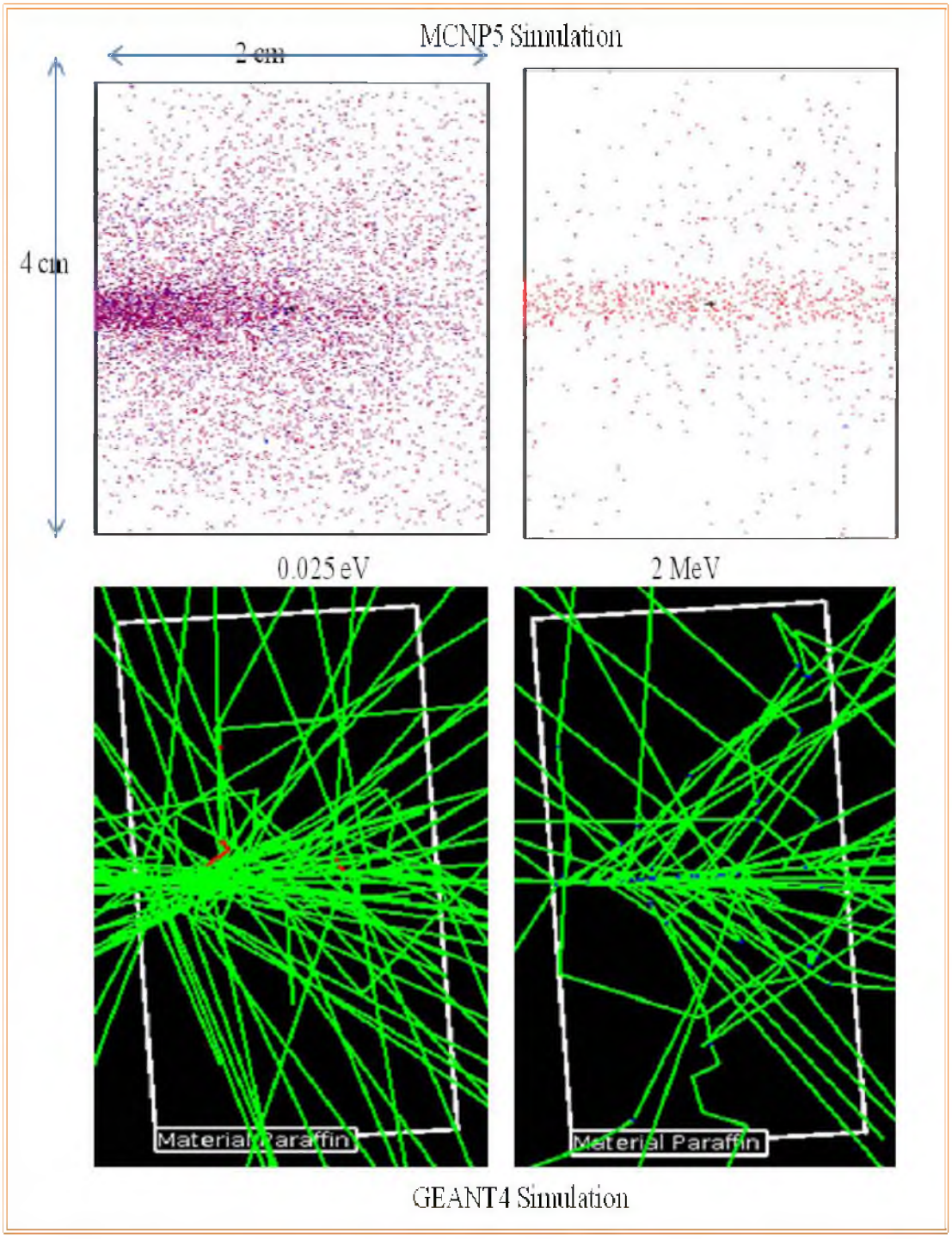

Figure 5-17. GEANT4 and MCNP5 simulation of neutron interactions with paraffin

Table 5-1. MCNP5 and GEANT4 comparison of neutron interactions

MCNP5 Simulation - 0.025 eV				
Material	Neutron-Flux n/cm^2	Neutron energy deposited- MeV/g	Gamma- Flux ɤ/cm^2	Gamma energy deposited - MeV/g
Boron	6.46×10^{5}	3.52×10^{-2}	3.74×10^{2}	4.74×10^{-4}
Lead	7.59×10^{2}	5.50×10^{-9}	9.23×10^{4}	1.39×10^{-4}
Paraffin	9.85×10^{5}	3.46×10^{-6}	3.97×10^{3}	7.15×10^{-5}
GEANT4.9.4 Simulation - 0.025 eV				
Material	Neutron-Flux n/cm^2	Neutron energy deposited- MeV/g	Gamma- Flux ɤ/cm^2	Gamma energy deposited - MeV/g
Boron	5.27×10^{5}	3.32×10^{-2}	3.42×10^{2}	4.31×10^{-4}
Lead	7.00×10^{2}	4.46×10^{-9}	9.16×10^{4}	1.06×10^{-4}
Paraffin	9.38×10^{2}	3.16×10^{-6}	3.68×10^{3}	6.51×10^{-5}
MCNP5 Simulation - 2 MeV				
Material	Neutron- Flux n/cm^2	Neutron energy deposited- MeV/g	Gamma- Flux ɤ/cm^2	Gamma energy deposited - MeV/g
Boron	6.38×10^{2}	9.97×10^{-3}	2.47×10^{3}	3.63×10^{-5}
Lead	6.84×10^{2}	3.69×10^{-5}	1.28×10^{4}	6.25×10^{-5}
Paraffin	7.22×10^{2}	1.61×10^{-2}	7.88×10^{1}	4.40×10^{-7}
GEANT4.9.4 Simulation - 2 MeV				
Material	Neutron- Flux n/cm^2	Neutron energy deposited- MeV/g	Gamma- Flux ɤ/cm^2	Gamma energy deposited - MeV/g
Boron	6.06×10^{2}	9.47×10^{-3}	2.34×10^{3}	3.44×10^{-5}
Lead	6.49×10^{2}	3.51×10^{-5}	1.21×10^{4}	5.93×10^{-5}
Paraffin	6.85×10^{2}	1.52×10^{-2}	7.48×10^{1}	4.18×10^{-7}

gamma fluence, and total energy deposited from neutrons and gammas are listed. At thermal neutron energy of 0.025 eV, as expected, the highest number of interactions occurred in boron-10 as compared to interactions of neutrons of energy 2 MeV. A smaller number of neutron interactions are recorded at thermal and fast neutron energies for lead. High thermal neutron interactions with paraffin were obtained at low neutron energy (0.025 eV) as compared to high neutron energy (2 MeV). In conclusion, comparison of GEANT4 and MCNP5 simulation of neutron interaction provides good agreement between the two simulations, as shown in Table 5-1.

5.6. Comparison between MCNP5 and GEANT4.9.4 Models of the Fast Neutron Pencil Beam Facility at the UUTR

MCNP5 and GEANT4.9.4 were used to model and simulate the UUTR FNPB design as described in previous sections. The MCNP5 input file (Appendix E) of the UUTR FNPB simulated the reactor core from which the fast neutron source was emitted from the fission process in the core. The reactor core was modeled at 90 kW power with all control rods out. Table 5-2 shows a summary of MCNP5 simulation of UUTR FNPB: the reactor remained critical with k_{eff} of 1.0065 (with good standard deviation and relative error of 0.00003 and 0.0275, respectively). The FNIF has an estimated fast neutron flux of ~ 10^{11} n/cm^2 s. The probability of fast neutron scattering into the UUTR FNPB sample holder is on the order of 1:10,000 based on the ration of neutrons recorded in the sample holder relative to the FNIF. The fast neutron flux of the FNPB is 6.52x10^7 n/cm^{2}s delivering a neutron dose of 4.24x10^4 rem/hr as shown in Table 5-2. The neutron spectrum, indicated in Figure 5-18 and Table 5-3, indicates that the maximum fast neutron flux is at neutron energy of 1 MeV. Gamma neutron flux in the UUTR FNPB is 1.14x10^8 ɣ/cm^{2}s, delivering a gamma dose of 4.54x10^3 rem/hr. Most of the gamma flux in the FNPB is emitted from the nuclear fission reaction in the reactor, core as shown in Table 5-4. Table 5-5 shows the gamma flux at different energies, and Figure 5-19 depicts the gamma spectrum in the FNPB sample holder.

Table 5-2. MCNP5 reactor physics neutron simulation of UUTR FNPB

Neutron Flux - n/cm^2 s	Neutron Dose - rem/hr	Error	k_{eff}	CPU time	Particles
6.52x10^7	4.24x10^4	0.0275	1.0065±0.00003	8.5 days	5.00x10^8

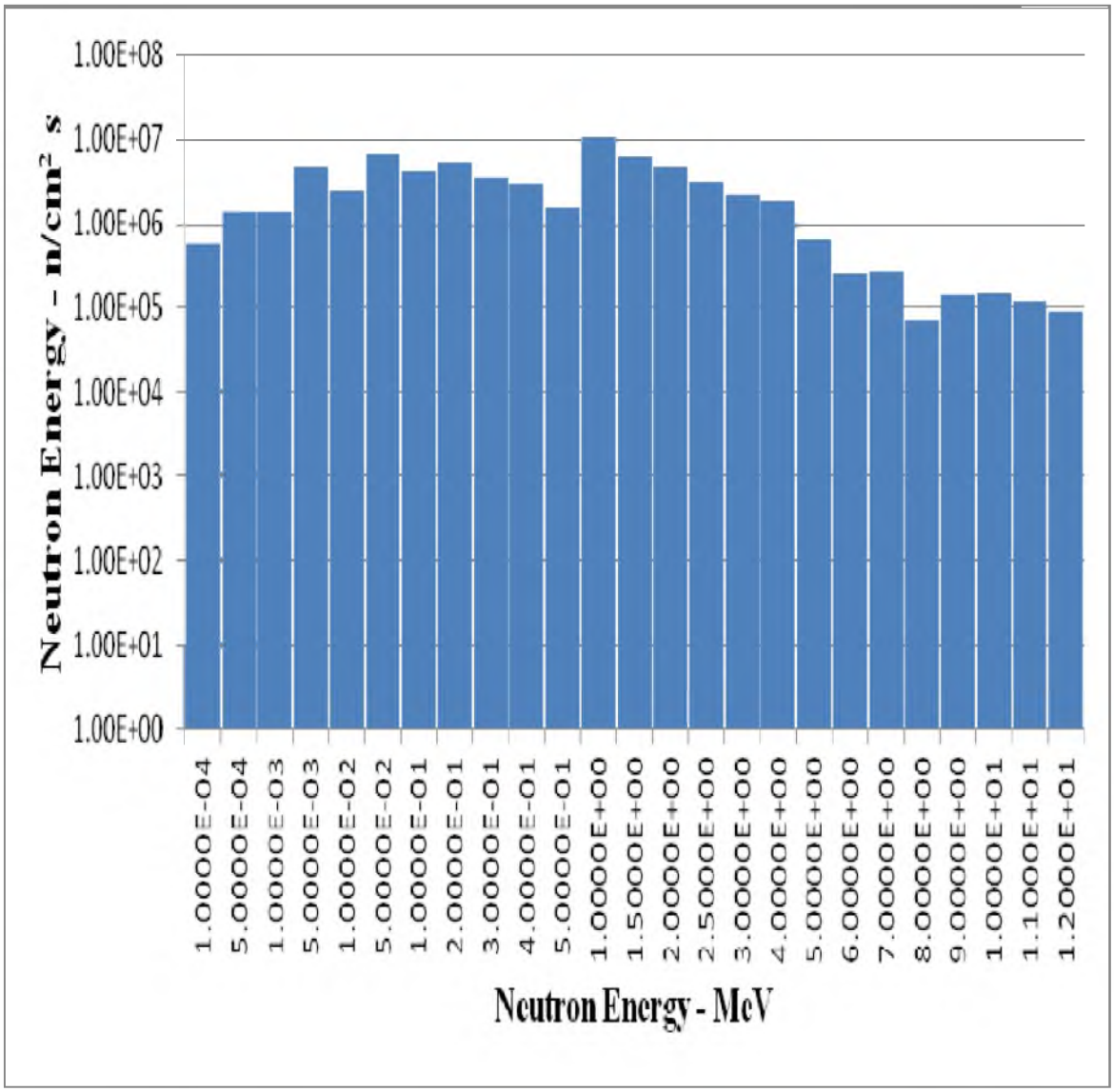

Figure 5-18. MCNP5 neutron spectrum in the UUTR FNPB

Table 5-3. MCNP5 neutron flux in UUTR FNPB

Neutron Energy - MeV	Neutron Flux - n/cm^2 s	Relative Error
$1.00\text{x}10^{-4}$	$5.67\text{x}10^{5}$	0.1206
$5.00\text{x}10^{-4}$	$1.40\text{x}10^{6}$	0.1122
$1.00\text{x}10^{-3}$	$1.38\text{x}10^{6}$	0.0841
$5.00\text{x}10^{-3}$	$4.70\text{x}10^{6}$	0.0985
$1.00\text{x}10^{-2}$	$2.47\text{x}10^{6}$	0.0983
$5.00\text{x}10^{-2}$	$6.74\text{x}10^{6}$	0.0837
$1.00\text{x}10^{-1}$	$4.12\text{x}10^{6}$	0.0804
$2.00\text{x}10^{-1}$	$5.48\text{x}10^{6}$	0.0936
$3.00\text{x}10^{-1}$	$3.45\text{x}10^{6}$	0.0923
$4.00\text{x}10^{-1}$	$2.86\text{x}10^{6}$	0.0122
$5.00\text{x}10^{-1}$	$1.56\text{x}10^{6}$	0.0166
$1.00\text{x}10^{0}$	$1.04\text{x}10^{7}$	0.0659
$1.50\text{x}10^{0}$	$6.46\text{x}10^{6}$	0.0844
$2.00\text{x}10^{0}$	$4.71\text{x}10^{6}$	0.0908
$2.50\text{x}10^{0}$	$3.06\text{x}10^{6}$	0.0976
$3.00\text{x}10^{0}$	$2.17\text{x}10^{6}$	0.0958
$4.00\text{x}10^{0}$	$1.90\text{x}10^{6}$	0.0971
$5.00\text{x}10^{0}$	$6.56\text{x}10^{5}$	0.1092
$6.00\text{x}10^{0}$	$2.60\text{x}10^{5}$	0.1022
$7.00\text{x}10^{0}$	$2.76\text{x}10^{5}$	0.1082
$8.00\text{x}10^{0}$	$7.10\text{x}10^{4}$	0.1081
$9.00\text{x}10^{0}$	$1.42\text{x}10^{5}$	0.1091
$1.00\text{x}10^{1}$	$1.52\text{x}10^{5}$	0.1094
$1.10\text{x}10^{1}$	$1.21\text{x}10^{5}$	0.1191
$1.20\text{x}10^{1}$	$9.16\text{x}10^{4}$	0.1284

Table 5-4. MCNP5 reactor physics gamma in the UUTR FNPB

Gamma Flux - ɣ/cm^2 s	Gamma Dose - rem/hr	Error	k_{eff}	Computer time	Particles
1.14x10^8	4.54x10^3	0.0275	1.0065±0.00003	8.5 days	5.00x10^8

Table 5-5. MCNP5 gamma flux in the UUTR FNPB

Gamma Energy - MeV	Gamma Flux - ɣ/cm^2 s	Relative Error
5.00x10^{-3}	2.72x10^4	0.1118
1.00x10^{-2}	3.40x10^4	0.0926
5.00x10^{-2}	1.36x10^7	0.0521
1.00x10^{-1}	6.52x10^7	0.0246
2.00x10^{-1}	3.82x10^7	0.0315
3.00x10^{-1}	5.60x10^7	0.0261
4.00x10^{-1}	7.06x10^7	0.0236
5.00x10^{-1}	1.01x10^8	0.0173
1.00x10^0	2.46x10^8	0.0131
1.50x10^0	1.24x10^8	0.0186
2.00x10^0	8.77x10^7	0.0213
2.50x10^0	1.86x10^8	0.0129
3.00x10^0	2.51x10^7	0.0453
4.00x10^0	3.47x10^7	0.0403
5.00x10^0	2.41x10^7	0.0433
6.00x10^0	1.59x10^7	0.0531
7.00x10^0	1.09x10^7	0.0563
8.00x10^0	3.01x10^7	0.0323
9.00x10^0	7.88x10^6	0.0642
1.00x10^1	2.18x10^6	0.1134

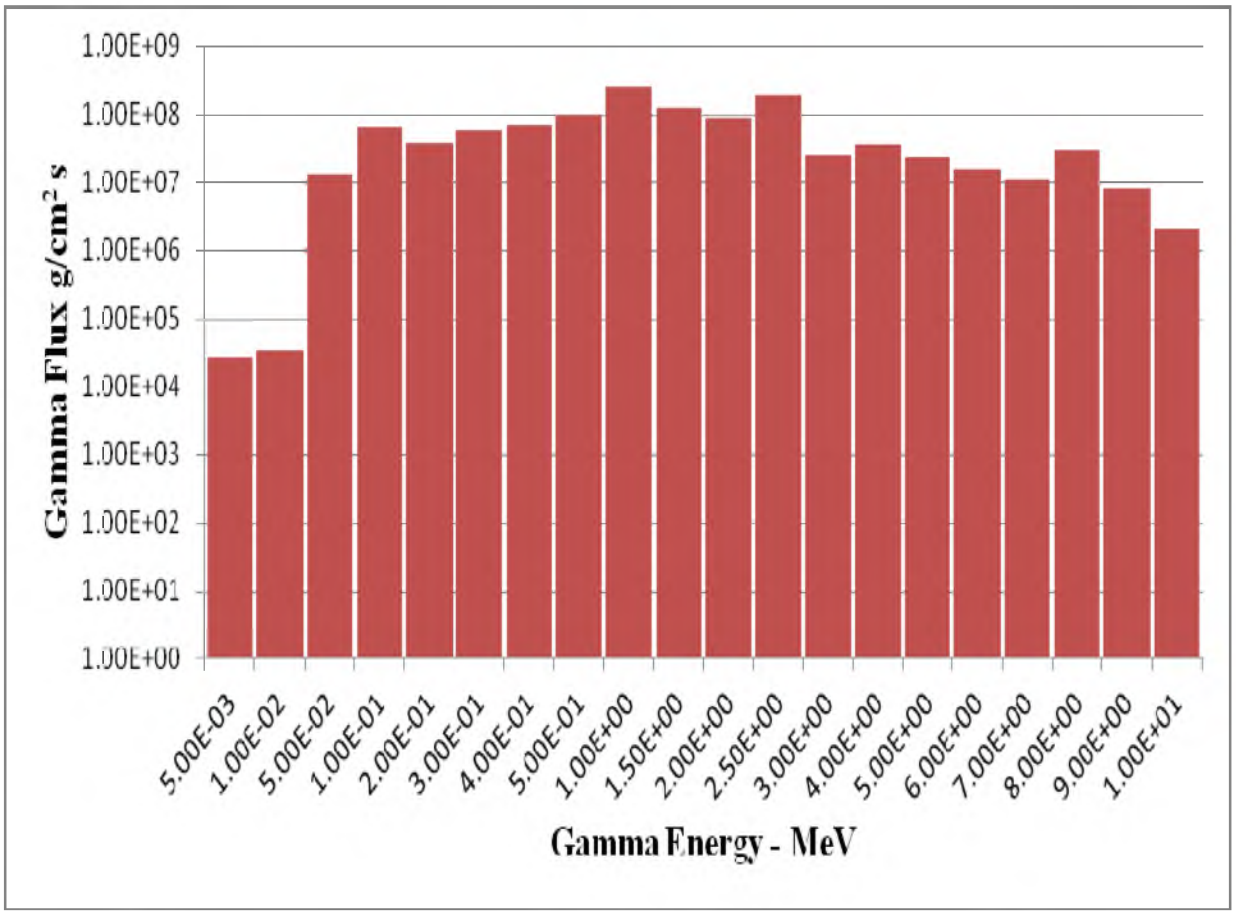

Figure 5-19. MCNP5 gamma spectrum of UUTR FNPB

GEANT4.9.4 was used to model and simulate the UUTR FNPB model (Appendix F). Since GEANT4.9.4 does not include the reactor physics calculations, the fast neutron source was simulated based on a Maxwellian distribution as a planar source. The simulated neutron fluence within the FNPB was 1.50×10^{7} n/cm^{2}s, delivering a calculated dose of 9.76×10^{3} rem/hr, and also the gamma fluence was 2.62×10^{7} γ/cm^2 s, delivering a calculated dose of 1.05×10^{8} rem/hr, as indicated in Tables 5-6 and 5-7. MCNP5 modeling and simulation of UUTR FNPB provides a more realistic model of the UUTR FNPB.

Table 5-6. GEANT4 summary of UUTR FNPB simulation

Neutron Flux n/cm^2 s	Neutron Dose rem/hr	Gamma Flux ɣ/cm^2 s	Gamma Dose rem/hr
1.50x10^7	9.76x10^3	2.62x10^7	1.05x10^3

Table 5-7. GEANT4 Simulation of neutron and gamma fluence in the UUTR FNPB

Energy - MeV	Neutron Flux n/cm^2 s	Gamma Flux ɣ/cm^2 s
5.00x10^{-3}	1.31x10^5	6.26x10^3
1.00x10^{-2}	3.21x10^5	7.83x10^3
5.00x10^{-2}	3.16x10^5	3.14x10^6
1.00x10^{-1}	1.08x10^6	1.50x10^7
2.00x10^{-1}	5.68x10^5	8.79x10^6
3.00x10^{-1}	1.55x10^6	1.29x10^7
4.00x10^{-1}	9.48x10^5	1.62x10^7
5.00x10^{-1}	1.26 x10^6	2.31x10^7
1.00x10^0	7.94x10^5	5.66x10^7
1.50x10^0	6.58x10^5	2.86x10^7
2.00x10^0	3.59x10^5	2.02x10^7
2.50x10^0	2.38x10^6	4.27x10^7
3.00x10^0	1.49x10^6	5.78x10^6
4.00x10^0	1.08x10^6	7.99x10^6
5.00x10^0	7.04x10^5	5.55x10^6
6.00x10^0	4.99x10^5	3.65x10^6
7.00x10^0	4.38x10^5	2.50x10^6
8.00x10^0	1.51x10^5	6.93x10^6
9.00x10^0	5.98x10^4	1.81x10^6
1.00x10^1	6.34x10^4	5.02x10^5

Comparison of MCNP5 simulation of UUTR FNPB with GEANT4 as shown in Table 5-8 indicates that MCNP5 gives a more realistic model of the fast neutron pencil beam with a neutron and gamma flux of $6.52x10^7$ n/cm^{2}s and $1.14x10^8$ ɤ /cm^{2}s, respectively, while the neutron and gamma flux recorded in GEANT4 were $1.50x10^7$ n/cm^2 s and $2.62x10^7$ ɤ/cm^2 s, respectively. The results indicate that both the neutron and gamma flux recorded via GEANT4 simulations were much less than MCNP5 simulation.

5.7. Comparison of UUTR FNPB Design with Other Fast Neutron Pencil Beam Facilities

Fast Neutron Pencil Beam (FNPB) facilities are applied in a couple of fields; most common amongst the applications are Fast Neutron Therapy for the cure of cancer and tumors and also for studying the radiation effects on electronic components' displacement damage and ionization, as discussed in Chapter 4. Research conducted by E. Bourhis-Martin [35] at the University of Essen, Strahlenklinik, Germany on the validation of a fast neutron pencil beam model-based treatment planning

Table 5-8. Comparison of MCNP5 and GEANT4.9.4 Simulation of UUTR FNPB

MCNP5			
Neutron Flux - n/cm^2 s	Neutron Dose - rem/hr	Gamma Flux - ɤ/cm^2 s	Gamma Dose - rem/hr
$6.52x10^7$	$4.24x10^4$	$1.14x10^8$	$4.54x10^3$
Preliminary GEANT4.9.4 Simulation			
Neutron Flux - n/cm^2 s	Neutron Dose - rem/hr	Gamma Flux - ɤ/cm^2 s	Gamma Dose - rem/hr
$1.50x10^7$	$9.76x10^3$	$2.62x10^7$	$1.05x10^3$

system for fast neutron therapy shows that the estimated fast neutron flux was within a range of ~10^6 to 10^8 n/cm^{2}s, as explained in Chapter 4. Results obtained from the UUTR FNPB simulation, explained in Chapter 5, shows that the simulated neutron flux obtained was 6.52x10^7 n/cm^{2}s, which is well within the estimated range of neutron flux obtained in existing facilities. Figure 5-20 depicts the comparison of fast neutron spectrum obtained from MCNP5 simulation of UUTR FNPB with fast neutron spectrum beam from research by Thomas B. Ucherl [43], showing that the two spectra have high neutron flux at fast neutron energy.

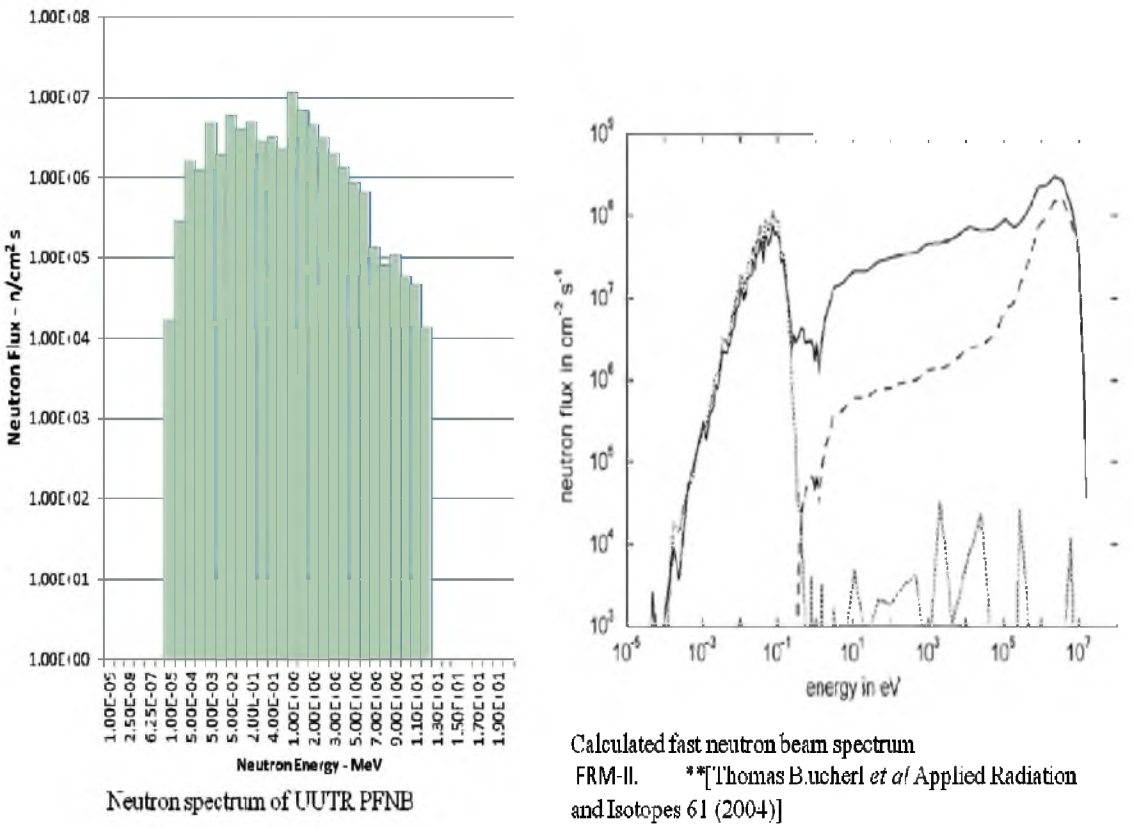

Figure 5-20. Comparison of UUTR FNPB spectrum with literature. Adapted from [43]

CHAPTER 6

CONCLUSION AND FUTURE WORK

6.1. Conclusion

The first objective of this thesis was to benchmark different versions of GEANT4 against experimental measurements and the MCNP5 model, pertaining to photon transport and interactions. Different versions of the GEANT4 codes (4.9.2, 4.9.3, and 4.9.4) were used to simulate the experimental set up, as described in Chapter 4. The results obtained from the simulations of different versions of GEANT4 were benchmarked against MCNP5 code as well, in addition to data obtained in the experiment. Gamma dose rate measured one foot away from the cesium source 27 mrem/hr decreased with distance away from the source 0.6 mR/hr. Even though the GEANT4 versions had different physics models implemented for photon interactions, the simulations of GEANT4 versions presented good agreement with experimental data and MCNP5 simulation. Statistical analysis of error propagation with both GEANT4 and MCNP5 indicates good accuracy with dose rate measured close to the source as compared to a further distance away from the detector (this is due to particle angular dispersion as the particle traverses distant away from the source). Also, a comparison of GEANT4 and MCNP5 simulation of neutron interactions at thermal and fast neutron energies of 0.025 eV and 2 MeV, respectively, were assessed for selected materials (lead, boron-10, and paraffin).

Comparison of simulations showed good agreement between GEANT4 and MCNP5 simulation codes for neutron interactions.

The second objective was to develop a preliminary model of Fast Neutron Pencil Beam Facility at the UUTR using MCNP5 and GEANT4.9.4. The fast neutron source was modeled in MCNP5 by running reactor physics simulations of the UUTR reactor core, while the fast neutron source in GEANT4.9.4 was simulated with a Maxwellian distribution as a planar source. The fast neutron flux obtained in MCNP5 simulation of the FNPB was 6.52×10^{7} n/cm^{2}s, delivering a neutron dose of 4.24×10^{4} rem/hr. The neutron spectrum, as discussed in Chapter 5, indicates that the maximum fast neutron flux obtained with the MCNP5 was at neutron energy of 1 MeV. MCNP5 gamma neutron flux of the UUTR FNPB was 1.14×10^{7} ɣ/cm^{2}s, delivering a gamma dose of 4.54×10^{3} rem/hr. The gamma flux in the FNPB was emitted from the nuclear fission reaction in the reactor core. GEANT4.9.4 simulation indicates that the neutron fluence within the FNPB was 1.50×10^{7} n/cm^{2}s, delivering a calculated dose of 9.76×10^{7} rem/hr, and also, the gamma fluence was 2.62×10^{7} ɣ/cm^{2}s, delivering a calculated dose of 1.05×10^{3} rem/hr.

In conclusion, MCNP5 modeling and simulation of UUTR FNPB provides a more realistic model of the UUTR FNPB since it can be used for reactor physics simulations to therefore give a more realistic prediction of the design.

6.2. Recommendations for Future Work

Developing a final design of a fast neutron pencil beam (FNPB) facility at the UNEP UUTR would enable an introduction of a wide range of experiments which might not be feasible with the current neutron irradiation ports, such as, but not limited to:

- Study of biological effect of fast neutrons on biological tissue and cells.
- Study of radiation damage to materials, and real-time analysis of radiation effect of materials.
- Study of fast neutron interaction effects on electrical components, and real-time analysis of electric circuits in electrical devices.
- Elemental analysis of various samples.

However, a complete optimized design of the FNPB facility will have to be performed, modeled, and built into the UUTR research reactor in order to be able to perform feasible scientific experiments, as mentioned above.

This thesis focused on the preliminary design of the fast neutron pencil beam facility, and further research has to be performed to optimize the UUTR FNPB model, such as but not limited to, the following;

- Further research concerning different type of compounds that could be used for collimation of fast neutrons such as borated polyethylene, borated graphite, or borated wood could be assessed.
- The gamma flux and gamma dose rate calculated in the preliminary design of UUTR FNPB sample holder was very high; therefore, further research

pertaining to good shielding material properties for attenuating gamma particles from the FNPB model should be done.

- Feasibility analysis of the optimization design of the fast neutron pencil beam should be re-examined to enhance the fast neutron flux within the FNPB.

Further improvement of the design will enhance the neutron flux and increase the wide range of research experiments that could be performed with the UUTR FNPB.

APPENDIX A

MCNP5 INPUT FILE FOR PHOTON EXPERIMENT

```
c ************************************************************
C BENCHMARK RESEARCH -CHRIS ADJEI
C ************************************************************
1    1 -1.29 -1 -5 4  imp:p=1                  $Air gap
2    2 -10.29 -2 -7 6 #1  imp:p=1          $Lead shielding
3    3 -8.06 -3 -7 6 #2 #1  imp:p=1            $StainlessSteeL
4    4 -3.667 8 -9 -10 11 -12 13  imp:p=2          $Detector
5    1 -1.29 14 -15 -16 17 18 -19 #4 #3 #2 #1 imp:p=1 $world volume
6    0       -14:15:-17:16:-18:19  imp:p=0         $ Outside
1     cz 0.721875          $ cell 1 - Air gap in Pig,
4     pz -6.0325           $ cell 1 - bottom of air gap in pig
5     pz -1.95             $ cell 1 - top of air gap in pig
2     cz 2.06375           $ cell 2 - radius of lead
6     pz -7.9375           $ cell 2 - bottom of lead shielding
7     pz 7.9375            $ cell 2 - top of lead shielding
3     cz 2.38125           $ cell 3 - radius of stianlesssteel
8     py -1.27             $ cell 4 - detector side on -y-axis
9     py 1.27              $ cell 4 - detector side on +y-axis
10    px -32.86125         $ cell 4 - detector side on x-axis
11    px -35.40125         $ cell 4 - detector side on y-axis
12    pz 1.27              $ cell 4 - detector side on +z-axis
13    pz -1.27             $ cell 4 - detector side on -Z-axis
14    py -10.0             $ cell 5 - world volume y-axis Box
15    py 10.0              $ cell 5 - world volume y-axis Box
16    pz 20.0              $ cell 5 - world volume z-axis Box
```

```
17     pz -10.0              $ cell 5 - world volume z-axis Box
18     px -50.0              $ cell 5 - world volume x-axis Box
19     px 10.0               $ cell 5 - world volume x-axis Box
mode p
SDEF ERG=0.6617 POS=0 0 -5.0 AXS= 0 0 1 RAD=d1 EXT=d2 PAR=2
SI1= 0 0.5
SP1= -21 0
SI2= -5.0 -4.0
SP2= -21 0
m1    7014 -0.78084
      8016 -0.2094
      18040 -0.00976
m2    82207 -1.0
m3    6012 -0.001
      14028 -0.007
      24052 -0.18
      25055 -0.01
      26056 -0.712
      28059 -0.09
m4    11023 -0.153373
      53127 -0.846627
F6:P 4
*F8:P 4
E8 0 1E-5 1E-1 2E-1 3E-1 4E-1 5E-1 6E-1 6.617E-1
FM6 6.845E8
de6 0.01 0.03 0.05 0.07 0.10 0.15 0.20 0.25 0.30 0.35
```

```
    0.40 0.45 0.50 0.55 0.60 0.65 0.70 0.80 1.00 1.40
    1.80 2.20 2.60 2.80 3.25 3.75 4.25 4.75 5.00
df6 3.96e-6 5.82e-7 2.90e-7 2.58e-7 2.83e-7 3.79e-7
    5.01e-7 6.31e-7 7.59e-7 8.78e-7 9.85e-7 1.08e-6
    1.17e-6 1.27e-6 1.36e-6 1.44e-6 1.52e-6 1.68e-6
    1.98e-6 2.51e-6 2.99e-6 3.42e-6 3.82e-6 4.01e-6
    4.41e-6 4.83e-6 5.23e-6 5.60e-6 5.80e-6
nps  1000000000
print
```

APPENDIX B

GEANT4.9.4 INPUT FILE FOR PHOTON EXPERIMENT

```
#include "ExN02DetectorConstruction.hh"
#include "G4Material.hh"
#include "G4Element.hh"
#include "G4Box.hh"
#include "G4VSolid.hh"
#include "G4Tubs.hh"
#include "G4Orb.hh"
#include "G4LogicalVolume.hh"
#include "G4ThreeVector.hh"
#include "G4PVPlacement.hh"
#include "G4NistManager.hh"
#include "G4VisAttributes.hh"
//....oooOO0OOooo........oooOO0OOooo........oooOO0OOooo........oooOO0OOooo......
ExN02DetectorConstruction::ExN02DetectorConstruction()
{
  expHall_x = expHall_y = expHall_z = 10*cm;
// lcylin_a = 0.*deg;
 // lcylin_b = 360.*deg;
  bubble_x = 1*cm;
  bubble_y = 2*cm;
  bubble_z = 2*cm;
 // bubble_a = 0.*deg;
 // bubble_b = 360.*deg;}
//....oooOO0OOooo........oooOO0OOooo........oooOO0OOooo........oooOO0OOooo......
ExN02DetectorConstruction::~ExN02DetectorConstruction(){;}
//....oooOO0OOooo........oooOO0OOooo........oooOO0OOooo........oooOO0OOooo......
```

```
G4VPhysicalVolume* ExN02DetectorConstruction::Construct()
{
//         ------------ Materials ------------
  G4double a, z, density;
  G4int nelements, natoms;
  G4int ncomponents;
  G4double fractionmass, temperature, pressure;
//Vacuum
pressure = 3.e-18*pascal; temperature = 293.15*kelvin;
density = universe_mean_density;
G4Material* Vacuum = new G4Material("Vacuum", 1., 1.01*g/mole, density,
kStateGas,temperature,pressure);
// Use NIST database for elements and materials whereever possible.
          G4NistManager* man = G4NistManager::Instance();
          man->SetVerbose(1);

          G4Element* C  = man->FindOrBuildElement("C");
          G4Element* Si = man->FindOrBuildElement("Si");
          G4Element* Cr = man->FindOrBuildElement("Cr");
          G4Element* Mn = man->FindOrBuildElement("Mn");
          G4Element* Fe = man->FindOrBuildElement("Fe");
          G4Element* Ni = man->FindOrBuildElement("Ni");
          G4Element* Na = man->FindOrBuildElement("Na");
          G4Element* I  = man->FindOrBuildElement("I");
          G4Element* Cd = man->FindOrBuildElement("Cd");
          G4Element* Al = man->FindOrBuildElement("Al");
        G4Element* B  = man->FindOrBuildElement("B");
```

```
        G4Material* StainlessSteel = new G4Material("StainlessSteel", density=
8.06*g/cm3, ncomponents=6);

        StainlessSteel->AddElement(C, fractionmass=0.001);

        StainlessSteel->AddElement(Si, fractionmass=0.007);

        StainlessSteel->AddElement(Cr, fractionmass=0.18);

        StainlessSteel->AddElement(Mn, fractionmass=0.01);

        StainlessSteel->AddElement(Fe, fractionmass=0.712);

        StainlessSteel->AddElement(Ni, fractionmass=0.09);

        G4Material* SodiumIodide = new G4Material("SodiumIodide", density=
3.667*g/cm3, ncomponents=2);

        SodiumIodide->AddElement(Na, fractionmass=0.153373);

        SodiumIodide->AddElement(I, fractionmass=0.846627);

        G4Material* Cadmium = new G4Material("Cadmium", density= 7.996*g/cm3,
ncomponents=1);

        Cadmium->AddElement(Cd, fractionmass=1.0);

      G4Material* Boron10 = new G4Material("Boron10", density= 2.08*g/cm3,
ncomponents=1);

        Boron10->AddElement(B, fractionmass=1.0);

// Air

G4Element* Pb = new G4Element("Lead", "Pb", z=82 , a=207*g/mole);

 G4Material* Lead = new G4Material("Lead", density=11.354*g/cm3, nelements=1);

Lead->AddElement(Pb, 100.*perCent);

  G4Element* N = new G4Element("Nitrogen", "N", z=7 , a=14.01*g/mole);

  G4Element* O = new G4Element("Oxygen"  , "O", z=8 , a=16.00*g/mole);

  G4Material* Air = new G4Material("Air", density=1.29*mg/cm3, nelements=2);

  Air->AddElement(N, 70.*perCent);

  Air->AddElement(O, 30.*perCent);

// Water
```

```
  G4Element* H = new G4Element("Hydrogen", "H", z=1 , a=1.01*g/mole);

  G4Material* Water = new G4Material("Water", density= 1.0*g/cm3, nelements=2);

  Water->AddElement(H, 2);

  Water->AddElement(O, 1);

  G4Material* Sapphire = new G4Material("Sapphire",density= 4.*g/cm3,
ncomponents=2);

  Sapphire->AddElement(Al, natoms=2);

  Sapphire->AddElement(O , natoms=3);

// Paraffin - Polythelene

   G4Material* Paraffin = new G4Material("Paraffin", density= 0.94*g/cm3,
nelements=2);

   Paraffin->AddElement(C, 85.6*perCent);

   Paraffin->AddElement(H, 14.4*perCent);

// The experimental Hall

  G4Box* expHall_box = new G4Box("World",expHall_x,expHall_y,expHall_z);

  G4LogicalVolume* expHall_log  = new
G4LogicalVolume(expHall_box,Vacuum,"World",0,0,0);

  G4VPhysicalVolume* expHall_phys = new
G4PVPlacement(0,G4ThreeVector(),expHall_log,"World",0,false,0);

// The Air Bubble

  G4Box* bubbleAir_box = new G4Box("Bubble",bubble_x,bubble_y,bubble_z);

  G4LogicalVolume* bubbleAir_log = new
G4LogicalVolume(bubbleAir_box,Paraffin,"Bubble",0,0,0);

G4VPhysicalVolume* bubbleAir_phys = new G4PVPlacement(0,G4ThreeVector(-
4*cm,0,0),bubbleAir_log,"Bubble",

                    expHall_log,false,0);
```

APPENDIX C

MCNP5 INPUT FILE FOR NEUTRON INTERACTION

NEUTRON INTERACTION WITH MATERIAL

C Cell Cards

1 5 -2.08 1 -7 -3 4 -5 6 imp:n=1 imp:p=1 $boron

5 3 -0.00115 10 -11 -12 13 -14 15 #1 imp:n=1 imp:p=1 $air

6 0 -10:11:12:-13:14:-15 imp:n=0 imp:p=0 $outside world

C Solution Cylinder Surface cards

1 px 0.0

3 pz 2.0

4 pz -2.0

5 py 2.0

6 py -2.0

7 px 2.0

10 px -5.0

11 px 15.0

12 py 4.0

13 py -4.0

14 pz 4.0

15 pz -4.0

C Material Cards

m1 1001 -0.2 $m1 is mix of H2O and Ca

  8016 -0.3

  20042 -0.5

m2 1001 -0.6667 $water

  8016 -0.3333

m3 7014 -0.78084 $Air - density - 0.00115

```
     8016 -0.2094
     18040 -0.00976
m4   1001.66c -0.143711        $polyethylene - density 0.94
     8016.66c -0.856289
m5   5010.66c -1.0             $Boron - density 2.08
m8   82000.50c    -1.0         $ Pb - density 11.354
SDEF PAR=1 ERG=2.5e-8 POS=0 0 0 AXS= 1 0 0 EXT=0 RAD=d1 VEC= 1 0 0 DIR=
1
SI1   0 0.2
SP1  -21 1
c  boroncell<--energy deposited (MeV/g)
F06:n   1
F16:p   1
F04:n   1
F14:p   1
mode  n p
nps   1e7
```

APPENDIX D

GEANT4.9.4 INPUT FILE FOR NEUTRON INTERACTION

```
//....oooOO0OOooo.....oooOO0OOooo.....oooOO0OOooo.....oooOO0OOooo.....
#include "ExN02DetectorConstruction.hh"
#include "G4Material.hh"
#include "G4Element.hh"
#include "G4Box.hh"
#include "G4VSolid.hh"
#include "G4Tubs.hh"
#include "G4Orb.hh"
#include "G4LogicalVolume.hh"
#include "G4ThreeVector.hh"
#include "G4PVPlacement.hh"
#include "G4NistManager.hh"
#include "G4VisAttributes.hh"
//....oooOO0OOooo.....oooOO0OOooo.....oooOO0OOooo.....oooOO0OOooo.....
ExN02DetectorConstruction::ExN02DetectorConstruction()
{
  expHall_x = expHall_y = expHall_z = 10*cm;
  bubble_x = 1*cm;
  bubble_y = 2*cm;
  bubble_z = 2*cm;
}
//....oooOO0OOooo.....oooOO0OOooo.....oooOO0OOooo.....oooOO0OOooo.....
ExN02DetectorConstruction::~ExN02DetectorConstruction(){;}

G4VPhysicalVolume* ExN02DetectorConstruction::Construct()
```

```
{
//          ------------ Materials ------------
  G4double a, z, density;
  G4int nelements, natoms;
  G4int ncomponents;
  G4double fractionmass, temperature, pressure;
//Vacuum
pressure = 3.e-18*pascal; temperature = 293.15*kelvin;
density = universe_mean_density;
G4Material* Vacuum = new G4Material("Vacuum", 1., 1.01*g/mole, density,
kStateGas,temperature,pressure);
// Use NIST database for elements and materials whereever possible.
          G4NistManager* man = G4NistManager::Instance();
          man->SetVerbose(1);
          G4Element* C  = man->FindOrBuildElement("C");
          G4Element* Si = man->FindOrBuildElement("Si");
          G4Element* Cr = man->FindOrBuildElement("Cr");
          G4Element* Mn = man->FindOrBuildElement("Mn");
          G4Element* Fe = man->FindOrBuildElement("Fe");
          G4Element* Ni = man->FindOrBuildElement("Ni");
          G4Element* Na = man->FindOrBuildElement("Na");
          G4Element* I  = man->FindOrBuildElement("I");
          G4Element* Cd = man->FindOrBuildElement("Cd");
          G4Element* Al = man->FindOrBuildElement("Al");
       G4Element* B  = man->FindOrBuildElement("B");
          G4Material* StainlessSteel = new G4Material("StainlessSteel", density=
8.06*g/cm3, ncomponents=6);
```

```
        StainlessSteel->AddElement(C, fractionmass=0.001);

        StainlessSteel->AddElement(Si, fractionmass=0.007);

        StainlessSteel->AddElement(Cr, fractionmass=0.18);

        StainlessSteel->AddElement(Mn, fractionmass=0.01);

        StainlessSteel->AddElement(Fe, fractionmass=0.712);

        StainlessSteel->AddElement(Ni, fractionmass=0.09);

        G4Material* SodiumIodide = new G4Material("SodiumIodide", density=
3.667*g/cm3, ncomponents=2);

        SodiumIodide->AddElement(Na, fractionmass=0.153373);

        SodiumIodide->AddElement(I, fractionmass=0.846627);

        G4Material* Cadmium = new G4Material("Cadmium", density= 7.996*g/cm3,
ncomponents=1);

        Cadmium->AddElement(Cd, fractionmass=1.0);

      G4Material* Boron10 = new G4Material("Boron10", density= 2.08*g/cm3,
ncomponents=1);

        Boron10->AddElement(B, fractionmass=1.0);

G4Element* Pb = new G4Element("Lead", "Pb", z=82 , a=207*g/mole);

 G4Material* Lead = new G4Material("Lead", density=11.354*g/cm3, nelements=1);

Lead->AddElement(Pb, 100.*perCent);

  G4Element* N = new G4Element("Nitrogen", "N", z=7 , a=14.01*g/mole);

  G4Element* O = new G4Element("Oxygen"  , "O", z=8 , a=16.00*g/mole);

  G4Material* Air = new G4Material("Air", density=1.29*mg/cm3, nelements=2);

  Air->AddElement(N, 70.*perCent);

  Air->AddElement(O, 30.*perCent);

// Water

  G4Element* H = new G4Element("Hydrogen", "H", z=1 , a=1.01*g/mole);

  G4Material* Water = new G4Material("Water", density= 1.0*g/cm3, nelements=2);
```

```
  Water->AddElement(H, 2);

  Water->AddElement(O, 1);

  G4Material* Sapphire = new G4Material("Sapphire",density= 4.*g/cm3,
ncomponents=2);

  Sapphire->AddElement(Al, natoms=2);

  Sapphire->AddElement(O , natoms=3);

// Paraffin - Polythelene

   G4Material* Paraffin = new G4Material("Paraffin", density= 0.94*g/cm3,
nelements=2);

   Paraffin->AddElement(C, 85.6*perCent);

   Paraffin->AddElement(H, 14.4*perCent);

// The experimental Hall

  G4Box* expHall_box = new G4Box("World",expHall_x,expHall_y,expHall_z);

  G4LogicalVolume* expHall_log  = new
G4LogicalVolume(expHall_box,Vacuum,"World",0,0,0);



  G4VPhysicalVolume* expHall_phys = new
G4PVPlacement(0,G4ThreeVector(),expHall_log,"World",0,false,0);

// The Air Bubble

  G4Box* bubbleAir_box = new G4Box("Bubble",bubble_x,bubble_y,bubble_z);

  G4LogicalVolume* bubbleAir_log = new
G4LogicalVolume(bubbleAir_box,Paraffin,"Bubble",0,0,0);

G4VPhysicalVolume* bubbleAir_phys = new G4PVPlacement(0,G4ThreeVector(-
4*cm,0,0),bubbleAir_log,"Bubble",

                  expHall_log,false,0);

  return expHall_phys;}

//....oooOO0OOooo.....oooOO0OOooo.....oooOO0OOooo.....oooOO0OOooo.....
```

APPENDIX E

MCNP5 INPUT FILE OF UUTR FNPB

```
UUTR FNPB PRILIMENARY MODEL
c New SS Fuel
100   1   -5.636 -2 11 -12              u=1   imp:n=1 imp:p=1 $Fuel Meat
101   2   -1.70  -2 12 -14              u=1   imp:n=1 imp:p=1 $Up Graphite
102   2   -1.70  -2 13 -11              u=1   imp:n=1 imp:p=1 $Down Graphite
103   3   -7.92  (-1 15 -16) (2:-13:14)   u=1   imp:n=1 imp:p=1 $Cladding
104   4   -1.0   1:-15:16 92 -93         u=1   imp:n=1 imp:p=1 $H2O
c Old SS Fuel
110 like 100 but mat=12 rho=-5.636        u=2   imp:n=1 imp:p=1 $Fuel Meat
111 like 101 but                          u=2   imp:n=1 imp:p=1 $Up Graphite
112 like 102 but                          u=2   imp:n=1 imp:p=1 $Down Graphite
113 like 103 but                          u=2   imp:n=1 imp:p=1 $Cladding
114 like 104 but                          u=2   imp:n=1 imp:p=1 $H2O
c Al Fuel
120   5   -6.143 -3 21 -22              u=3   imp:n=1 imp:p=1 $Fuel Meat
121   2   -1.70  -3 22 -24              u=3   imp:n=1 imp:p=1 $Up Graphite
122   2   -1.70  -3 23 -21              u=3   imp:n=1 imp:p=1 $Down Graphite
123   6   -2.70  (-1 25 -26) (3:-23:24)   u=3   imp:n=1 imp:p=1 $Cladding
124   4   -1.0   1:-25:26 92 -93         u=3   imp:n=1 imp:p=1 $H2O
c Instrumental Fuel
130 like 110 but                          u=4   imp:n=1 imp:p=1 $Fuel Meat
131 like 111 but                          u=4   imp:n=1 imp:p=1 $Up Graphite
132 like 112 but                          u=4   imp:n=1 imp:p=1 $Down Graphite
133 like 113 but                          u=4   imp:n=1 imp:p=1 $Cladding
134 like 114 but                          u=4   imp:n=1 imp:p=1 $H2O
c Graphite
```

```
140   2   -1.70   -3 23 -24            u=6   imp:n=1 imp:p=1 $Graphite
143   like 123 but                     u=6   imp:n=1 imp:p=1 $Cladding
144   like 124 but                     u=6   imp:n=1 imp:p=1 $H2O
c Heavy Water
150   7   -1.056  -3 23 -24            u=7   imp:n=1 imp:p=1 $D2O
153   like 123 but                     u=7   imp:n=1 imp:p=1 $Cladding
154   like 124 but                     u=7   imp:n=1 imp:p=1 $H2O
c Water
160   4   -1.0    -1 92 -93            u=8   imp:n=1 imp:p=1 $H2O
161   4   -1.0     1 92 -93            u=8   imp:n=1 imp:p=1 $H2O
c Safety Control Rod
170   9   -2.52   -46 11 -93           u=10  imp:n=1 imp:p=1 $B4C
171   6   -2.7     46 -47 11 -93       u=10  imp:n=1 imp:p=1 $Al Cladding
172   4   -1.0    (47 -50 11 -93):(-50 -11 92)  u=10  imp:n=1 imp:p=1 $H2O
173   6   -2.7     50 -1 92 -93        u=10  imp:n=1 imp:p=1 $Al Tube
174   4   -1.0     1 92 -93            u=10  imp:n=1 imp:p=1 $H2O
c Shim Control Rod
180   9   -2.52   -46 11 -93           u=11  imp:n=1 imp:p=1 $B4C
181   6   -2.7     46 -47 11 -93       u=11  imp:n=1 imp:p=1 $Al Cladding
182   4   -1.0    (47 -50 11 -93):(-50 -11 92)  u=11  imp:n=1 imp:p=1 $H2O
183   6   -2.7     50 -1 92 -93        u=11  imp:n=1 imp:p=1 $Al Tube
184   4   -1.0     1 92 -93            u=11  imp:n=1 imp:p=1 $H2O
c Reg Control Rod
190   9   -2.52   -48 11 -93           u=12  imp:n=1 imp:p=1 $B4C
191   6   -2.7     48 -49 11 -93       u=12  imp:n=1 imp:p=1 $Al Cladding
192   4   -1.0    (49 -50 11 -93):(-50 -11 92)  u=12  imp:n=1 imp:p=1 $H2O
```

```
193   6   -2.7     50 -1 92 -93          u=12  imp:n=1 imp:p=1 $Al Tube
194   4   -1.0     1 92 -93              u=12  imp:n=1 imp:p=1 $H2O
c Empty Control Rod
196   4   -1.0     -50 92 -93            u=5   imp:n=1 imp:p=1 $H2O
197   6   -2.7     50 -1 92 -93          u=5   imp:n=1 imp:p=1 $Al Tube
198   4   -1.0     1 92 -93              u=5   imp:n=1 imp:p=1 $H2O
c Brand New SS Fuel, more U235
c 310 like 100 but mat=5  rho=-5.781        u=15   imp:n=1 imp:p=1 $Fuel Meat
c 311 like 101 but                          u=15   imp:n=1 imp:p=1 $Up Graphite
c 312 like 102 but                          u=15   imp:n=1 imp:p=1 $Down Graphite
c 313 like 103 but                          u=15   imp:n=1 imp:p=1 $Cladding
c 314 like 104 but                          u=15   imp:n=1 imp:p=1 $H2O
c Lattice
200   4   -1.0   -101 102 -103 104 -105 106 92 -93    lat=2    u=9
              fill=-7:7 -7:7 0:0
              0 0 0 0 0 0 0 9 9 9 9 9 9 9 9
               0 0 0 0 0 0 9 8 7 8 7 8 7 8 9
                0 0 0 0 0 9 3 2 3 1 1 3 2 7 9
                 0 0 0 0 9 1 3 1 1 1 1 3 3 8 9
                  0 0 0 9 1 1 3 1 3 1 5 3 3 7 9
                   0 0 9 3 1 1 4 1 2 2 1 2 3 7 9
                    0 9 3 3 1 3 2 2 2 4 2 3 3 7 9
                     9 8 7 2 5 1 1 5 1 1 8 3 1 6 9
                      9 8 7 1 2 2 1 1 1 2 1 3 6 9 0
                       9 8 7 1 3 8 2 2 1 3 1 6 9 0 0
                        9 8 7 1 1 2 2 5 3 3 6 9 0 0 0
```

```
                    9 8 7 8 1 1 1 1 1 6 9 0 0 0 0

                    9 8 6 6 6 6 6 6 6 6 9 0 0 0 0 0

                    9 8 8 8 8 8 8 8 8 9 0 0 0 0 0 0 0

                    9 9 9 9 9 9 9 9 9 0 0 0 0 0 0 0 0 imp:n=1 imp:p=1

201   4   -1.0   -111 112 -113 114 -115 116 92 -93  fill=9  imp:n=1 imp:p=1 $Lattices

202   6   -2.7   (-121 122 -123 124 -125 126) 91 -94

          (111:-112:113:-114:115:-116)          imp:n=1 imp:p=1  $Al Wall

203   6   -2.7   -111 112 -113 114 -115 116 91 -92          imp:n=1 imp:p=1   $Lower Al
Plate

204   6   -2.7  -111 112 -113 114 -115 116 93 -94 41 43 45  imp:n=1 imp:p=1 $Upper
Al Plate

206   4   -1.0  -131 94 -97 41 43 45 #402 #404 #405 #406 #408 #410 #418

                    #412 #414 #416 #424 imp:n=1 imp:p=1 $Top Water

207   4   -1.0   -131 96 -91                    imp:n=1 imp:p=1      $Bottom Water

208   10  -2.30  -131 -96 95                     imp:n=1 imp:p=1     $Bottom Concrete

301   9   -2.52  -40 93 -97      imp:n=1 imp:p=1 $Safety Rod above core region

302   6   -2.7    40 -41 93 -97  imp:n=1 imp:p=1

303   9   -2.52  -42 93 -97      imp:n=1 imp:p=1 $Shim Rod above core region

304   6   -2.7    42 -43 93 -97  imp:n=1 imp:p=1

305   9   -2.52  -44 93 -97      imp:n=1 imp:p=1 $Reg Rod above core region

306   6   -2.7    44 -45 93 -97  imp:n=1 imp:p=1

c FNIF

400   11  -0.00115  -141 #402 #418 #420 #422 imp:n=2 imp:p=2  $ FNIF Air

401   8   -11.34  -140 141          imp:n=1 imp:p=1  $ FNIF Pb

402   8   -11.34  -142              imp:n=1 imp:p=1  $ Lead base of PFNB

404   11  -0.00115 -246 -244 248     imp:n=4 imp:p=4  $ pencil beam inner cone
```

```
418   6   -2.7  -145 #420 #422          imp:n=2 imp:p=2  $ Aluminum casing of PFNB in
FNIF

420   8   -11.34  -147                  imp:n=1 imp:p=1  $ Lead block in aluminum casing

422   11  -0.00115  -149                imp:n=4 imp:p=4  $ Air gap in aluminum casing

405   11  -0.00115  -144                imp:n=4 imp:p=4  $ Air Collimator box

406   11  -0.00115  -240 -250 244       imp:n=4 imp:p=4  $ pencil mouth of collimator
cylinder

424   17  -2.08    -262 -264 266        imp:n=4 imp:p=4  $ Boron window - PFNB

408    8  -11.34   -252 #410 #406 #424       imp:n=2 imp:p=2  $ SAMPLER  CASING

410   11  -0.00115 -254                  imp:n=16 imp:p=16  $ Inner sAMPLER holder - AIR

412   14  -0.94  -260 #402 #404 #405 #406 #408 #410 #424 imp:n=2 imp:p=2 $
Collimator box

414   6   -2.7   -256  258   imp:n=2 imp:p=2  $ Aluminum cladding of PFNB

416   17   -2.08  -258 260              imp:n=2 imp:p=2  $boron shielding in collimator

c Heavy water block

500   11  -0.00115   -159 160 -161      imp:n=1 imp:p=1  $ Heavy water Air

501   6   -2.7   159 -158 160 -161      imp:n=1 imp:p=1

502   7   -1.056 158 154 -155 156 157 160 -161  imp:n=1 imp:p=1

503   6   -2.7   (-154:155:-156:-157)
              150 -151 152 153 160 -161    imp:n=1 imp:p=1

c

900   4   -1.0   -131 91 -94 140
            (-150:151:-152:-153:-160:161)
          (121:-122:123:-124:125:-126) #402 #404 #405 #406 #408 #410 #412
            #414 #416 #418 #424 imp:n=1 imp:p=1 $Water Arround Core

999   0          131:-95:97   imp:n=0 imp:p=0

C Surface Cards
```

```
1    cz    1.873  $Outer Radius
2    cz    1.82   $Inner Radius
3    cz    1.79   $Inner Radius for Aluminum Container
11   pz   -19.05   $SS Fuel Meat Bottom (7.5 inch * 2)
12   pz    19.05   $SS Fuel Meat Top
13   pz   -29.21   $SS Fuel Graphite Bottom (4 inch)
14   pz    29.21   $SS Fuel Graphite Top
15   pz   -30.39   $SS Cladding Bottom (1.18 cm)
16   pz    30.39   $SS Cladding Top (1.18 cm)
21   pz   -17.78   $Al Fuel Meat Bottom (7 inch * 2)
22   pz    17.78   $Al Fuel Meat Top
23   pz   -27.94   $Al Fuel Graphite Bottom (4 inch)
24   pz    27.94   $Al Fuel Graphite Top
25   pz   -29.12   $Al Cladding Bottom (1.18 cm)
26   pz    29.12   $Al Cladding Top (1.18 cm)
40   c/z   6.555 -11.354 1.00  $Safety Control Rod
41   c/z   6.555 -11.354 1.11  $Safety Control Rod Cladding
42   c/z -13.11    0.0   1.00  $Shim Control Rod
43   c/z -13.11    0.0   1.11  $Shim Control Rod Cladding
44   c/z   6.555  11.354 0.200 $Reg Control Rod
45   c/z   6.555  11.354 0.318 $Reg Control Rod Cladding
46   cz    1.00   $ Safety and Shim Rod in Unit
47   cz    1.11   $ Safety and Shim Rod in Unit Cladding
48   cz    0.200  $ Reg Rod in Unit
49   cz    0.318  $ Reg Rod in Unit Cladding
50   cz    1.750  $ Inner radius of Al tube for control rod
```

```
91    pz   -33.43   $Lower Plate Bottom
92    pz   -30.89   $Lower Plate Top (1 inch)
93    pz    30.89   $Upper Plate Bottom
94    pz    32.79   $Upper Plate Top (0.75 inch)
95    pz   -55.0    $Concrete Bottom
96    pz   -43.09   $Water Bottom (2 inch)
97    pz    100.0    $Water Top
C Lattice Cells
101   px    2.185
102   px   -2.185
103   p     0.5   0.8660254  0   2.185
104   p     0.5   0.8660254  0  -2.185
105   p    -0.5   0.8660254  0   2.185
106   p    -0.5   0.8660254  0  -2.185
c Frame Boundary
111   p     1.732038    1   0    50.460
112   p     1.732038    1   0   -50.460
113   p     1.732038   -1   0    50.460
114   p     1.732038   -1   0   -50.460
115   py   25.230
116   py  -25.230
c Al Wall
121   p     1.732038    1   0    54.270
122   p     1.732038    1   0   -54.270
123   p     1.732038   -1   0    54.270
124   p     1.732038   -1   0   -54.270
```

```
125   py   27.135
126   py  -27.135
C Reflector Surfaces
131   cz   65.0      $ Water reflector
c 131   p    1.732038    1    0  83.259682
c 132   p    1.732038    1    0 -83.259682
c 133   p    1.732038   -1    0  83.259682
c 134   p    1.732038   -1    0 -83.259682
c 135   py   41.629841
c 136   py  -41.629841
c FNIF
140   BOX -15.88 -26.77 -30.48   -15.24 26.40 0   -22.00 -12.70 0   0 0 60.96
141   BOX -22.82 -24.91 -30.48   -10.16 17.60 0   -08.80 -05.10 0   0 0 60.96
142   BOX -22.87 -24.86 -30.48   -10.11 17.50 0   -08.75 -05.05 0   0 0 05.08
145   BOX -22.87 -24.86 -25.40   -10.11 17.50 0   -08.75 -05.05 0   0 0 55.88
144   BOX -22.97 -24.96  31.00   -10.01 17.40 0   -08.65 -04.95 0   0 0 20.08
147   BOX -22.97 -24.96 -24.90   -10.01 17.40 0   -08.65 -04.95 0   0 0 02.54
149   BOX -22.97 -24.96 -22.36   -10.01 17.40 0   -08.65 -04.95 0   0 0 52.34
252   BOX -27.66 -21.33  73.00   -05.00 08.50 0   -04.50 -02.70 0   0 0 07.00
254   BOX -28.15 -21.20  73.50   -04.60 08.10 0   -04.10 -02.30 0   0 0 06.00
256   BOX -15.88 -26.77  30.48   -15.24 26.40 0   -22.00 -12.70 0   0 0 50.00
258   BOX -16.88 -26.90  31.00   -14.24 25.40 0   -21.00 -11.70 0   0 0 49.00
260   BOX -17.88 -27.00  31.00   -13.24 24.40 0   -20.00 -10.70 0   0 0 49.00
c Heavy water beside core
150   p    1.732038    1   0    54.270  $ Al oute
151   p    1.732038    1   0    84.670
```

```
152   py    0.0
153   p     1.732038   -1   0     0.0
154   p     1.732038    1   0    54.670  $ Al outer
155   p     1.732038    1   0    84.270
156   py    0.2
157   p     1.732038   -1   0     0.4
158   c/z   30.08 17.37 5.7  $ Air tub Al wall
159   c/z   30.08 17.37 5.5  $ Air tub
160   pz   -30.0           $ Heavy water top
161   pz    30.0           $ Heavy water bottom
201 pz -18.5
202 pz -17.5
203 pz -16.5
204 pz -15.5
205 pz -14.5
206 pz -13.5
207 pz -12.5
208 pz -11.5
209 pz -10.5
210 pz -9.5
211 pz -8.5
212 pz -7.5
213 pz -6.5
214 pz -5.5
215 pz -4.5
216 pz -3.5
```

217 pz -2.5

218 pz -1.5

219 pz -0.5

220 pz 0.5

221 pz 1.5

222 pz 2.5

223 pz 3.5

224 pz 4.5

225 pz 5.5

226 pz 6.5

227 pz 7.5

228 pz 8.5

229 pz 9.5

230 pz 10.5

231 pz 11.5

232 pz 12.5

233 pz 13.5

234 pz 14.5

235 pz 15.5

236 pz 16.5

237 pz 17.5

238 pz 18.5

240 c/z -32 -19 1.5

244 pz 67.48

246 k/z -32 -19 71.48 0.17 -1

248 pz 51.08

```
250 pz  73
262 c/z -32 -19 1.5
264 pz 73.5
266 pz 73
mode n p
kcode 100000 1.0 100 5000
ksrc   -15.2950   -18.9227     0.0000
       -10.9250   -18.9227     0.0000
        -6.5550   -18.9227     0.0000
        -2.1850   -18.9227     0.0000
         2.1850   -18.9227     0.0000
         6.5550   -18.9227     0.0000
        10.9250   -18.9227     0.0000
       -17.4800   -15.1381     0.0000
       -13.1100   -15.1381     0.0000
        -8.7400   -15.1381     0.0000
        -4.3700   -15.1381     0.0000
         0.0000   -15.1381     0.0000
         4.3700   -15.1381     0.0000
         8.7400   -15.1381     0.0000
        13.1100   -15.1381     0.0000
       -19.6650   -11.3536     0.0000
       -15.2950   -11.3536     0.0000
       -10.9250   -11.3536     0.0000
        -6.5550   -11.3536     0.0000
        -2.1850   -11.3536     0.0000
```

```
       2.1850   -11.3536     0.0000
      10.9250   -11.3536     0.0000
      15.2950   -11.3536     0.0000
     -21.8500    -7.5691     0.0000
       8.7400    15.1381     0.0000
      13.1100    15.1381     0.0000
m1     1001.66c    -0.015896   $ new SS meat, H/Zr=1.6. 0.59% burn-up
     40000.66c    -0.899104
     92235.66c    -0.016728
m2     6000.66c     1.0        $ graphite
mt2    grph.60t
m3     6000.66c    -0.0004     $ ss cladding
     14000.60c    -0.0046
     24000.50c    -0.190
     25055.66c    -0.009
     26000.50c    -0.699
     28000.50c    -0.097
m4     1001.66c     2.0        $ H2O
      8016.66c     1.0
mt4    lwtr.60t
m5     1001.66c    -0.010    $ Al meat, H/Zr=1.0, 8.91% burnup
     40000.66c    -0.905
     92235.66c    -0.01533
     92238.66c    -0.06967
mt5    h/zr.60t
      zr/h.60t
```

```
m6    13027.66c     1.0        $ Al
m7     1001.66c     0.64       $ D20 (68% atom)
       1002.66c     1.36
       8016.66c     1.00
m8    82000.50c     1.0        $ Pb
m9     5010.66c    -0.1566     $ b4c
       5011.66c    -0.6264
       6000.66c    -0.217
m10    1001.66c    -0.00619    $ Concrete
       6000.66c    -0.17520
       8016.66c    -0.41020
      11023.66c    -0.00027
      12000.66c    -0.03265
      13027.66c    -0.01083
      14000.60c    -0.03448
      19000.66c    -0.00114
      20000.66c    -0.32130
      26000.50c    -0.00778
m11    7014.66c     0.0000381259 $Air
       8016.66c     0.0000095012
      18000.59c     0.0000001664
m12    1001.66c    -0.015896    $ Old SS meat, H/Zr=1.6, 8.77% burnup
      40000.66c    -0.899104
      92235.66c    -0.015354
      92238.66c    -0.069646
m13   26054.66c -1.0            $iron - density 7.874
```

```
m14   1001.66c -0.143711        $polyethylene - density 0.94
      8016.66c -0.856289
m15   1001.66c -0.148605        $paraffin wax - density 0.93
      8016.66c -0.851395
m16  1001.66c -0.06             $wood - density 1.4
      8016.66c -0.44
      6000.66c -0.50
m17  5010.66c -1.0              $Boron - density 2.08
c New SS Fuel (u=1)
f47:n  (130<200[-1 -2 0]<201)  (130<200[2 -1 0]<201)
FS47 -201 -202 -203 -204 -205 -206 -207 -208 -209 -210 -211 -212 -213 -214
     -215 -216 -217 -218 -219 -220 -221 -222 -223 -224 -225 -226 -227 -228
     -229 -230 -231 -232 -233 -234 -235 -236 -237 -238
E54 0 1E-9 5E-9 2.5E-8 1E-7 6.25E-7 2E-6 1E-5 1E-4 5E-4 1E-3 5E-3 0.01 0.05 0.1
      0.2 0.3 0.4 0.5 1 1.5 2 2.5 3 4 5 6 7 8 9 10 11 12 13 14 15 16 17 18 19 20
f64:n  410   $ SAMPLER
E64 0 1E-9 5E-9 2.5E-8 1E-7 6.25E-7 2E-6 1E-5 1E-4 5E-4 1E-3 5E-3 0.01 0.05 0.1
      0.2 0.3 0.4 0.5 1 1.5 2 2.5 3 4 5 6 7 8 9 10 11 12 13 14 15 16 17 18 19 20
f74:p  410   $ SAMPLER
FMESH84:n GEOM=rec ORIGIN=-40 -40 -40
          IMESH=40 IINTS=40
          JMESH=40 JINTS=40
          KMESH=40 KINTS=40
          EMESH=2.5E-8 6.25E-7 0.1 20 EINTS=1 1 1 1  OUT=ij
```

APPENDIX F

GEANT4.9.4 INPUT FILE OF UUTR FNPB

```
//....oooOO0OOooo........oooOO0OOooo........oooOO0OOooo........oooOO0OOooo......

ExN02DetectorConstruction::ExN02DetectorConstruction()

{

  // world volume

  world_x = world_y = world_z = 10*m;

  // FNIF-lead

  FNIF_x = 12.7*cm;

  FNIF_y = 13.5*cm;

  FNIF_z = 30.48*cm;

  // FNIF-Air

  FNIFa_x = 5.08*cm;

  FNIFa_y = 8.42*cm;

  FNIFa_z = 30.48*cm;

  //FNPB - Aluminum casing

  FNPBAli_x = 12.7*cm;

  FNPBAli_y = 13.5*cm;

  FNPBAli_z = 25*cm;

  //FNPB - Boron shielding inside FNPB

  FNPBB_x = 12.4*cm;

  FNPBB_y = 13*cm;

  FNPBB_z = 25*cm;

  //FNPB - collimator paraffin

  FNPBcoll_x = 11.7*cm;

  FNPBcoll_y = 12.5*cm;
```

```
FNPBcoll_z = 25*cm;
//FNPB - sampler casing
Casing_x = 2.5*cm;
Casing_y = 4*cm;
Casing_z = 3*cm;
//FNPB - sampler casing
sampler_x = 2*cm;
sampler_y = 3.5*cm;
sampler_z = 2.5*cm;
//Pencil tip
pencil_x = 0*cm;
pencil_y = 1.5*cm;
pencil_z = 2.5*cm;
pencil_a = 0.*deg;
pencil_b = 360.*deg;
// Air collimator box
Calor_x = 5.08*cm;
Calor_y = 8.42*cm;
Calor_z = 15*cm;
//cone tip
dx1 =5.08*cm;
dx2 =1.5*cm;
dy1 =8.42*cm;
dy2 =1.5*cm;
```

```
  dz  = 5*cm;
  //Fuel Box
  Fbox_x = 1.8*cm;
  Fbox_y = 13.5*cm;
  Fbox_z = 30.48*cm;
  //fuel pin}
//....oooOO0OOooo........oooOO0OOooo........oooOO0OOooo........oooOO0OOooo.....
ExN02DetectorConstruction::~ExN02DetectorConstruction(){;}
//....oooOO0OOooo........oooOO0OOooo........oooOO0OOooo........oooOO0OOooo.....
G4VPhysicalVolume* ExN02DetectorConstruction::Construct()
  G4double a, z, density;
  G4int nelements, natoms;
  G4int ncomponents;
  G4double fractionmass, temperature, pressure;
//Define stainless steel
// Use NIST database for elements and materials whereever possible.
        G4NistManager* man = G4NistManager::Instance();
        man->SetVerbose(1);
        G4Element* C  = man->FindOrBuildElement("C");
        G4Element* Si = man->FindOrBuildElement("Si");
        G4Element* Cr = man->FindOrBuildElement("Cr");
        G4Element* Mn = man->FindOrBuildElement("Mn");
        G4Element* Fe = man->FindOrBuildElement("Fe");
        G4Element* Ni = man->FindOrBuildElement("Ni");
```

```
        G4Element* Na = man->FindOrBuildElement("Na");

        G4Element* I  = man->FindOrBuildElement("I");

        G4Element* Cd = man->FindOrBuildElement("Cd");

        G4Element* Al = man->FindOrBuildElement("Al");

      G4Element* B  = man->FindOrBuildElement("B");

        G4Material* Cadmium = new G4Material("Cadmium", density= 7.996*g/cm3,
ncomponents=1);

        Cadmium->AddElement(Cd, fractionmass=1.0);

      G4Material* Boron10 = new G4Material("Boron10", density= 2.08*g/cm3,
ncomponents=1);

Boron10->AddElement(B, fractionmass=1.0);

   G4Material* Aluminum = new G4Material("Aluminum", density= 2.7*g/cm3,
ncomponents=1);

Aluminum->AddElement(Al, fractionmass=1.0);

// Air

G4Element* Pb = new G4Element("Lead", "Pb", z=82 , a=207*g/mole);

 G4Material* Lead = new G4Material("Lead", density=11.354*g/cm3, nelements=1);

Lead->AddElement(Pb, 100.*perCent);

  G4Element* N = new G4Element("Nitrogen", "N", z=7 , a=14.01*g/mole);

  G4Element* O = new G4Element("Oxygen"  , "O", z=8 , a=16.00*g/mole);

  G4Material* Air = new G4Material("Air", density=1.29*mg/cm3, nelements=2);

  Air->AddElement(N, 70.*perCent);

  Air->AddElement(O, 30.*perCent);

// Water

  G4Element* H = new G4Element("Hydrogen", "H", z=1 , a=1.01*g/mole);

  G4Material* Water = new G4Material("Water", density= 1.0*g/cm3, nelements=2);
```

```
  Water->AddElement(H, 2);

  Water->AddElement(O, 1);

  G4Material* Sapphire = new G4Material("Sapphire",density= 4.*g/cm3,
ncomponents=2);

  Sapphire->AddElement(Al, natoms=2);

  Sapphire->AddElement(O , natoms=3);

// Paraffin - Polythelene

  G4Material* Paraffin = new G4Material("Paraffin", density= 0.94*g/cm3,
nelements=2);

  Paraffin->AddElement(C, 85.6*perCent);

  Paraffin->AddElement(H, 14.4*perCent);

//=============================================================

//   Description of FNPB Geometry

//=============================================================

// The WORLD VOLUME

  G4Box* world_box = new G4Box("World",world_x,world_y,world_z);

  G4LogicalVolume* world_log  = new
G4LogicalVolume(world_box,Water,"World",0,0,0);

  G4VPhysicalVolume* world_phys = new
G4PVPlacement(0,G4ThreeVector(),world_log,"World",0,false,0);

// FNIF-Lead

  G4VSolid* FINFLead_box = new G4Box("FNIF", FNIF_x, FNIF_y, FNIF_z);

 G4LogicalVolume* FINFLead_log = new
G4LogicalVolume(FINFLead_box,Lead,"FNIF",0,0,0);

 G4VPhysicalVolume* FINFLead_phys = new
G4PVPlacement(0,G4ThreeVector(0,0,0),FINFLead_log,"FNIF",

  world_log,false,0);
```

```
// FNIF-Air

  G4VSolid* FNIF_Box = new G4Box("FNIF-air",FNIFa_x,FNIFa_y,FNIFa_z);

  G4LogicalVolume* FNIF_log = new G4LogicalVolume(FNIF_Box,Air,"FNIF-
air",0,0,0);\

  G4VPhysicalVolume* FNIF_phys = new
G4PVPlacement(0,G4ThreeVector(2.54*cm,0,0),FNIF_log,"FNIF-
air",world_log,false,0);

// FNPB-Aluminum

  G4VSolid* FNPBAli_box = new G4Box("FNPB-ali", FNPBAli_x, FNPBAli_y,
FNPBAli_z);

  G4LogicalVolume* FNPBAli_log = new
G4LogicalVolume(FNPBAli_box,Aluminum,"FNPB-ali",0,0,0);

  G4VPhysicalVolume* FNPBAli_phys = new
G4PVPlacement(0,G4ThreeVector(0,0,55.48*cm),FNPBAli_log,"FNPB-ali",

  world_log,false,0)

// FNPB-Boron

  G4VSolid* FNPBB_box = new G4Box("FNPBBoron", FNPBB_x, FNPBB_y,
FNPBB_z);

 G4LogicalVolume* FNPBB_log = new
G4LogicalVolume(FNPBB_box,Boron10,"FNPBBoron",0,0,0);

 G4VPhysicalVolume* FNPBB_phys = new
G4PVPlacement(0,G4ThreeVector(0,0,55.48*cm),FNPBB_log,"FNPBBoron",

 world_log,false,0);

// FNPB-Collimator

  G4VSolid* FNPBcollim_box = new G4Box("collimator", FNPBcoll_x, FNPBcoll_y,
FNPBcoll_z);

 G4LogicalVolume* FNPBcollim_log = new

G4LogicalVolume(FNPBcollim_box,Paraffin,"collimator",0,0,0);
```

```
G4VPhysicalVolume* FNPBcollim_phys = new
G4PVPlacement(0,G4ThreeVector(0,0,55.48*cm),FNPBcollim_log,"collimator",

 world_log,false,0);

G4VSolid* Casing_box = new G4Box("Casing", Casing_x, Casing_y,
Casing_z);G4LogicalVolume* Casing_log = new
G4LogicalVolume(Casing_box,Lead,"Casing",0,0,0);

 G4VPhysicalVolume* Casing_phys = new
G4PVPlacement(0,G4ThreeVector(2.54*cm,0,77.48*cm),Casing_log,"Casing",

world_log,false,0);

// Sampler-Air

 G4VSolid* sampler_box = new G4Box("sampler", sampler_x, sampler_y, sampler_z);

G4LogicalVolume* sampler_log = new
G4LogicalVolume(sampler_box,Air,"sampler",0,0,0);

 G4VPhysicalVolume* sampler_phys = new
G4PVPlacement(0,G4ThreeVector(2.54*cm,0,77.98*cm),sampler_log,"sampler",

 world_log,false,0);

// Pencil tip of colliator

  G4Tubs* pencil_tip = new G4Tubs("pencil",pencil_x,pencil_y,pencil_z,
pencil_a,pencil_b);

  G4LogicalVolume* pencil_log = new G4LogicalVolume(pencil_tip,Air,"pencil",0,0,0);

  G4VPhysicalVolume* pencil_phys = new
G4PVPlacement(0,G4ThreeVector(2.54*cm,0,72.98*cm),pencil_log,"pencil",

 world_log,false,0);

//Collimator Box

  G4Box* Collimator_Box = new G4Box("AirCollimator",Calor_x,Calor_y,Calor_z);

  G4LogicalVolume* Collimator_log = new
G4LogicalVolume(Collimator_Box,Air,"AirCollimator",0,0,0);
```

```
  G4VPhysicalVolume* Collimator_phys = new
G4PVPlacement(0,G4ThreeVector(2.54*cm,0,45.48*cm),Collimator_log,"AirCollimat
or",

 world_log,false,0);

//Collimator cone

  G4Trd* Collimator_con = new G4Trd("Collimator_con",dx1,dx2,dy1,dy2,dz);

  G4LogicalVolume* con_log = new
G4LogicalVolume(Collimator_con,Air,"Collimator_con",0,0,0);

  G4VPhysicalVolume* con_phys = new
G4PVPlacement(0,G4ThreeVector(2.54*cm,0,65.48*cm),con_log,"Collimator_co
world_log,false,0);

  G4Box* fuel_Box = new G4Box("fuelbox",Fbox_x,Fbox_y,Fbox_z);

  G4LogicalVolume* fuelbox_log = new
G4LogicalVolume(fuel_Box,Air,"fuelbox",0,0,0);

  G4VhysicalVolume* fuelbox_phys = new
G4PVPlacement(0,G4ThreeVector(14.4*cm,0,0),fuelbox_log,"fuelbox",

                world_log,false,0);

  G4Tubs* fuel = new G4Tubs("fuel",fuel_x,fuel_y,fuel_z, fuel_a,fuel_b);

  G4LogicalVolume* fuel_log = new G4LogicalVolume(fuel,Air,"fuel",0,0,0);

  G4VPhysicalVolume* fuel_phys = new
G4PVPlacement(0,G4ThreeVector(14.4*cm,0,0*cm),fuel_log,"fuel",

 world_log,false,0);

  G4Tubs* fuel1 = new G4Tubs("fuel1",fuel1_x,fuel1_y,fuel1_z, fuel1_a,fuel1_b);

  G4LogicalVolume* fuel1_log = new G4LogicalVolume(fuel1,Air,"fuel1",0,0,0);

  G4VPhysicalVolume* fuel1_phys = new
G4PVPlacement(0,G4ThreeVector(14.4*cm,3.2*cm,0*cm),fuel1_log,"fuel1",

                world_log,false,0);

  G4Tubs* fuel2 = new G4Tubs("fuel2",fuel2_x,fuel2_y,fuel2_z, fuel2_a,fuel2_b);
```

```
  G4LogicalVoume* fuel2_log = new G4LogicalVolume(fuel2,Air,"fuel2",0,0,0);

  G4VPhysicalVolume* fuel2_phys = new
G4PVPlacement(0,G4ThreeVector(14.4*cm,6.5*cm,0*cm),fuel2_log,"fuel2",

                world_log,false,0);

  G4Tubs* fuel3 = new G4Tubs("fuel3",fuel3_x,fuel3_y,fuel3_z, fuel3_a,fuel3_b);

  G4LogicalVolume* fuel3_log = new G4LogicalVolume(fuel3,Air,"fuel3",0,0,0);

  G4VPhysicalVolume* fuel3_phys = new
G4PVPlacement(0,G4ThreeVector(14.4*cm,9.8*cm,0*cm),fuel3_log,"fuel3",

   world_log,false,0);

  G4Tubs* fuel4 = new G4Tubs("fuel4",fuel4_x,fuel4_y,fuel4_z, fuel4_a,fuel4_b);

  G4LogicalVolume* fuel4_log = new G4LogicalVolume(fuel4,Air,"fuel4",0,0,0);

  G4VPhysicalVolume* fuel4_phys = new
G4PVPlacement(0,G4ThreeVector(14.4*cm,-3.2*cm,0*cm),fuel4_log,"fuel4",

   world_log,false,0);

  G4Tubs* fuel5 = new G4Tubs("fuel5",fuel5_x,fuel5_y,fuel5_z, fuel5_a,fuel5_b);

  G4LogicalVolume* fuel5_log = new G4LogicalVolume(fuel5,Air,"fuel5",0,0,0);

  G4VPhysicalVolume* fuel5_phys = new
G4PVPlacement(0,G4ThreeVector(14.4*cm,-6.5*cm,0*cm),fuel5_log,"fuel5",

   world_log,false,0);

  G4Tubs* fuel6 = new G4Tubs("fuel6",fuel6_x,fuel6_y,fuel6_z, fuel6_a,fuel6_b);

  G4LogicalVolume* fuel6_log = new G4LogicalVolume(fuel6,Air,"fuel6",0,0,0);

  G4VPhysicalVolume* fuel6_phys = new
G4PVPlacement(0,G4ThreeVector(14.4*cm,-9.8*cm,0*cm),fuel6_log,"fuel6",

                world_log,false,0);

  return world_phys;

//....oooOO0OOooo.....oooOO0OOooo.....oooOO0OOooo.....oooOO0OOooo.....
```

REFERENCES

1. GEANT4 Simulation code, Introduction to GEANT4 user documentation, 2012.Web,http://geant4.web.cern.ch/geant4/UserDocumentation/Welcome/IntroductionToGeant.

2. X-5 Monte Carlo Team. MCNP – A General Monte Carlo N-Particle Transport Code, Version 5, LA-UR-03-1987 (2003).

3. ATLAS Liquid Argon HEC Collaboration (B. Dowler et al.), Nucl. Instr. and Meth. A 482 (2002) 94.

4. Geant4 Collaboration (S. Agostinelli *et al.*), Nucl. Instr. and Meth. A 506 (2003) 250.

5. BABAR Computing Group (D.H. Wright et al.), CHEP-2003-TUMT006, May 2003, 7pp. Proceedings of the International Conference CHEP'03, La Jolla, California, 2003, e-Print Archive: hep-ph/0305240.

6. F. Salvat, et al., PENELOPE: a code system for monte carlo simulation of electron and photon transport, in: Workshop Proceedings, OECD Nuclear Energy Agency, Issyles Moulineaux, 2001.

7. GEANT4 Simulation code, 2012. Web, http:://www.info.cern.ch/asd/geant4/

8. GEANT4 Simulation code, Introduction to GEANT4 – Physics references, 2012. Web,http://geant4.web.cern.ch/geant4/UserDocumentation/UsersGuides/PhysicsReference

9. S. Agostinelli et al., Geant4 – a simulation toolkit Nucl. Instr. Meth. A506 (2003) 250.

10. J. Apostolakis et al., Geometry and physics of the Geant4 toolkit for high and medium energy applications. Rad. Phys. Chem. 78 (2009) 859.

11. L.M. Chounet, J.M. Gaillard, and M.K. Gaillard, Phys. Reports 4C, 199 (1972).

12. Review of Particle Physics, The European Physical Journal C, 15 (2000).

13. H.Fesefeldt GHEISHA, The Simulation of Hadronic Showers 149 RWTH/PITHA 85/02 (1985)

14. G.A.P. Cirrone et al., Validation of the Geant4 electromagnetic photon cross-section for elements and compound. Nuclear Inst. and meth in physics research. A 618 (2010) 315-322.

15. V.N. Ivanchenko, Geant4: Physics potential for instrumentation in space and medicine; Nuclear instruments & methods in physics research. A 525 (2004) 402-405.

16. GEANT4 Simulation code, electromagnetic physics models - benchmark, 2012. Web, http://indico.cern.ch/getFile.py/102427

17. F. Salvat, J.F Fernandez-Varea, J. Sempau, X. Llovet, Rad. Phys. and Chem., 75 (2006) 1201-1219.

18. GEANT4 Simulation code, electromagnetic physics models, 2012. Web, https://indico.fnal.gov/getFile.py/4535

19. Monte Carlo Method, 2012 Web, http://en.wikipedia.org/wiki/Monte_Carlo_method

20. Berg, Bernd A., *Markov Chain Monte Carlo Simulations and Their Statistical Analysis (With Web-Based Fortran Code)*. Hackensack, NJ: World Scientific. ISBN 981-238-935-0 (2004).

21. P. Arce, *et al.*, Nucl. Instr. and Meth. A 502 (2003) 687.

22. F. Brown, B. Kiedrowski *et al.,* Verification of MCNP5-1.60, LA-UR-10-05611, 836 (07/2006).

23. Y. Danon, E. Liu *et al.*, Benchmark Experiment of Neutron Resonance Scattering Models in Monte Carlo Codes, International conference of mathematics, computational methods & reactor physics, May (2009).

24. H. Koivunoro et al., Accuracy of the Electron in MCNP5 and its Suitability for Ionization Chamber Response Simulations: A Comparison with the EGSNRC and PENELOPE Codes, Med. Phys. 39 (3), March (2012).

25. Decay scheme of Cesium-137, 2012, Web, http://atom.kaeri.re.kr/cgi-bin/decay?Cs-137%20B-

26. Description of changes and additions in GEANT4.9.3, 2012, Web, http://geant4.cern.ch/support/ReleaseNotes4.9.3.html

27. Discovery of Neutron, 2012, Web, http://en.wikipedia.org/wiki/Neutron#Discovery

28. Sir James Chadwick's Discovery of Neutrons. ANS Nuclear Cafe. Retrieved on 2012-09-16

29. Fast neutrons, 2012, Web, http://en.wikipedia.org/wiki/Neutron_temperature

30. D. L. Chichester, J. D. Simpson, Compact Accelerator Neutron Generators, The Industrial Physicist, vol-9, iss-6, p22.

31. C. Adreani, A. Pietropaolo *et al.*, Facility for fast neutron irradiation tests of electronics at the ISIS Spallation neutron source, American Institute of Physics, vol-92, iss-11, (2008).

32. Michigan State University courses, 2012, Web, http://www2.chemistry.msu.edu/courses/CEM988Nuclear/lectures/Chem988_S09-Ch15.pdf

33. NIST accelerator facility, 2012, Web, http://www.nist.gov/pml/div682/grp02/accelerator-facilities.cfm

34. B. A. Ludewigt, D. L. Bleuel *et al.*, Accelerator-driven neutron source for cargo screening, Nuclear instruments and methods, physics research. vol-261, Iss 1-2, pp. 303-306, (2007).

35. E. Bourhis-martin et al., Empirical description and Monte Carlo simulation of fast neutron pencil beams as basis of a treatment planning system. Med. Phys. 29 (8), August (2002).

36. D. King, P. Griffin et al., Test simulation of neutron damage to electronic components using accelerator facilities. Sandia National Laboratories, May (2009).

37. F. M. Wagner *et al.*, Neutron medical treatment tumors – a survey of facilities. IOP publishing for SISSA Media Lab, march (2012).

38. General Atomics Electronic Systems, TRIGA Nuclear Reactors, 2012. Web, http://www.ga-esi.com/triga/

39. University of Utah - Safety Analysis Report, 2012. Web, http://pbadupws.nrc.gov/docs/ML1032/ML103210041.pdf

40. J. D. Bess. Designing A High-Flux Trap In The University Of Utah TRIGA Reactor. Masters Thesis. University of Utah; 2005

41. J. S. Bennion. Characterization and Qualification of a Quasi-fission Neutron Irradiation Environment for Neutron Hardness Assurance Testing of Electronic Devices and other Materials Damage Investigations. Doctoral Dissertation. University of Utah; 1996

42. Table of Nuclides, Cross section plotter, 2012, Web, http://atom.kaeri.re.kr/

43. T. Bucherl. Radiography and tomography with fast neutrons at the FRM-II-a status report. Applied Radiation and Isotopes 61 (2004) 537–540